TO APPEAR IN THE ASTROPHYSICAL JOURNAL, SUPPLEMENT SERIES
Preprint typeset using LaTeX style emulateapj v. 05/12/14

arXiv:1511.06819v1 [astro-ph.SR] 21 Nov 2015

LIGHT CURVE ANALYSIS OF NEON NOVAE

IZUMI HACHISU
Department of Earth Science and Astronomy, College of Arts and Sciences, The University of Tokyo, 3-8-1 Komaba, Meguro-ku, Tokyo 153-8902, Japan
AND
MARIKO KATO
Department of Astronomy, Keio University, Hiyoshi, Kouhoku-ku, Yokohama 223-8521, Japan
to appear in the Astrophysical Journal, Supplement Series

ABSTRACT

We analyzed light curves of five neon novae, QU Vul, V351 Pup, V382 Vel, V693 CrA, and V1974 Cyg, and determined their white dwarf (WD) masses and distance moduli on the basis of theoretical light curves composed of free-free and photospheric emission. For QU Vul, we obtained a distance of $d \sim 2.4$ kpc, reddening of $E(B-V) \sim 0.55$, and WD mass of $M_{\rm WD} = 0.82 - 0.96\ M_\odot$. This suggests that an oxygen-neon WD lost a mass of more than $\sim 0.1\ M_\odot$ since its birth. For V351 Pup, we obtained $d \sim 5.5$ kpc, $E(B-V) \sim 0.45$, and $M_{\rm WD} = 0.98 - 1.1\ M_\odot$. For V382 Vel, we obtained $d \sim 1.6$ kpc, $E(B-V) \sim 0.15$, and $M_{\rm WD} = 1.13 - 1.28\ M_\odot$. For V693 CrA, we obtained $d \sim 7.1$ kpc, $E(B-V) \sim 0.05$, and $M_{\rm WD} = 1.15 - 1.25\ M_\odot$. For V1974 Cyg, we obtained $d \sim 1.8$ kpc, $E(B-V) \sim 0.30$, and $M_{\rm WD} = 0.95 - 1.1\ M_\odot$. For comparison, we added the carbon-oxygen nova V1668 Cyg to our analysis and obtained $d \sim 5.4$ kpc, $E(B-V) \sim 0.30$, and $M_{\rm WD} = 0.98$–$1.1\ M_\odot$. In QU Vul, photospheric emission contributes 0.4 – 0.8 mag at most to the optical light curve compared with free-free emission only. In V351 Pup and V1974 Cyg, photospheric emission contributes very little (0.2 – 0.4 mag at most) to the optical light curve. In V382 Vel and V693 CrA, free-free emission dominates the continuum spectra, and photospheric emission does not contribute to the optical magnitudes. We also discuss the Maximum Magnitude versus Rate of Decline (MMRD) relation for these novae based on the universal decline law.

Keywords: novae, cataclysmic variables — stars: individual (QU Vul, V351 Pup, V382 Vel, V693 CrA, V1974 Cyg)

1. INTRODUCTION

A classical nova is a thermonuclear runaway event on a mass-accreting white dwarf (WD) in a binary system, in which mass is transferred from the companion to the WD via Roche lobe overflow or winds. When the hydrogen-rich envelope mass reaches a critical value, hydrogen ignites to trigger a shell flash at the bottom of the hydrogen-rich envelope. The photosphere of the envelope expands to a giant size of $\sim 100 R_\odot$, and the binary becomes a bright classical nova.

It is widely known that nova ejecta are enriched with heavy elements such as C, O, and Ne (e.g., Gehrz et al. 1998). These elements are thought to originate from the WD cores, because such amounts of heavy elements cannot be synthesized in hydrogen burning on the WDs. Thus, a nova having ejecta enriched by carbon and oxygen occurs on a carbon–oxygen (CO) WD. A nova is enriched by neon if it outbursts on an oxygen-neon (ONe) WD.

Neon novae are a subclass of classical novae that show neon emission lines stronger than the permitted lines in the nebular phase. If the neon in the ejecta comes from the core material of an ONe WD (e.g., Gehrz et al. 1998), its natal WD mass is likely greater than $\gtrsim 1.07\ M_\odot$ (e.g., Umeda et al. 1999), or $\gtrsim 1.0\ M_\odot$ (e.g., Weidemann 2000). Evolution calculations suggest that a natal WD has a thin helium-rich layer above a carbon–oxygen-rich mantle, e.g., a $0.035\ M_\odot$ CO mantle for a $1.09\ M_\odot$ ONe core (Gil-Pons & García-Berro 2001). Such a WD may undergo a number of nova explosions before the thin helium-rich layer is blown off. Subsequently, the WD further undergoes a number of nova explosions before the CO mantle on the ONe core is blown off. If the mass accretion rate is $\sim 10^{-9} M_\odot$ yr^{-1}, the ignition mass is $\sim 10^{-5} M_\odot$, and the same amount of WD material is dredged up in every nova outburst, we can expect that 3,000 to 4,000 outbursts (in a total time of at least 30 – 40 Myr) must occur before the WD is deprived of its $0.035\ M_\odot$ carbon–oxygen-rich mantle and significant neon is detected in the ejecta. This could be a lower estimate because a carbon–oxygen-rich mantle is more massive for the lower mass limit of the ONe core (as massive as $\sim 0.1\ M_\odot$, Gil-Pons et al. 2003). Therefore, the minimum masses could be slightly smaller than $\sim 1.0\ M_\odot$. In this paper, we determine the WD masses and other parameters of various neon novae on the basis of our model light curve fitting. It should be noted that, however, a modest enrichment in neon could be originated even from a CO core (Livio & Truran 1994, see discussion in Section 8.1).

The optical light curves of novae show overall similarity despite their wide variety of timescales and shapes (e.g., Payne-Gaposchkin 1957; Duerbeck 1981; Strope et al. 2010; Hachisu & Kato 2014). Optical and near infrared (NIR) spectra of some novae are consistent with that of free-free emission in the early decline phase (e.g., Gallagher & Ney 1976). Kato and her collaborators developed optically thick wind theory as summarized in Kato & Hachisu (1994), in which they calculated hydrogen-rich envelope models in the decay phase of novae for various WD masses and chemical compositions. Hachisu & Kato (2006) calculated free-free emission model light curves on the basis of Kato & Hachisu's wind mass loss solutions for various sets of WD masses and chemical compositions. They found a universal decline law from theoretical analysis and

hachisu@ea.c.u-tokyo.ac.jp

showed that several well observed novae follow the law in the optical and infrared (IR) light curves. We show such examples of light curve fitting between the universal decline law (theoretical) and the observed ones (Figures 1 and 2), which will be described in more detail in later. These figures suggest that there is a similarity in the light curves both for optical and UV as well as color evolutions. They found that the time-normalized light curves are independent of the WD mass, chemical composition of ejecta, and wavelength. They also showed that the UV 1455 Å light curves (Cassatella et al. 2002), interpreted as photospheric blackbody emission, can also be time-normalized by the same factor as in the optical and IR (Figures 1 and 2). This strongly support the reliability of the universal decline law, as it appears to be independent of the emission mechanism, be that free-free (optical/IR) or blackbody emission (UV). Because the time-stretching factor is closely related to the WD mass, the authors determined the WD masses and other parameters from the light curve fittings for a number of relatively well-observed novae, e.g., V1500 Cyg, V1668 Cyg, V1974 Cyg, V838 Her, V598 Pup, V382 Vel, V4743 Sgr, V1281 Sco, V597 Pup, V1494 Aql, V2467 Cyg, V5116 Sgr, V574 Pup, V458 Vul (see, e.g., Hachisu & Kato 2007, 2010, 2014, 2015; Hachisu et al. 2008; Kato & Hachisu 2007; Kato et al. 2009).

In fast novae, free-free emission dominates the spectrum in optical and NIR bands. The free-free emission is radiated from optically thin plasma outside the photosphere and its flux is calculated from $\dot{M}_{\rm wind}^2/v_{\rm ph}^2 R_{\rm ph}$ in Hachisu & Kato (2006), where $\dot{M}_{\rm wind}$ is the wind mass-loss rate, $v_{\rm ph}$ the photospheric velocity, and $R_{\rm ph}$ the photospheric radius of the nova envelope. Faster novae blow stronger winds with larger mass-loss rates (Kato & Hachisu 1994). So faster novae show brighter optical maxima. In slower novae, their wind mass-loss rates are smaller than those of fast novae, so the brightness of free-free emission is much fainter than that of fast novae. As a result, the brightness of free-free emission becomes as faint as or fainter than that of photospheric emission. So we must take into account photospheric emission, which is calculated from the blackbody emission at the photosphere (e.g., Kato & Hachisu 1994). Hachisu & Kato (2015) calculated three model light curves of free-free emission (radiated from optically thin plasma outside the pseudophotosphere), photospheric emission (blackbody radiation from the pseudophotosphere), and their sum for various WD masses with various chemical compositions, and fitted the total V flux with the observed data for several slower novae, e.g., PW Vul, V705 Cas, GQ Mus, V723 Cas, HR Del, V5558 Sgr, and RR Pic. Thus, in these novae, the photospheric emission cannot be neglected compared with free-free emission to accurately determine the WD mass and other properties of a nova.

In the present paper, we select five neon novae, QU Vul, V351 Pup, V382 Vel, V693 CrA, and V1974 Cyg with a supplemental analysis of V1668 Cyg, and analyze in detail, including both the free-free emission and photospheric emission. These novae are selected from the following reasons: (1) well observed in optical/IR; (2) chemical composition is known; (3) *International Ultraviolet Explore (IUE)* UV data or supersoft X-ray/on or X-ray/off epoch data are obtained, which specifies the evolution timescale for different emission mechanisms of individual novae. We need the chemical composition of ejecta to accurately determine the WD mass because the nova model light curves depends not only on the WD mass but also slightly on the chemical composition. The chemical compositions of eleven neon novae were obtained as listed in Table 1. The UV 1455Å light curves are extremely useful for our light curve analysis (see, e.g., Hachisu & Kato 2006, 2015). Five out of the eleven neon novae, i.e., QU Vul, V351 Pup, V838 Her, V1974 Cyg, and V693 CrA were well observed with the *IUE* satellite that provided plenty of UV 1455Å light curve data (Cassatella et al. 2002). Among them, V838 Her was already analyzed by Kato et al. (2009) and its WD mass was estimated to be $\gtrsim 1.35\ M_\odot$, so we exclude V838 Her in the present analysis. We include V382 Vel in our analysis because the end of hydrogen shell-burning of V382 Vel was detected with X-ray (e.g., Ness et al. 2005), supporting our multiwavelength light curve analysis. Although V1668 Cyg was not identified as a neon nova, we reanalyze V1668 Cyg because its WD mass is close to the lower mass boundary of ONe WDs and the optical, especially medium-band y magnitude, and *IUE* UV data are so rich.

Our method for nova light curve analysis is introduced in Section 2 for V1668 Cyg, which is a carbon-oxygen (CO) nova but observed well in multiwavelength bands. Then, we analyze the neon nova QU Vul in Section 3. Subsequently, we examine V351 Pup in Section 4, V382 Vel in Section 5, V693 CrA in Section 6, and V1974 Cyg in Section 7. Discussion and conclusions follow in Sections 8 and 9, respectively. Nova evolution is discussed using the color-color (Section 8.2) and color-magnitude (Section 8.3) diagrams. Our time-stretching method for obtaining the distance modulus of a nova is also described in Appendix A. The absolute magnitudes of the nova light curves are estimated from our universal decline law in Appendix B.

2. NUMERICAL METHOD AND REANALYSIS OF V1668 CYG

V1668 Cyg was well observed with *IUE* and the chemical composition of ejecta was obtained as listed in Table 1. Hachisu & Kato (2006) calculated free-free emission model light curves for various WD masses and chemical compositions and fitted their free-free emission model light curves with the V and y light curves of V1668 Cyg. They further fitted their blackbody emission UV 1455Å model light curves with the *IUE* UV 1455Å observation, and estimated the WD mass. In this section, we reanalyze the light curves of V1668 Cyg including contribution of photospheric emission, which is not considered in the previous analysis of V1668 Cyg. V1668 Cyg is a CO nova but its WD mass is close to the lower mass bound of natal pure ONe WD. We will discuss its implication on binary evolution in Section 8.1.

It has been argued that nova envelopes reach steady-state after optical maximum. Using this assumption, Kato & Hachisu (1994) calculated evolution of nova envelopes for various WD masses and several sets of chemical compositions. They numerically obtained optically thick winds of nova envelopes. The wind mass loss rate, $\dot{M}_{\rm wind}$, is obtained as an eigen-value of the steady-state envelope solution, whose hydrogen-rich envelope mass is $M_{\rm env}$. The time evolution of a hydrogen-rich nova envelope is calculated from $\dot{M}_{\rm env} = \dot{M}_{\rm acc} - \dot{M}_{\rm wind} - \dot{M}_{\rm nuc}$, where $\dot{M}_{\rm env}$ is the mass decreasing rate of the hydrogen-rich envelope, $\dot{M}_{\rm acc}$ the mass accretion rate to the WD, $\dot{M}_{\rm wind}$ the wind mass loss rate, and $\dot{M}_{\rm nuc} \equiv L_{\rm n}/XQ$ the mass decreasing rate by nuclear burning, $L_{\rm n}$ the hydrogen nuclear burning luminosity, X the hydrogen content, and $Q = 6.4 \times 10^{18}$ erg s^{-1} the energy generation

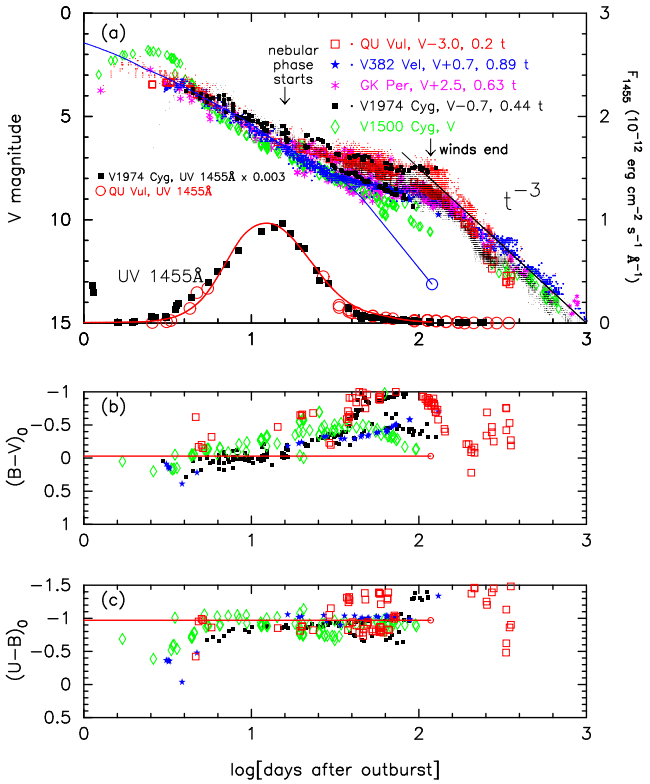

Figure 1. Five neon novae follow a universal decline law (blue solid line) in the decay phase. (a) V band and UV 1455 Å band light curves, (b) $(B-V)_0$, and (c) $(U-B)_0$ color curves, for QU Vul (red open squares), V382 Vel (blue filled star marks), GK Per (magenta asterisks), V1974 Cyg (black filled squares), and V1500 Cyg (green open diamonds). To make them overlap in the early decline phase, we shift horizontally the logarithmic time of QU Vul, V382 Vel, GK Per, and V1974 Cyg, by $-0.70 = \log 0.2$, $-0.05 = \log 0.89$, $-0.20 = \log 0.63$, and $-0.36 = \log 0.63$, and vertically their magnitudes by –3.0, +0.7, +2.5, and –0.7 mag, respectively, against V1500 Cyg. UV 1455 Å fluxes of V1974 Cyg are also rescaled against that of QU Vul as indicated in the figure. Model light curves (blue solid line for optical, red solid line for UV 1455 Å) are also added for QU Vul (a 0.96 $M_\odot$ WD with the envelope chemical composition of Ne Nova 3 in Table 2). Colors of optically thick free-free emission are also added by red solid lines, i.e., $(B-V)_0 = -0.03$ in panel (b) and $(U-B)_0 = -0.97$ in panel (c). The t^{-3} law (black solid line) indicates the trend of free-free flux for a freely expanding nebula with no mass supply. See text for the sources of the observed data.

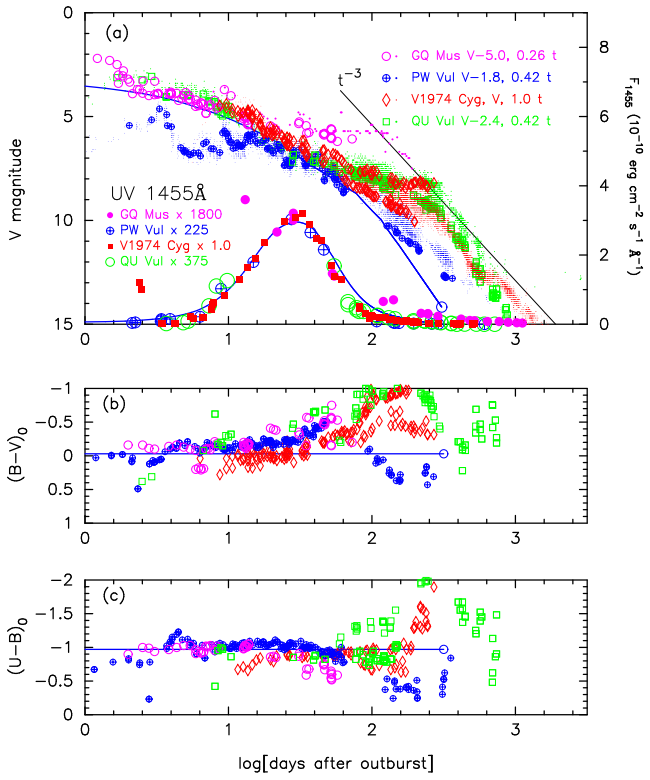

Figure 2. Four novae follow a universal decline law (blue solid line). The UV 1455 Å light curves are also overlapped each other with the same stretching factor as that of the optical light curve. (a) V band and UV 1455 Å band light curves, (b) $(B-V)_0$, and (c) $(U-B)_0$ color curves, for QU Vul (green open squares), PW Vul (blue open circles with a plus sign inside), GQ Mus (magenta open circles), and V1974 Cyg (red open diamonds). To make them overlap in the early decline phase, we shift horizontally their logarithmic time of QU Vul, GQ Mus, and PW Vul against V1974 Cyg, by $-0.38 = \log 0.42$, $-0.585 = \log 0.26$, and $-0.38 = \log 0.42$, and vertically their magnitudes by –2.4, –5.0, and –1.8 mag, respectively, as indicated in the figure. The UV 1455 Å light curves are also rescaled against that of V1974 Cyg as indicated in the figure. We also added our free-free emission and UV 1455Å model light curves (blue solid lines) of 0.83 $M_\odot$ WD with CO Nova 4 (as the best-fit model of PW Vul). See text for the sources of the observational data.

per unit mass by hydrogen burning. Kato & Hachisu (1994) obtained a sequence of envelope solutions, in which various physical values such as $\dot{M}_{\rm wind}$ and $\dot{M}_{\rm nuc}$ are given as a function of the envelope mass $M_{\rm env}$. If the initial envelope mass $M_{\rm env,0}$ is given, we follow the evolution of the hydrogen-rich envelope mass by integrating $\dot{M}_{\rm env} = \dot{M}_{\rm acc} - \dot{M}_{\rm wind} - \dot{M}_{\rm nuc}$, and obtain the time evolutions of various physical values such as $\dot{M}_{\rm wind}$, the photospheric radius $R_{\rm ph}$, photospheric temperature $T_{\rm ph}$, and photospheric velocity $v_{\rm ph}$. The mass accretion rate is usually very small compared with the wind mass loss rate or the nuclear burning rate, i.e., $\dot{M}_{\rm acc} \ll \dot{M}_{\rm wind} + \dot{M}_{\rm nuc}$ in classical novae, so we set $\dot{M}_{\rm acc} = 0$ in our model light curves. Because Kato & Hachisu's solutions are applied only to a steady-state envelope, that is, in the decay phase of a nova after optical maximum, we use our model light curves only for the decay phase of novae.

The optical V flux is calculated from the sum of the free-free and photospheric blackbody emission. The blackbody emission was described in Kato & Hachisu (1994), and the free-free emission was calculated from $F_\nu \propto \dot{M}_{\rm wind}^2 / v_{\rm ph}^2 R_{\rm ph}$ in Hachisu & Kato (2006) (see also Equation (B2) in Appendix B). The UV 1455 Å band flux is useful for determining the WD mass. This is a narrow-band (1445–1465 Å) flux that represents well the continuum fluxes of novae (Cassatella et al. 2002). The flux in the UV 1455 Å band was calculated from the blackbody emission at the pseudophotosphere of the optically thick wind solutions of Kato & Hachisu (1994) and is presented in Hachisu & Kato (2006) for various WD masses and chemical compositions.

2.1. *Light curve fitting of V1668 Cyg*

Figure 3 show the optical and UV light curves of V1668 Cyg and our model light curves. The visual magnitudes are taken from the archive of the American Association of Variable Star Observers (AAVSO) and those of V magnitudes are from di Paolantonio et al. (1981), Piccioni et al. (1984), Hopp (1979), Kolotilov (1980), Mallama & Skillman (1979), and Duerbeck et al. (1980). The data of the y magnitudes are from Gallagher et al. (1980). The UV 1455 Å band, a 20Å width at the center of 1455Å, was defined by Cassatella et al. (2002) as one of the two UV narrow bands that can represent the UV continuum

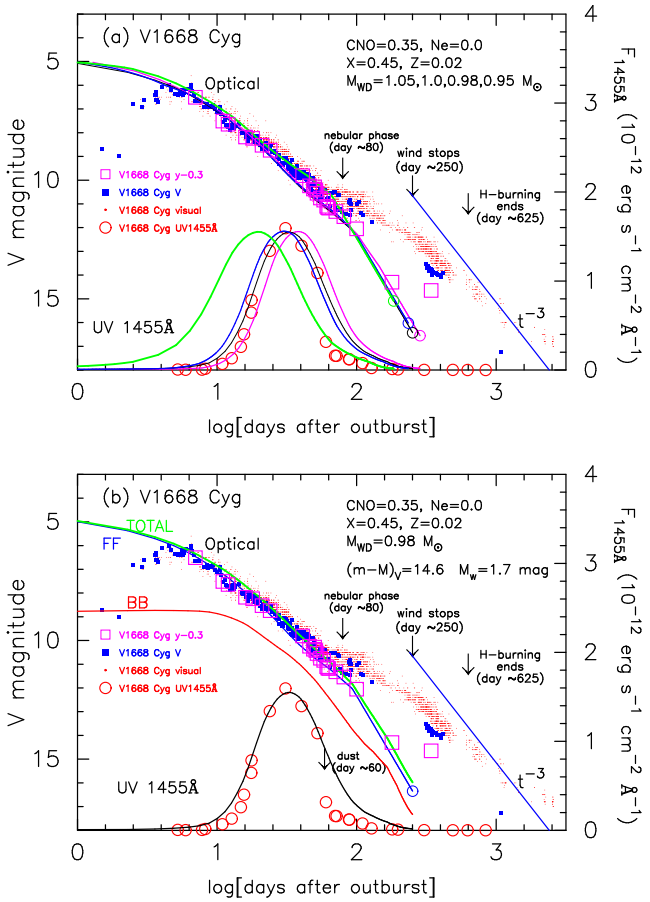

Figure 3. (a) Free-free emission and UV 1455 Å model light curves of 0.95 $M_\odot$ (magenta solid lines), 0.98 $M_\odot$ (black thin solid lines), 1.0 $M_\odot$ (blue solid lines), and 1.05 $M_\odot$ (green solid lines) WDs with CO Nova 3 as well as visual (small red dots), V (blue filled sqaures), $y-0.3$ (magenta open squares), and UV 1455 Å (red open circles) light curves of V1668 Cyg. (b) Assuming that $(m-M)_V = 14.6$, we plot three model light curves of the 0.98 $M_\odot$ WD. Here, we assume that $M_w = 1.7$ mag for the free-free emission model light curve. The green, blue, and red solid lines show the total (labeled "TOTAL"), free-free (labeled "FF"), and blackbody (labeled "BB") V fluxes. The black solid line denotes the UV 1455 Å flux. An optically thin dust shell formed ~ 60 days after the outburst (e.g., Gehrz et al. 1980). Optically thick winds and hydrogen shell-burning end approximately 250 days and 625 days after the outburst, respectively, for the 0.98 $M_\odot$ WD model. The t^{-3} law (blue solid line) indicates the trend of free-free flux for a freely expanding nebula with no mass supply. See text for the sources of the observational data.

flux. The UV 1455 Å fluxes are taken from Cassatella et al. (2002). An optically thin dust shell formed ~ 60 days after the outburst (e.g., Gehrz et al. 1980), so we observed a drop of the UV 1455Å flux after this epoch as indicated by the downward arrow in Figure 3(b) (see also Hachisu & Kato 2006).

Table 2 shows our model composition designed for various classical novae (see, e.g., Hachisu & Kato 2006). In Table 2, X is the mass fraction of hydrogen, Y the mass fraction of helium, $X_{\rm CNO}$ and $X_{\rm Ne}$ are the mass fractions of carbon–nitrogen–oxygen and neon, respectively, and $Z = 0.02$ is the mass fraction of heavy elements with the same ratio as the solar abundance. Model light curves of free-free emission and UV 1455 Å were already published in Hachisu & Kato (2006) for these sets of chemical composition. The flux of free-free emission is calculated from $F_\nu \propto \dot{M}_{\rm wind}^2/v_{\rm ph}^2 R_{\rm ph}$ (or $F_\nu = C[\dot{M}_{\rm wind}^2/v_{\rm ph}^2 R_{\rm ph}]$) in Hachisu & Kato (2006), where

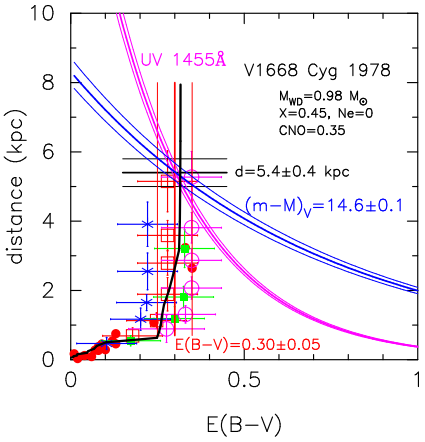

Figure 4. Distance-reddening relations toward V1668 Cyg. The blue solid lines show the distance-reddening relations calculated from Equation (1) with $(m-M)_V = 14.6 \pm 0.1$. The magenta solid lines show the distance-reddening relations calculated from Equation (2) with the UV 1455 Å flux fitting in Figure 3(b), i.e., for CO nova 3. We also plot other three distance-reddening relations toward V1668 Cyg. One is taken from Slovak & Vogt (1979) (red filled circles) and the others are relations given by Marshall et al. (2006): distance-reddening relations toward four directions close to V1668 Cyg, $(l,b) = (90.^\circ8373, -6.^\circ7598)$; that is, $(l,b) = (90.^\circ75, -6.^\circ75)$ (red open squares), $(91.^\circ00, -6.^\circ75)$ (green filled squares), $(90.^\circ75, -7.^\circ00)$ (blue asterisks), and $(91.^\circ00, -7.^\circ00)$ (magenta open circles), and given by Green et al. (2015) (black solid line).

$\dot{M}_{\rm wind}$ is the wind mass-loss rate, $v_{\rm ph}$ the photospheric velocity, and $R_{\rm ph}$ the photospheric radius of the nova envelope, and are obtained from the optically thick wind solutions of novae (Kato & Hachisu 1994). We must know the proportionality constant C to evaluate the absolute magnitude of free-free emission light curve. This was done by comparing the model light curve with a nova whose distance modulus is known (see also Appendix B). The absolute magnitudes of the free-free emission model light curves were published for "CO nova 2" and "Ne nova 2" in Hachisu & Kato (2010) and for "CO nova 4" in Hachisu & Kato (2015). For the other chemical compositions, the absolute magnitudes of the free-free emission model light curves are calibrated in the present paper (see Table 2).

For each set of chemical composition, we calculate WD mass models in coarser steps of 0.05 $M_\odot$ and then in finer steps of 0.01 $M_\odot$, and select one by eye as the best-fit WD mass model among them. The light curve flux fit in the vertical direction is usually done by the least square method with the already given best-fit WD mass model, but sometimes by eye if the least square fit is not good.

First we adopt CO nova 3 as the chemical composition of V1668 Cyg, because it is close to the observational estimate of chemical compositions (see Table 1). We plot our free-free and UV 1455 Å model light curves in Figure 3(a). The free-free emission model light curves are calculated from $F_\nu \propto \dot{M}_{\rm wind}^2/v_{\rm ph}^2 R_{\rm ph}$ (see Equation (B2) in Appendix B). Because we have not yet calibrated the absolute magnitude of free-free emission light curves for the chemical composition of CO nova 3, we vertically move the free-free emission model light curves as it lies just on the V observation. The shapes of free-free emission model light curves follow the observed V and especially y magnitudes. However, we cannot select the best-fit one only from fitting with the V or y observation because the shapes of model light curves are very similar to each other among the 0.95, 0.98, 1.0, and 1.05 $M_\odot$ WDs. So, we use the UV 1455Å flux. The UV 1455Å flux

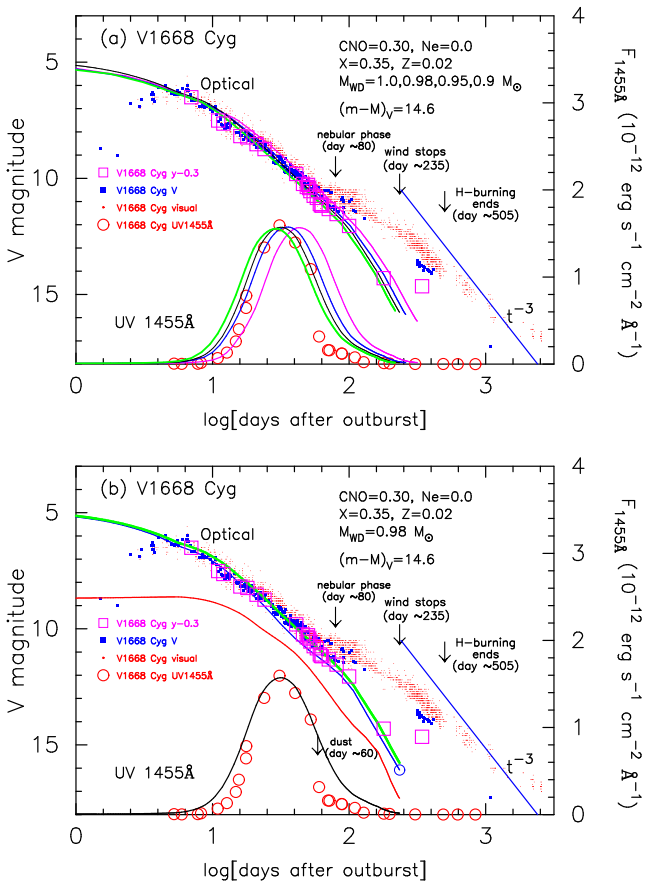

Figure 5. Similar to Figure 3, but for CO Nova 2. (a) Assuming that $(m-M)_V$ = 14.6, we plot total V and UV 1455 Å model light curves of 0.9 $M_\odot$ (magenta solid lines), 0.95 $M_\odot$ (blue solid lines), 0.98 $M_\odot$ (black thin solid lines), and 1.0 $M_\odot$ (green solid lines) WDs. (b) Assuming also that $(m-M)_V$ = 14.6, we plot three (total, free-free, blackbody) model light curves of the 0.98 $M_\odot$ WD. Optically thick winds and hydrogen shell-burning end approximately 235 days and 505 days after the outburst, respectively, for the 0.98 $M_\odot$ WD.

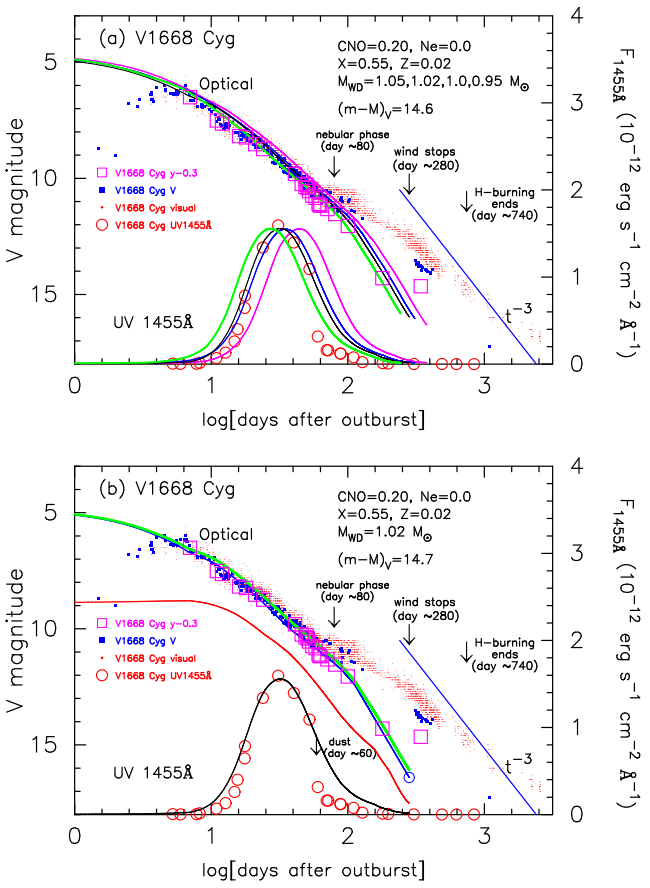

Figure 6. Same as Figure 5, but for CO Nova 4. (a) Assuming that $(m-M)_V$ = 14.6, we plot model light curves of 0.95 $M_\odot$ (magenta solid lines), 1.0 $M_\odot$ (blue solid lines), 1.02 $M_\odot$ (black thin solid lines), and 1.05 $M_\odot$ (green solid lines) WDs. (b) Assuming that $(m-M)_V$ = 14.7, we plot three model light curves of the 1.02 $M_\odot$ WD. Optically thick winds and hydrogen shell-burning end approximately 280 days and 740 days after the outburst, respectively, for the 1.02 $M_\odot$ WD.

is calculated from the blackbody emission at the pseudophotosphere (see Kato & Hachisu 1994; Hachisu & Kato 2006). Figure 3(a) shows that the 0.98 $M_\odot$ model reproduces well the UV 1455 Å light curve. The accuracy of our mass determination depends on how we select the UV 1455Å data points involved in our fitting. In Figure 3(a), we omit the UV 1455Å data later than 60 days after the outburst because the UV flux could be cut by dust. We estimated that the accuracy is as good as 0.01 $M_\odot$, that is, $M_{\rm WD} = 0.98 \pm 0.01\ M_\odot$. This means that we accept $M_{\rm WD}$ = 0.99 $M_\odot$ but do not $M_{\rm WD}$ = 1.0 $M_\odot$ from fitting in the figure. Our flux fitting of UV 1455Å in the vertical direction typically has a $\sim$ 10% accuracy because the UV 1455Å observed fluxes typically have a $\sim$ 10% error.

We must calibrate the absolute magnitude of free-free emission model light curve for CO nova 3. We estimated the distance modulus in the V band to V1668 Cyg as $\mu_V = (m-M)_V$ = 14.6 in Appendix A based on the time-stretching method. Assuming a trial value for the proportionality constant C in Equation (B4) of Appendix B.1, we obtain the absolute magnitude of the free-free model light curve (blue solid line labeled "FF") of the 0.98 $M_\odot$ WD in Figure 3(b). We also calculate the blackbody light curve model of the 0.98 $M_\odot$ WD in the V band (red solid line labeled "BB") in Figure 3(b). The total absolute flux (green solid line labeled "TOTAL") is the sum of these two fluxes. However, this total flux generally does not fit the observed data well. We assume a different value of C until it reproduces the observed V flux. Figure 3(b) shows our final flux fit.

We directly read $m_{\rm w}$ = 16.3 from Figure 3(b), where $m_{\rm w}$ is the apparent magnitude at the end of the wind phase (open circle at the end of the blue solid line labeled "FF"). Then, we obtain $M_{\rm w} = m_{\rm w} - (m-M)_V = 16.3 - 14.6 = 1.7$, where $M_{\rm w}$ is the absolute magnitude of the free-free model light curve at the end of the wind phase. Thus, we can specify the proportionality constant by $M_{\rm w}$ = 1.7 for the 0.98 $M_\odot$ WD model of V1668 Cyg. In other words, this value fixes the proportionality constant C in Equation (B4) of Appendix B.1. Then, we obtain $M_{\rm w}$ for the other WD mass models from Equation (B11). The absolute magnitudes are specified by the value of $M_{\rm w}$ and are listed in Table 3 for 0.55–1.2 $M_\odot$ WDs in steps of 0.05 $M_\odot$. Once the calibrated free-free model light curves are given by the absolute magnitude of $M_{\rm w}$ at the end point of the wind phase, we calculate the absolute magnitudes of the total V flux (free-free plus blackbody emission).

In Figure 3(b), optically thick winds and hydrogen shell burning end approximately 250 and 625 days after the outburst, respectively. The total V light curve model agrees well the V magnitude observation and the shape of UV 1455 Å light curve model fits the observation well. After the wind

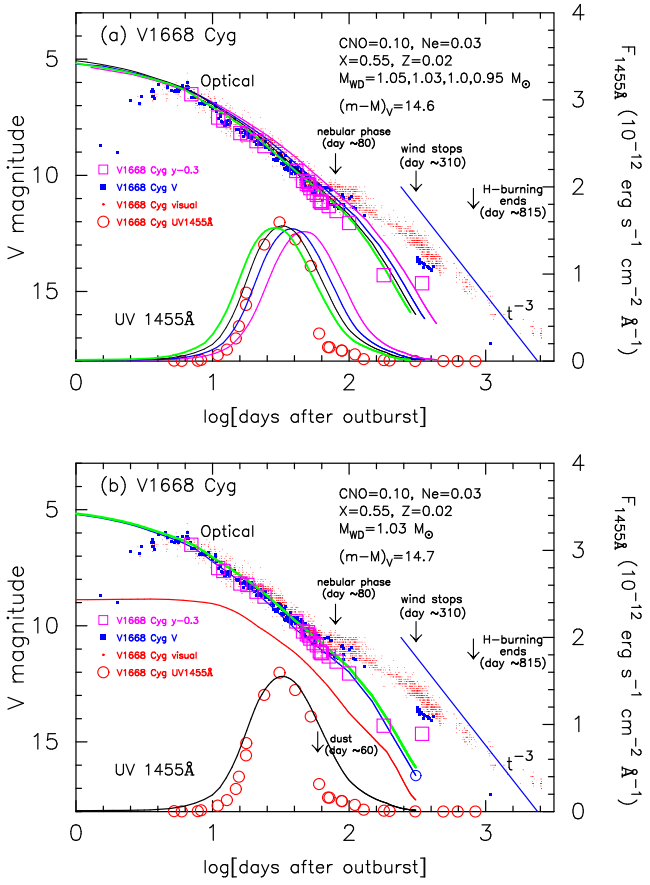

Figure 7. Same as Figure 5, but for Ne Nova 2. (a) Assuming that $(m-M)_V = 14.6$, we plot model light curves of 0.95 $M_\odot$ (magenta solid lines), 1.0 $M_\odot$ (blue solid lines), 1.03 $M_\odot$ (black thin solid lines), and 1.05 $M_\odot$ (green solid lines) WDs. (b) Assuming that $(m-M)_V = 14.7$, we plot three model light curves of the 1.03 $M_\odot$ WD. Optically thick winds and hydrogen shell-burning end approximately 310 days and 815 days after the outburst, respectively, for the 1.03 $M_\odot$ WD.

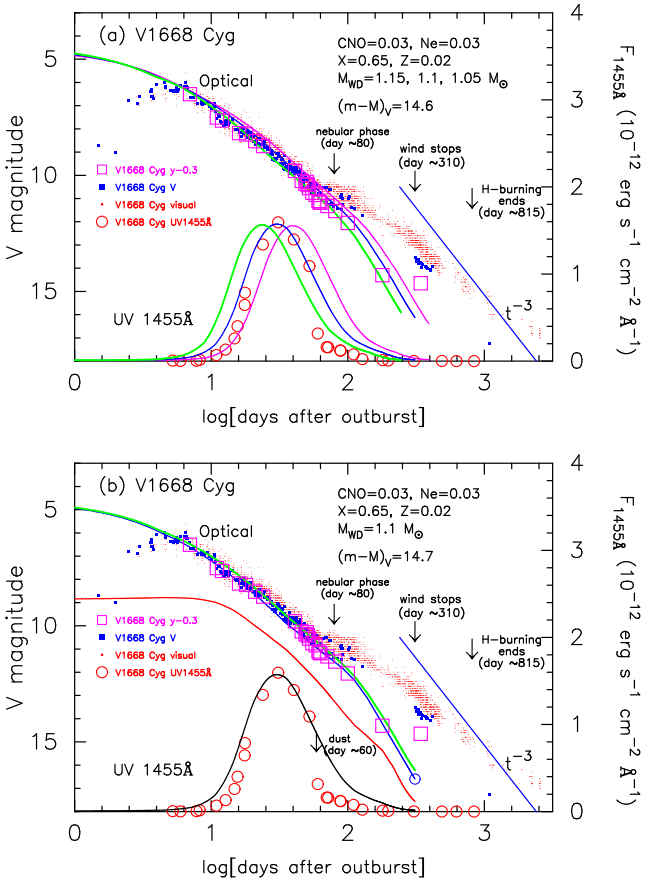

Figure 8. Same as Figure 5, but for Ne Nova 3. (a) Assuming that $(m-M)_V = 14.6$, we plot model light curves of 1.05 $M_\odot$ (magenta solid lines), 1.1 $M_\odot$ (blue solid lines), and 1.15 $M_\odot$ (green solid lines) WDs. (b) Assuming that $(m-M)_V = 14.7$, we plot three model light curves of the 1.1 $M_\odot$ WD. Optically thick winds and hydrogen shell-burning end approximately 310 days and 815 days after the outburst, respectively, for the 1.1 $M_\odot$ WD.

stops, the ejecta mass $M_{\rm ej}$ is constant in time because of no mass supply from the WD. We estimate the free-free flux by assuming that the ejecta expand homologously. Then the free-free emission light curve changes its decline shape as expressed by Equation (B3), i.e., $\propto t^{-3}$. We also plot this trend by the black solid line labeled "t^{-3}" in Figure 3.

We should note that the strong emission lines such as [O III] significantly contribute to the V and visual magnitudes in the nebular phase. V1668 Cyg entered the nebular phase at $m_V \approx$ 10.4, about 80 days after the outburst (e.g., Klare et al. 1980). Our model light curves (free-free plus blackbody) begins to deviate from the observed V and visual magnitude as shown in Figure 3 (see also Figure 11 of Hachisu & Kato 2006, for a schematic illustration). The intermediate y band (magenta open squares), which is designed to avoid such strong emission lines, reasonably follows our model light curve which represents the continuum spectrum.

2.2. *Distance and reddening toward V1668 Cyg*

We obtain two distance-reddening relations toward V1668 Cyg from the two model light curve fittings (V and UV 1455 Å) of CO nova 3, which are shown in Figure 4. The distance modulus in the V band, $\mu_V = (m-M)_V$, is obtained using the time-stretching method (Hachisu & Kato 2010) for nova light curves, which yielded a value of

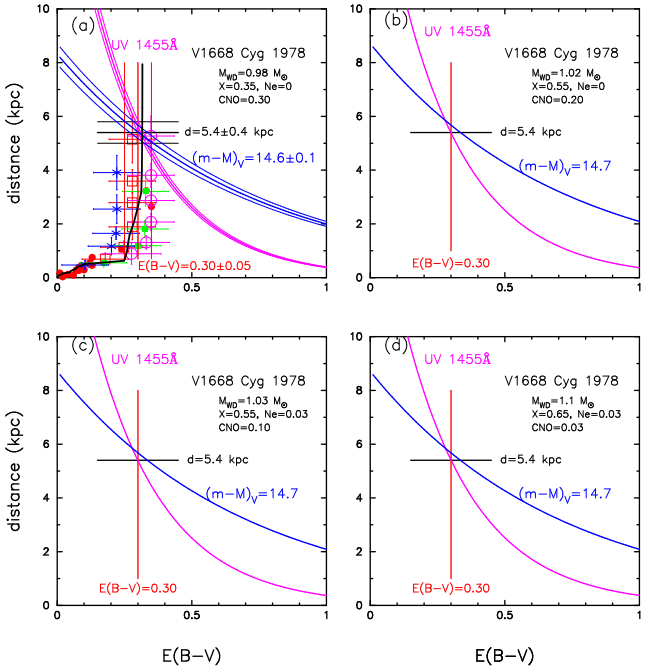

Figure 9. Same as Figure 4, but for (a) CO nova 2 in Figure 5, (b) CO nova 4 in Figure 6, (c) Ne nova 2 in Figure 7, and (d) Ne nova 3 in Figure 8. Symbols and lines are the same as those in Figure 4.

$(m-M)_{V,\mathrm{V1668\ Cyg}} = 14.6 \pm 0.1$ (see Appendix A). Adopting $(m-M)_V = 14.6 \pm 0.1$ for V1668 Cyg, we obtain a distance-reddening relation of

$$(m-M)_V = 5\log\left(\frac{d}{10\ \mathrm{pc}}\right) + 3.1E(B-V), \quad (1)$$

and plot this in Figure 4 by a thick blue line flanked by thin blue lines.

The UV 1455 Å light curve fitting gives another distance-reddening relation of

$$2.5\log F_{1455}^{\mathrm{mod}} - 2.5\log F_{1455}^{\mathrm{obs}} = 5\log\left(\frac{d}{10\ \mathrm{kpc}}\right) + 8.3\times E(B-V). \quad (2)$$

The magenta solid lines show Equation (2) with $F_{1455}^{\mathrm{mod}} = 11.8\times10^{-12}$ erg cm^{-2} s^{-1} Å^{-1} as the calculated model flux of the upper bound of Figure 3(b) at the distance of 10 kpc and $F_{1455}^{\mathrm{obs}} = (4.0\pm0.3)\times10^{-12}$ erg cm^{-2} s^{-1} Å^{-1} as the observed flux corresponding to that of the upper bound in Figure 3(b). Here we assume an absorption of $A_\lambda = 8.3\times E(B-V)$ at $\lambda = 1455$ Å (Seaton 1979).

We further plot other distance-reddening relations toward V1668 Cyg in Figure 4: that given by Slovak & Vogt (1979) (large red filled circles), that given by Marshall et al. (2006), and that given by Green et al. (2015). The galactic distance-reddening relation was presented by Marshall et al. (2006) with a grid of $\Delta l = 0.^\circ25$ and $\Delta b = 0.^\circ25$ for $-100.^\circ0 \le l \le 100.^\circ0$ and $-10.^\circ0 \le b \le 10.^\circ0$, respectively. The galactic coordinates of V1668 Cyg are $(l,b) = (90.^\circ8373, -6.^\circ7598)$. Here we plot four nearby directions using data from Marshall et al. (2006): $(l,b) = (90.^\circ75, -6.^\circ75)$ (red open squares), $(91.^\circ00, -6.^\circ75)$ (green filled squares), $(90.^\circ75, -7.^\circ00)$ (blue asterisks), and $(91.^\circ00, -7.^\circ00)$ (magenta open circles). Green et al. (2015) published the data of the galactic extinction map which covers a much wider range of the galactic coordinates (over three quarters of the sky) with much more finer grids of $3.'4$ to $13.'7$ and a maximum distance resolution of 25%. We added Green et al.'s distance-reddening line (best fitted one of their examples) by the black thick solid line in Figure 4.

All these trends/lines cross at $d \sim 5.4$ kpc and $E(B-V) \sim 0.30$. Therefore, we conclude that $d \sim 5.4 \pm 0.4$ kpc and $E(B-V) \sim 0.30 \pm 0.05$ for V1668 Cyg. This is consistent with the galactic dust absorption map of $E(B-V) = 0.29 \pm 0.02$ in the direction toward V1668 Cyg at the NASA/IPAC Infrared Science Archive[1], which is calculated on the basis of data from Schlafly & Finkbeiner (2011). Hachisu & Kato (2014) proposed a new method of determining the reddening of classical novae. They identified a general course of dereddened UBV color-color evolution and determined the reddening for a number of novae by comparing the observed track of a target nova with the general course (see Section 8.2 below). Their value is $E(B-V) \sim 0.35 \pm 0.05$ for V1668 Cyg, being also consistent with our new value of $E(B-V) \sim 0.30 \pm 0.05$.

2.3. *Light curve fitting for other various chemical compositions*

For the other chemical compositions, we plot the V and UV 1455 Å model light curves as shown in Figures 5 – 8. Here we include two sets of chemical composition of neon novae to see the dependence of neon abundance. Our theoretical light curves are insensitive to the neon content. The wind acceleration occurs mainly near the iron-peak of OPAL opacity ($\log T(\mathrm{K}) \sim 5.2$), which hardly changes if we replace neon by oxygen. On the other hand, nuclear burning is dominated by the CNO cycle, which depends on the hydrogen mass fraction X and the CNO mass fraction X_{CNO}, but not on the neon mass fraction X_{Ne}. Thus, the nova model light curves depends not only on the WD mass but also slightly on the chemical composition of X and X_{CNO}. We must know the chemical composition of hydrogen-rich envelope to accurately determine the WD mass.

Using the absolute magnitude of model light curves in Figures 5 – 8, we calculated the distance modulus in the V band, $\mu_V = (m-M)_V$, for each best-fit model. We first determine the WD mass from the UV 1455Å light curve fitting as shown in Figures 5(a) – 8(a) and, for this WD mass model, we calculate the absolute V magnitude of the total V flux (free-free plus blackbody) from the absolute magnitude of M_{w} in tables of Hachisu & Kato (2010), Hachisu & Kato (2015), and the present paper as shown in Figures 5(b) – 8(b). Then, we obtain the distance modulus in the V band, $(m-M)_V$, by fitting our total V model light curve with the observed V magnitudes. Thus, we chose the $M_{\mathrm{WD}} = 0.98\ M_\odot$ and $(m-M)_V = 14.6$ for CO nova 2 in Figure 5(b), $M_{\mathrm{WD}} = 1.02\ M_\odot$ and $(m-M)_V = 14.7$ for CO nova 4 in Figure 6(b), $M_{\mathrm{WD}} = 1.03\ M_\odot$ and $(m-M)_V = 14.7$ for Ne nova 2 in Figure 7(b), and $M_{\mathrm{WD}} = 1.1\ M_\odot$ and $(m-M)_V = 14.7$ for Ne nova 3 in Figure 8(b). Optically thick winds and hydrogen shell burning end approximately 235 and 505 days after the outburst, respectively, for the 0.98 $M_\odot$ WD with CO nova 2, 280 days and 740 days, respectively, for the 1.02 $M_\odot$ WD with CO nova 4, 310 days and 815 days, respectively, for the 1.03 $M_\odot$ WD with Ne nova 2, and 310 days 815 days, respectively, for the 1.1 $M_\odot$ WD with Ne nova 3.

Note that we obtain the best fit at $(m-M)_V = 14.7$ for the 1.02 $M_\odot$ WD with CO nova 4, and for the 1.03 $M_\odot$ WD with Ne nova 2, and for the 1.1 $M_\odot$ WD with Ne nova 3, which is slightly brighter than at $(m-M)_V = 14.6$ of CO nova 2. All the total V light curve models agree well with the V observation and all the shapes of UV 1455 Å light curve models fit the observation well. The photospheric emission contributes slightly to the total V light curve and it is ~ 0.2 – 0.4 mag at most.

For these chemical compositions, we also obtained two distance-reddening relations from the model light curve fittings of V and UV 1455 Å, which are shown in Figure 9. Figure 9(a) is for the two distance-reddening relations for CO nova 2. The blue solid lines show the distance-reddening relation of Equation (1) with $(m-M)_V = 14.6 \pm 0.1$. The magenta solid lines show the distance-reddening relation of Equation (2) with $F_{1455}^{\mathrm{mod}} = 11.3\times10^{-12}$ erg cm^{-2} s^{-1} Å^{-1} and $F_{1455}^{\mathrm{obs}} = (4.0\pm0.3)\times10^{-12}$ erg cm^{-2} s^{-1} Å^{-1}. These trends/lines cross approximately at $d \sim 5.4$ kpc and $E(B-V) \sim 0.30$, which are consistent with the conclusion that $d \sim 5.4 \pm 0.4$ kpc and $E(B-V) \sim 0.30 \pm 0.05$ obtained for CO nova 3 in Section 2.2.

The distance-reddening relations for CO nova 4, Ne nova 2, and Ne nova 3 are plotted in Figures 9(b), 9(c), and 9(d). All the cross points of the two lines deviate slightly from $d = 5.4$ kpc and $E(B-V) = 0.30$, but within $d = 5.4 \pm 0.4$ kpc and $E(B-V) = 0.30 \pm 0.05$.

To summarize, our model light curve fittings give a rea-

[1] http://irsa.ipac.caltech.edu/applications/DUST/

sonable set of solutions for the distance and reddening toward V1668 Cyg even if the chemical composition is not so accurately constrained. Therefore, we safely conclude that $(m-M)_V = 14.6 \pm 0.1$, $d = 5.4 \pm 0.4$ kpc, and $E(B-V) = 0.30 \pm 0.05$. If we adopt CO nova 3, then we obtain the WD mass of $M_{\rm WD} = 0.98\,M_\odot$ and the hydrogen-rich envelope mass of $M_{\rm env} = 1.38 \times 10^{-5}\,M_\odot$ at optical maximum (see Table 6). We suppose that the envelope mass at the optical maximum approximately represents the ignition mass of the nova.

2.4. *Comparison with previous results*

The timescale of a nova evolution is governed by the wind mass loss rate because the decreasing rate of the hydrogen-rich envelope mass is determined mainly by the wind mass loss rate. Kato & Hachisu (1994) calculated optically thick wind solutions as the structure of hydrogen-rich envelope of novae. Then, they applied their model to light curve analysis of novae. The WD mass of V1668 Cyg was estimated by Kato & Hachisu (1994) to be 0.9–1.0 $M_\odot$ from optical and UV light curve fittings based on their optically thick wind solutions and blackbody photospheric emission models. Their result is not so different from our result (0.98 $M_\odot$) partly because the timescale of nova evolution is the same. However, they adopted the blackbody emission flux for optical light curve, which is too faint to reproduce the optical light curves of V1668 Cyg (labeled "BB") as shown in Figure 3(b). As a result, their distance estimate is 2.87 kpc and it is too short to be compared with our new estimate of $d = 5.4$ kpc.

Hachisu & Kato (2006) proposed the free-free emission model for optical light curves and obtained the WD mass of 0.95 $M_\odot$ based mainly on the UV 1455Å light curve fitting. They could not fix the proportionality constant C in their models and did not estimate the distance modulus. Using the time-stretching method of the universal decline law, Hachisu & Kato (2010) obtained the absolute magnitude of their free-free emission model light curves and applied their light curve model to V1668 Cyg and obtained the distance modulus in the V band as $(m-M)_V = 14.25$ and the WD mass of 0.95 $M_\odot$. Including the effect of photospheric emission as well as free-free emission, we reanalyzed the optical light curve of V1668 Cyg and now fix $M_{\rm WD} = 0.98\,M_\odot$ and $(m-M)_V = 14.6$ for the chemical composition of CO nova 3.

3. QU VUL 1984#2

QU Vul was discovered by P. Collins on UT 1984 December 22.13 at about 6.8 mag (Collins et al. 1984). We plot the V and visual light curves and $B-V$ and $U-B$ color evolutions in Figure 10. The optical data are taken from IAU Circular No. 4033, Kolotilov (1988), Bergner et al. (1988), Rosino et al. (1992), and the AAVSO archive. The UV 1455 Å data are compiled from the *IUE* Newly Extracted Spectra (INES) archive data sever[2] (see Cassatella et al. 2002, for the UV 1455 Å band). It rose to $m_V \approx 5.5$ at maximum on UT December 27 (e.g., Rosino et al. 1992). Then it gradually declined, with $t_2 = 22$ days and $t_3 = 49$ days (e.g., Downes & Duerbeck 2000). The nova was identified as a fast neon nova by Gehrz et al. (1985). An orbital period of 2.68 hr was detected by Shafter et al. (1995).

3.1. *Reddening and distance*

[2] http://sdc.cab.inta-csic.es/ines/index2.html

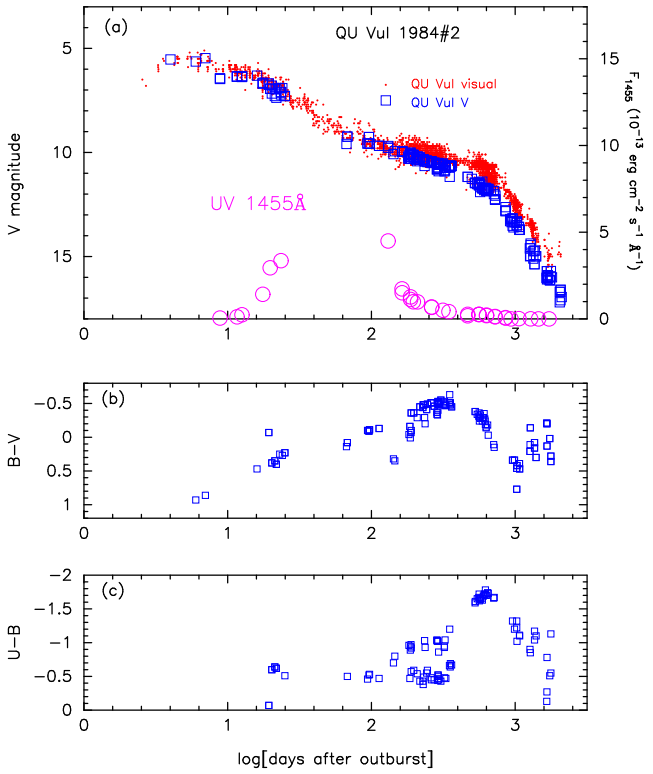

Figure 10. (a) V (blue open squares), visual (red dots), and UV 1455 Å (magenta open circles) band light curves, (b) $B-V$, and (c) $U-B$ color curves, for QU Vul. Here, we assume the start of the day ($t = 0$) as JD 2446054.0 for QU Vul. See text for the sources of the data.

The reddening toward QU Vul was estimated as $E(B-V) = A_V/3.1 \sim 1.0/3.1 = 0.3$ by Gehrz et al. (1986) from the galactic absorption, as $E(B-V) = 0.5$ by Rosino et al. (1992) from the spectral type of the nova at optical maximum, and as $E(B-V) = 0.61 \pm 0.1$ by Saizar et al. (1992) from the He II 1640/4686 Å ratio and from the 2200 Å UV spectral feature. della Valle et al. (1997) adopted $E(B-V) = A_V/3.1 \sim 1.7/3.1 = 0.55$ for dereddening the spectra. Using Saizar et al.'s $E(B-V) = 0.61$, Schwarz (2002) obtained UV fluxes that were consistent with the optical fluxes.

For the galactic extinction, the NASA/IPAC galactic dust absorption map gives $E(B-V) = 0.55 \pm 0.03$ in the direction of QU Vul, whose galactic coordinates are $(l,b) = (68.^\circ5108, -6.^\circ0263)$. Hachisu & Kato (2014) proposed a new method of determining the reddening of classical novae. They identified a general course of dereddened UBV color-color evolution and determined the reddening for a number of novae by comparing the observed track of a target nova with the general course. Their obtained value is $E(B-V) = 0.55 \pm 0.05$ for QU Vul (see Figure 31(c) of Hachisu & Kato 2014) which is shown again in Figure 11(a). These estimates strongly suggest that $E(B-V) = 0.55 \pm 0.05$. Therefore, we adopt $E(B-V) = 0.55 \pm 0.05$ in this paper.

The distance toward QU Vul was estimated as $d = 3.6$ kpc by Taylor et al. (1987) using the radio image expansion parallax method, and as $d = 2.6$ kpc by della Valle et al. (1997) using the optical shell expansion parallax method. On the basis of the shell structure observed by *Hubble Space Telescope (HST)*, Downes & Duerbeck (2000) obtained $d = 1.5$ kpc using the expansion velocity of 1500 km s^{-1} and $d = 2.0$ kpc using the velocity observed by Andreaë et al. (1991). Downes & Duerbeck (2000) summarized the value

Table 1
Chemical abundances of selected neon novae

object	H	CNO	Ne	Na-Fe	reference
Sun (solar)	0.71	0.014	0.0018	0.0034	Grevesse & Anders (1989)
V1370 Aql 1982	0.053	0.23	0.52	0.11	Snijders et al. (1987)
V1370 Aql 1982	0.044	0.28	0.56	0.017	Andreä et al. (1994)
V1370 Aql 1982	0.065	0.13	0.69	···	Arkhipova et al. (1997)
V723 Cas 1995[a]	0.52	0.064	0.052	0.042	Iijima (2006)
V693 CrA 1981	0.29	0.25	0.17	0.016	Williams et al. (1985)
V693 CrA 1981	0.16	0.36	0.26	0.030	Andreä et al. (1994)
V693 CrA 1981	0.40	0.14	0.23	···	Vanlandingham et al. (1997)
V693 CrA 1981	0.29	0.21	0.17	···	Arkhipova et al. (1997)
CP Cru 1996	0.47	0.18	0.047	0.0026	Lyke et al. (2003)
V1500 Cyg 1975	0.57	0.149	0.0099	···	Lance et al. (1988)
V1500 Cyg 1975	0.49	0.275	0.023	···	Ferland & Shields (1978)
V1668 Cyg 1978[b]	0.45	0.33	···	···	Andreä et al. (1994)
V1668 Cyg 1978[b]	0.45	0.32	0.0068	···	Stickland et al. (1981)
V1974 Cyg 1992	0.19	0.375	0.11	0.0051	Austin et al. (1996)
V1974 Cyg 1992	0.30	0.14	0.037	0.075	Hayward et al. (1996)
V1974 Cyg 1992	0.23	0.14	0.43	0.0018	Arkhipova et al. (1997)
V1974 Cyg 1992	0.55	0.12	0.06	···	Vanlandingham et al. (2005)
V838 Her 1991	0.78	0.041	0.081	0.0003	Vanlandingham et al. (1996)
V838 Her 1991	0.59	0.030	0.067	0.0003	Vanlandingham et al. (1997)
V838 Her 1991	0.56	0.038	0.070	0.015	Schwarz et al. (2007)
V351 Pup 1991	0.37	0.26	0.13	···	Saizar et al. (1996)
V977 Sco 1989	0.51	0.072	0.26	0.0027	Andreä et al. (1994)
V4160 Sgr 1991	0.465	0.125	0.065	0.011	Schwarz et al. (2007)
V382 Vel 1999	0.47	0.0018	0.0099	0.0069	Augusto & Diaz (2003)
V382 Vel 1999	0.66	0.043	0.027	0.0030	Shore et al. (2003)
QU Vul 1984 #2	0.30	0.06	0.040	0.0049	Saizar et al. (1992)
QU Vul 1984 #2	0.33	0.25	0.086	0.063	Andreä et al. (1994)
QU Vul 1984 #2	0.36	0.26	0.18	0.0014	Austin et al. (1996)
QU Vul 1984 #2	0.63	0.029	0.032	0.009	Schwarz (2002)

[a] V723 Cas was not identified as a neon nova, but the neon lines were very strong and the neon abundance obtained by Iijima (2006) is as large as those of other neon novae. See Section 8.1.
[b] V1668 Cyg was not identified as a neon nova. See Section 2.

Table 2
Chemical compositions of nova models

novae case	X	Y	$X_{\rm CNO}$	$X_{\rm Ne}$	Z[a]	mixing[b]	calibration[c]	comments
Ne nova 1	0.35	0.33	0.20	0.10	0.02	100%	V351 Pup	this work; Table 5
Ne nova 2[d]	0.55	0.30	0.10	0.03	0.02	25%	V1500 Cyg	Hachisu & Kato (2010)
Ne nova 3	0.65	0.27	0.03	0.03	0.02	8%	QU Vul	this work; Table 4
CO nova 1	0.35	0.13	0.50	0.0	0.02	100%	···	···
CO nova 2[e]	0.35	0.33	0.30	0.0	0.02	100%	GQ Mus	Hachisu & Kato (2010)
CO nova 3	0.45	0.18	0.35	0.0	0.02	55%	V1668 Cyg	this work; Table 3
CO nova 4[f]	0.55	0.23	0.20	0.0	0.02	25%	PW Vul	Hachisu & Kato (2015)
Solar	0.70	0.28	0.0	0.0	0.02	0%	···	···

[a] Carbon, nitrogen, oxygen, and neon are also included in $Z = 0.02$ with the same ratio as the solar abundance (Grevesse & Anders 1989).
[b] Mixing between the helium layer + core material and the accreted matter with solar abundances, which is calculated from $\eta_{\rm mix} = (0.7/X) - 1$.
[c] Absolute magnitudes of free-free emission model light curve are calibrated with each nova whose distance modulus is known. Adopted chemical composition of each nova in the present paper (V1668 Cyg, V351 Pup, QU Vul) or in our separate papers (V1500 Cyg, GQ Mus, PW Vul).
[d] Free-free light curves of Ne nova 2 are tabulated in Table 3 of Hachisu & Kato (2010).
[e] Free-free emission light curves of CO nova 2 are tabulated in Table 2 of Hachisu & Kato (2010).
[f] Free-free light curves of CO nova 4 are tabulated in Table 4 of Hachisu & Kato (2015).

Table 3
Free-free Light Curves of CO Novae 3[a]

$m_{\rm ff}$ (mag)	$0.55M_\odot$ (day)	$0.6M_\odot$ (day)	$0.65M_\odot$ (day)	$0.7M_\odot$ (day)	$0.75M_\odot$ (day)	$0.8M_\odot$ (day)	$0.85M_\odot$ (day)	$0.9M_\odot$ (day)	$0.95M_\odot$ (day)	$1.0M_\odot$ (day)	$1.05M_\odot$ (day)	$1.1M_\odot$ (day)	$1.15M_\odot$ (day)	$1.2M_\odot$ (day)
4.000	0.0	0.0	0.0	0.0	0.0	0.0	0.0	0.0	0.0	0.0	0.0	0.0	0.0	0.0
4.250	8.030	4.350	3.320	32.72	2.110	1.530	1.200	1.020	0.8900	0.7900	0.7020	0.6480	0.6160	0.5600
4.500	17.32	10.02	6.680	35.35	4.270	3.250	2.470	2.070	1.810	1.610	1.413	1.309	1.198	1.110
4.750	27.26	17.54	10.17	39.40	6.470	4.960	3.810	3.180	2.770	2.440	2.163	1.990	1.771	1.670
5.000	38.18	25.06	16.25	43.67	8.800	6.950	5.180	4.390	3.800	3.280	2.973	2.700	2.424	2.230
5.250	49.80	33.44	22.70	48.15	12.41	9.430	6.920	5.670	4.870	4.300	3.870	3.427	3.164	2.810
5.500	64.69	43.53	29.55	53.15	16.41	12.03	9.270	7.070	6.290	5.570	5.168	4.562	4.036	3.460
5.750	81.31	54.09	36.91	58.81	20.68	14.97	11.76	8.970	8.040	6.980	6.446	5.806	5.092	4.340
6.000	99.21	65.91	45.96	64.84	25.23	18.10	14.12	11.13	9.770	8.290	7.506	6.675	5.980	5.320
6.250	118.4	79.36	55.85	71.45	30.18	21.40	16.55	13.16	11.26	9.640	8.596	7.543	6.710	6.030
6.500	138.8	94.36	66.44	79.26	35.47	25.23	19.17	15.18	12.86	11.03	9.716	8.453	7.460	6.660
6.750	159.2	108.9	77.80	87.86	41.38	29.32	22.19	17.35	14.64	12.51	10.91	9.413	8.240	7.300
7.000	181.6	124.1	89.70	97.18	47.95	33.79	25.45	19.77	16.62	14.08	12.21	10.44	9.070	7.950
7.250	206.5	140.1	102.5	106.9	55.08	38.74	29.00	22.44	18.76	15.84	13.64	11.56	9.950	8.610
7.500	233.9	157.3	115.3	116.8	62.70	44.16	32.90	25.31	21.08	17.77	15.20	12.79	10.88	9.310
7.750	265.0	176.6	129.2	127.4	70.47	50.04	37.16	28.39	23.71	19.88	16.89	14.11	11.89	10.03
8.000	300.6	199.7	144.5	139.0	78.80	56.12	41.76	31.75	26.42	22.09	18.55	15.42	12.92	10.82
8.250	344.3	225.9	163.4	151.5	88.12	62.39	46.70	35.37	29.22	24.32	20.33	16.81	13.98	11.65
8.500	394.4	257.0	184.8	166.0	98.52	69.25	51.88	39.28	32.15	26.73	22.25	18.32	15.13	12.49
8.750	445.3	292.4	209.1	183.8	110.2	77.58	57.46	43.42	35.48	29.24	24.42	19.98	16.40	13.40
9.000	503.2	331.7	237.3	203.9	124.5	86.85	64.37	47.93	39.24	32.29	27.08	22.12	17.97	14.39
9.250	544.6	371.8	270.4	226.0	140.7	98.15	72.08	53.82	43.82	35.79	30.06	24.50	19.83	15.52
9.500	589.1	411.5	299.3	251.5	158.9	111.6	81.43	60.45	49.23	40.28	33.79	27.48	22.10	16.94
9.750	639.5	447.2	324.1	280.9	179.8	126.4	92.64	68.51	55.48	45.31	38.00	30.82	24.76	18.60
10.00	692.0	483.0	352.4	300.0	204.0	142.0	104.8	78.04	63.14	51.51	43.40	35.12	28.00	20.73
10.25	735.4	518.2	384.6	321.2	219.4	160.1	117.9	88.29	71.90	58.72	49.47	39.93	31.79	23.19
10.50	780.8	551.1	421.2	345.1	235.6	175.6	132.8	99.09	81.57	66.84	55.41	44.75	35.72	26.15
10.75	829.0	585.4	450.9	372.0	253.7	187.9	146.8	111.3	91.87	75.19	61.93	49.91	39.78	29.41
11.00	879.9	622.0	479.5	401.6	273.8	201.8	159.9	121.2	100.8	83.10	69.01	55.57	44.16	32.78
11.25	933.9	660.7	509.7	425.1	296.4	217.1	170.8	129.6	107.8	90.50	74.09	60.00	48.46	36.18
11.50	990.9	701.8	541.8	450.3	315.3	234.1	182.0	138.9	115.4	98.00	79.36	64.32	52.40	39.53
11.75	1052.	745.3	575.7	477.0	334.7	250.7	193.9	149.1	123.4	105.2	85.05	68.93	56.15	42.72
12.00	1116.	791.4	611.6	505.3	355.3	266.7	206.4	160.1	131.8	112.1	91.15	73.87	59.83	45.85
12.25	1184.	840.1	649.7	535.3	377.0	283.8	219.7	171.4	140.8	119.4	97.63	79.12	63.75	48.99
12.50	1256.	891.9	690.1	567.0	400.1	301.7	233.8	182.8	150.3	127.1	104.0	84.35	67.84	52.34
12.75	1332.	946.6	732.8	600.6	424.5	320.8	248.7	194.9	160.3	135.3	110.4	89.53	72.07	56.17
13.00	1413.	1005.	778.0	636.2	450.4	341.0	264.5	207.7	171.0	144.0	117.2	95.02	76.59	60.23
13.25	1498.	1066.	825.9	673.9	477.9	362.4	281.2	221.3	182.3	153.2	124.4	100.8	81.40	64.54
13.50	1589.	1132.	876.7	713.9	506.9	385.1	298.9	235.7	194.2	162.9	132.0	107.0	86.50	69.10
13.75	1685.	1200.	930.5	756.2	537.7	409.0	317.7	250.9	206.9	173.2	140.1	113.5	91.91	73.93
14.00	1787.	1274.	987.1	801.0	570.2	434.5	337.5	267.0	220.3	184.2	148.6	120.4	97.62	79.05
14.25	1894.	1351.	1048.	848.6	604.8	461.4	358.6	284.1	234.5	195.7	157.7	127.7	103.7	84.47
14.50	2008.	1433.	1112.	898.9	641.3	489.9	380.9	302.2	249.5	208.0	167.3	135.5	110.1	90.18
14.75	2129.	1520.	1179.	952.1	680.1	520.1	404.5	321.3	265.4	221.0	177.4	143.7	116.9	96.28
15.00	2257.	1611.	1251.	1009.	721.1	552.1	429.5	341.6	282.3	234.7	188.2	152.4	124.1	102.8
X-ray[b]	5075	3827	2942	2278	1643	1186	847	604	443	331	225	151	102	67.5
$\log f_{\rm s}$[c]	0.84	0.73	0.63	0.57	0.44	0.33	0.23	0.17	0.055	–0.03	–0.13	–0.23	–0.30	–0.42
$M_{\rm w}$[d]	5.2	4.7	4.3	3.7	3.2	2.7	2.4	2.1	1.9	1.6	1.45	1.3	1.0	0.7

[a] Chemical composition of the envelope is assumed to be that of CO nova 3 in Table 2.
[b] Duration of supersoft X-ray phase in units of days.
[c] Stretching factor against V1668 Cyg UV 1455 Å observation in Figure 53.
[d] Absolute magnitudes at the bottom point in Figure 56 by assuming $(m-M)_V$ = 14.6 (V1668 Cyg).

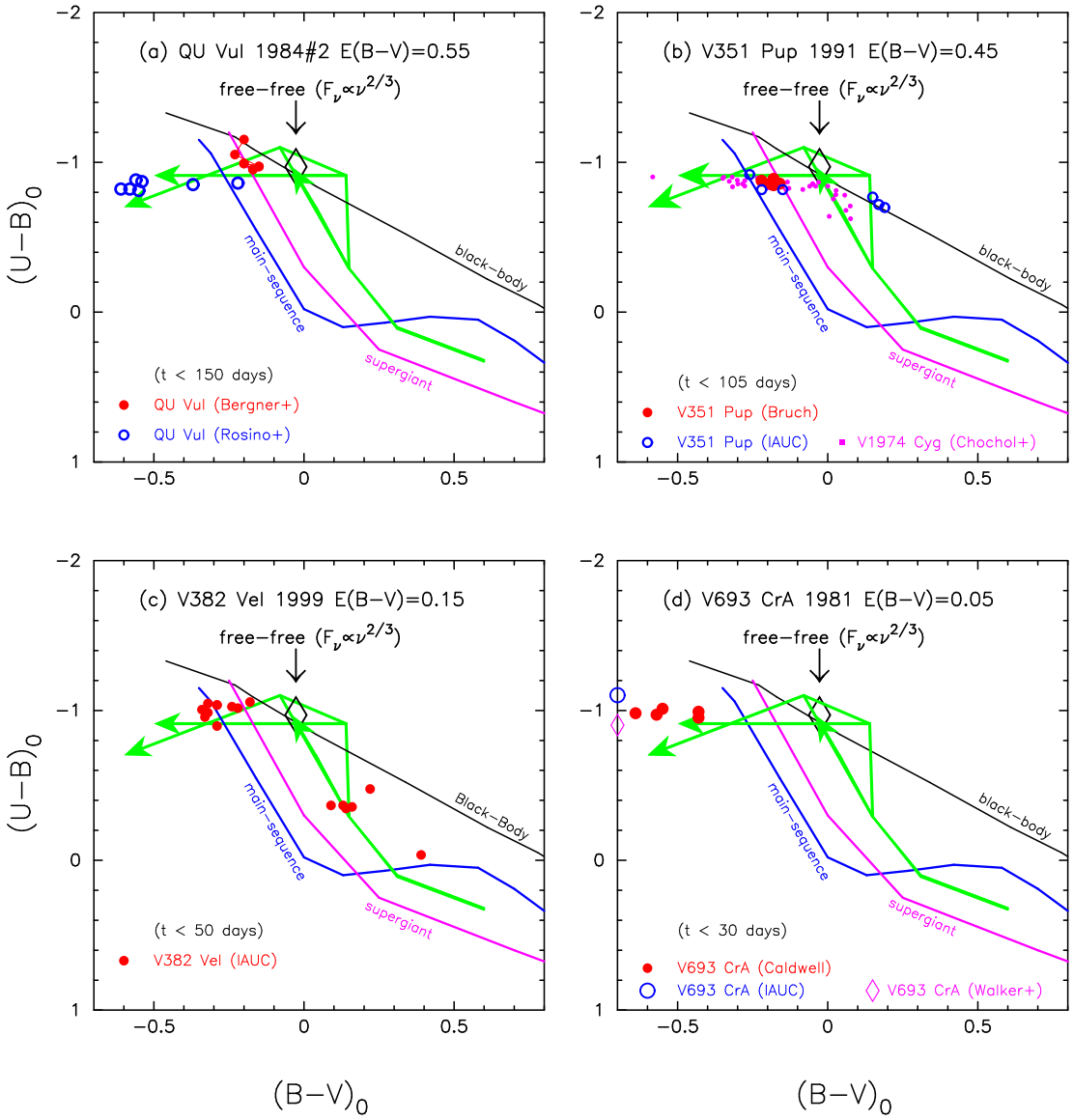

Figure 11. Color-color diagram for five neon novae in outburst as well as the general course of novae (green solid lines), blackbody (black solid line), main-sequence (blue solid line), and supergiant (magenta solid line) sequences. The data of these sequences are the same as those of Figure 28 of Hachisu & Kato (2014). (a) $(B-V)_0$ versus $(U-B)_0$ color-color diagram of QU Vul for a reddening of $E(B-V) = 0.55$. The data of QU Vul are taken from Rosino et al. (1992) and Bergner et al. (1988). (b) V351 Pup for $E(B-V) = 0.45$ as well as V1974 Cyg for $E(B-V) = 0.30$. The data of V351 Pup are taken from Bruch (1992) and IAU Circulars. The data of V1974 Cyg are taken from Chochol et al. (1993). (c) V382 Vel for $E(B-V) = 0.15$. The data of V382 Vel are taken from IAU Circulars. (d) V693 CrA for $E(B-V) = 0.05$. The data of V693 CrA are taken from Caldwell (1981), Walker & Marino (1982), and IAU Circulars.

as $d = 1.75 \pm 0.25$ kpc and concluded that this range of the distance is in reasonable agreement with estimates based on other methods ($d = 1.9 \pm 0.5$ kpc). The expansion parallax method of nova shells depends basically on the assumptions that (1) nova shells expand isotropically and (2) the expansion velocity is constant in time. Even if the shell size is the same, this method gives different distances with different expansion velocities and anisotropic velocity fields. The arithmetic mean of the above four values is 2.4 kpc.

The distance modulus in the V band, $\mu_V = (m-M)_V$, is obtained using the time-stretching method (Hachisu & Kato 2010) for nova light curves, which yielded a value of $(m-M)_{V,\mathrm{QU\ Vul}} = 13.6 \pm 0.2$ (see Appendix A). We plot various distance-reddening relations toward QU Vul in Figure 12. Adopting $(m-M)_V = 13.6 \pm 0.2$ for QU Vul, we plot the relation of Equation (1) in Figure 12 by a thick blue line flanked by thin blue lines. We also plot distance-reddening relations at four nearby directions using data from Marshall et al. (2006): (l, b) = (68.°50, −6.°00) (red open squares), (68.°75, −6.°00) (green filled squares), (68.°50, −6.°25) (blue asterisks), and (68.°75, −6.°25) (magenta open circles). We also add Green et al.'s (2015) relation (black solid line).

All the three trends, $E(B-V) = 0.55 \pm 0.05$ (vertical red solid lines), $(m-M)_V = 13.6 \pm 0.2$ (blue solid lines), and the distance-reddening relation of Marshall et al. (2006), approximately cross at $E(B-V) \sim 0.55$ and $d \sim 2.4$ kpc in Figure 12, although Green et al.'s relation deviates slightly from this cross point. This is consistent with the NASA/IPAC galactic dust absorption map of $E(B-V) = 0.55 \pm 0.03$ in the direction toward QU Vul. Thus, we adopt $E(B-V) = 0.55 \pm 0.05$ and $d = 2.4 \pm 0.3$ kpc in this paper.

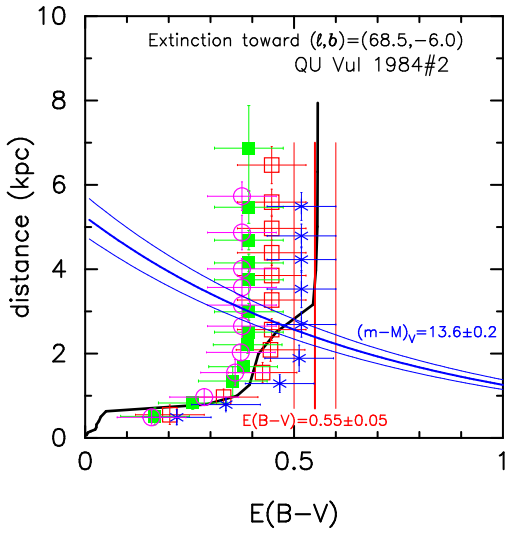

Figure 12. Various distance-reddening relations toward QU Vul, whose galactic coordinates are $(l,b) = (68.^\circ5108, -6.^\circ0263)$. Blue solid line flanking two thin solid lines: the distance-reddening relation calculated from Equation (1) with $(m-M)_V = 13.6 \pm 0.2$. Red vertical solid line flanking two thin solid lines: the reddening estimate of $E(B-V) = 0.55 \pm 0.05$. We add the galactic distance-reddening relations toward four directions close to QU Vul: $(l,b) = (68.^\circ50, -6.^\circ00)$ (red open squares), $(68.^\circ75, -6.^\circ00)$ (green filled squares), $(68.^\circ50, -6.^\circ25)$ (blue asterisks), and $(68.^\circ75, -6.^\circ25)$ (magenta open circles), the data for which are taken from Marshall et al. (2006). We further add Green et al.'s (2015) relation (black solid line).

3.2. *Chemical abundance of ejecta*

The chemical abundance of the ejecta was estimated by several groups. The estimated values are summarized in Table 1. WD core material such as carbon, oxygen, neon, and magnesium is generally mixed into hydrogen-rich envelopes before nova explosions and ejected in nova winds. If we assume that the abundance of the accreted matter is solar ($X = 0.70$, $Y = 0.28$, and $Z = 0.02$), we roughly calculate the degree of mixing as $\eta_{\rm mix} = (0.7/X) - 1$. Here, X, Y, and Z are the mass fractions of hydrogen, helium, and heavy elements, respectively, in the hydrogen-rich envelopes of novae.

Saizar et al. (1992), Andreä et al. (1994), and Austin et al. (1996) obtained chemical compositions with a relatively high degree of mixing. The average value of these three estimates is $X \sim 0.33$, i.e., $\eta_{\rm mix} \sim 1.1$ (110%). On the other hand, Schwarz (2002) presented a low degree of mixing of $X \sim 0.63$, i.e., $\eta_{\rm mix} \sim 0.11$ (11%).

First, we adopt the chemical abundance of Ne nova 2 and examine the light curves of QU Vul because we have the absolute magnitudes of optical light curves for Ne nova 2. This case corresponds to a relatively low degree of mixing, $X = 0.55$, i.e., $\eta_{\rm mix} = 0.25$ (25%), which is lower than the estimates made by the above three groups (Saizar et al. 1992; Andreä et al. 1994; Austin et al. 1996) but higher than the estimate of Schwarz (2002). Second, for comparison, assuming different degrees of mixing for CO novae, i.e., 100% of CO nova 2, and 25% of CO nova 4, we obtain model light curves and compare them with the light curves of QU Vul. Because Schwarz's estimate is close to that of Ne nova 3, i.e., a low degree of mixing, $X = 0.65$ ($\eta_{\rm mix} = 0.08$), we finally examine this case of Ne nova 3, assuming that $(m-M)_V = 13.6$.

3.3. *Light curve analysis of QU Vul*

We calculate three model light curves of free-free emission, photospheric emission (blackbody approximation), and their sum for various WD masses with various chemical compositions, and fitted the total V flux with the observed data. The blackbody emission was described in Kato & Hachisu (1994) and the free-free emission in Hachisu & Kato (2006). The UV 1455 Å band flux is also useful for determining the WD mass. The flux in the UV 1455 Å band was calculated from the blackbody emission of a pseudophotosphere based on the optically thick wind solutions of Kato & Hachisu (1994) and Hachisu & Kato (2006, 2010, 2015). Unfortunately, no *IUE* observation is available around the UV 1455 Å peak as shown in Figure 10(a). Thus, we added the UV 1455 Å light curve of PW Vul in Figure 13 (black open circles). The shapes of the UV 1455 Å and optical light curves of novae show a remarkable similarity among different timescales, if we can squeeze/stretch the light curves in the direction of time as demonstrated in Figures 1 and 2. Using this time-scaled similarity, we fit our model light curves with the UV 1455 Å data for both QU Vul and PW Vul.

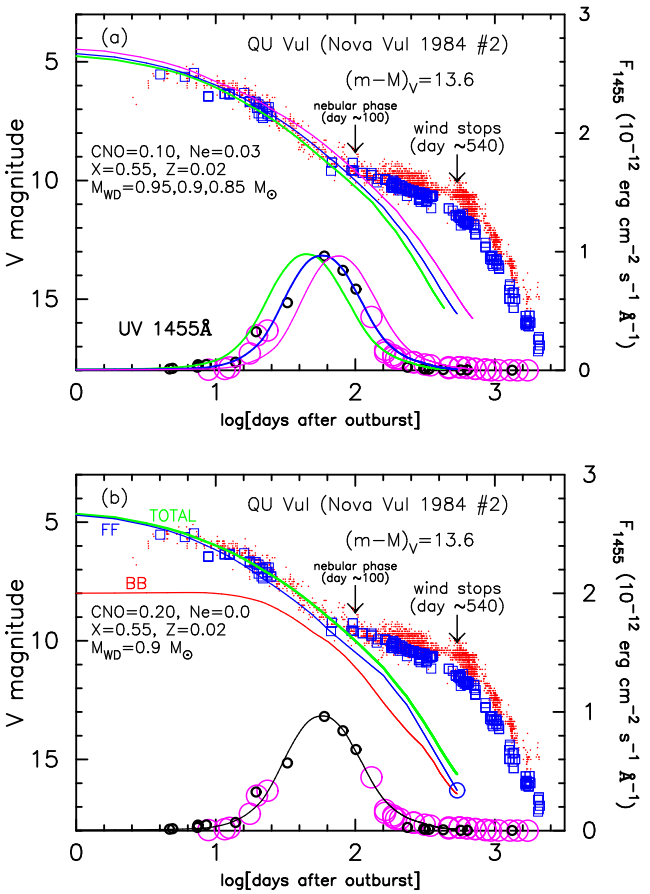

Figure 13. (a) Model light curves of 0.85 $M_\odot$ (magenta solid lines), 0.9 $M_\odot$ (blue solid lines), and 0.95 $M_\odot$ (green solid lines) WDs with the chemical composition of Ne Nova 2 for the distance modulus of $(m-M)_V = 13.6$ as well as V band (blue open squares), visual (red dots), and UV 1455 Å (large magenta open circles) light curves of QU Vul. The V, visual, and UV 1455 Å light curves of QU Vul are the same as those in Figure 10, but we added UV 1455 Å fluxes of PW Vul (small black open circles) to estimate the peak flux of QU Vul. (b) Model light curves of the 0.9 $M_\odot$ WD for the distance modulus of $(m-M)_V = 13.6$. Optically thick winds stop approximately 540 days after the outburst for the 0.9 $M_\odot$ WD. The green solid line labeled "TOTAL" shows the total V flux of free-free plus blackbody, whereas the blue (labeled "FF") and red (labeled "BB") solid lines show the V fluxes of free-free emission and blackbody emission, respectively. The black solid line shows the UV 1455 Å flux.

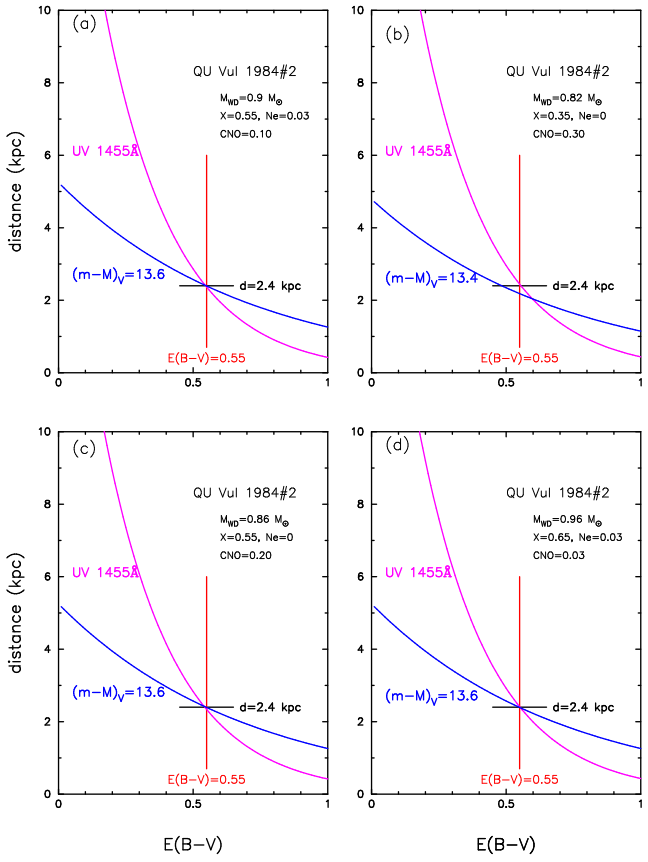

Figure 14. Distance-reddening relations toward QU Vul for the V and UV 1455 Å light curve fittings of (a) 0.9 $M_\odot$ WD with the chemical composition of Ne nova 2, (b) 0.82 $M_\odot$ WD with CO nova 2, (c) 0.86 $M_\odot$ WD with CO nova 4, and (d) 0.96 $M_\odot$ WD with Ne nova 3. The blue solid lines show the results obtained from the V model light curve fittings. The magenta solid lines show the results calculated from the UV 1455 Å flux fittings. Two other constraints are also plotted; the distance of d = 2.4 kpc and the reddening of $E(B-V)$ = 0.55, which are estimated in Section 3.1.

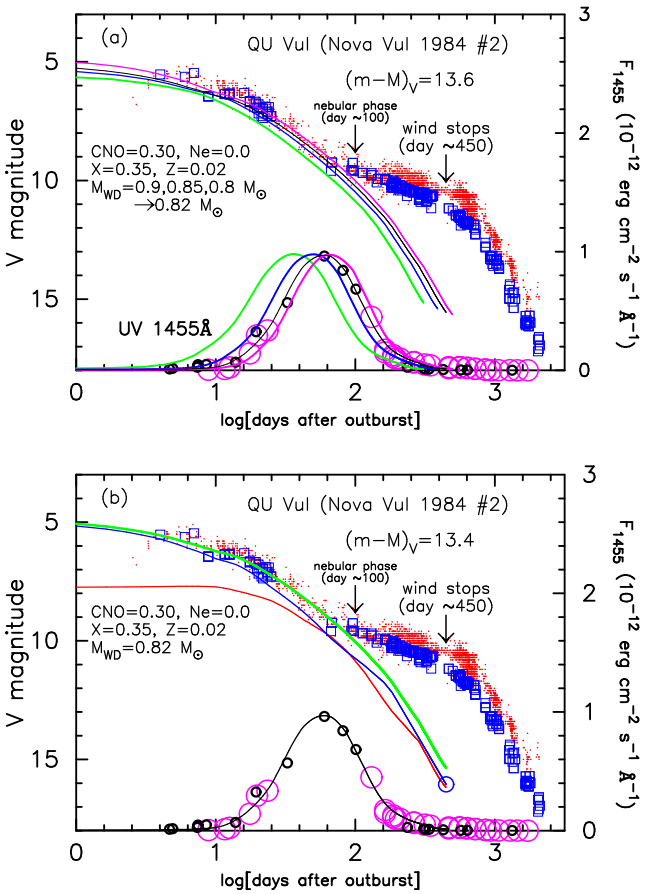

Figure 15. Same as Figure 13, but for CO nova 2. (a) Model light curves of 0.8 $M_\odot$ (magenta solid lines), 0.82 $M_\odot$ (black thin solid lines), 0.85 $M_\odot$ (blue solid lines), and 0.9 $M_\odot$ (green solid lines) WDs with CO Nova 2 for $(m-M)_V$ = 13.6. (b) Model light curves of the 0.82 $M_\odot$ WD for $(m-M)_V$ = 13.4. Optically thick winds stop approximately 450 days after the outburst for the 0.82 $M_\odot$ WD. The green solid line shows the total V flux, whereas the blue and red solid lines show the V fluxes of free-free emission and blackbody emission, respectively. The black solid line shows the UV 1455 Å flux.

3.3.1. *Ne nova 2*

First, we consider a relatively low degree of mixing, 25%, i.e., Ne nova 2 in Table 2. The absolute magnitudes of the model light curves were published in Hachisu & Kato (2010). In Figure 13(a), we plot our total V and UV 1455 Å model light curves for WDs with 0.85 (magenta solid lines), 0.9 (blue solid lines), and 0.95 $M_\odot$ (green solid lines), assuming that the distance modulus in the V band is $\mu_V = (m-M)_V$ = 13.6. The model of $M_{\rm WD}$ = 0.9 $M_\odot$ agrees well with the V and UV 1455 Å observations. In Figure 13(b), we plot three model light curves of the blackbody emission (red solid line), free-free emission (blue solid line), and total flux (green solid line) for the 0.9 $M_\odot$ WD.

Figure 14(a) shows the distance-reddening relation of Equation (1) for $(m-M)_V$ = 13.6 (blue solid line labeled "$(m-M)_V$ = 13.6"). The UV 1455 Å light curve fitting gives another distance-reddening relation of Equation (2), where we adopted $F_{1455}^{\rm mod} = 11.3 \times 10^{-12}$ erg cm^{-2} s^{-1} Å^{-1} as the calculated model flux of the upper bound of Figure 13(a) at a distance of 10 kpc and $F_{1455}^{\rm obs} = 3.0 \times 10^{-12}$ erg cm^{-2} s^{-1} Å^{-1} as the observed flux corresponding to that of the upper bound in Figure 13(a). This distance-reddening relation is also plotted as a magenta solid line (labeled "UV1455 Å") in Figure 14(a). The two distance-reddening relations cross each other at $E(B-V) \approx 0.55$ and $d \approx 2.4$ kpc. These two values are consistent with our estimates in Section 3.1.

It should be noted that our model light curve fits the early V and visual light curves well but deviates from the V and visual observation in the later phase, that is, in the nebular phase. QU Vul entered the nebular phase in April 1985 at $m_V \approx 9.6$ (about 100 days after the outburst) (Rosino & Iijima 1987; Rosino et al. 1992). This deviation is due to strong emission lines such as [O III], which are not included in our model light curves (Hachisu & Kato 2006). The medium-band y is designed to avoid such strong emission lines. If y magnitude data of QU Vul were available, like in Figures 3, and 5 – 8 for V1668 Cyg, our model light curves could follow the observed y light curve even in the nebular phase of QU Vul.

3.3.2. *CO nova 2*

Next, we consider a relatively high degree of mixing, 100%, i.e., CO nova 2 in Table 2 for comparison. The absolute magnitudes of the model light curves for this chemical composition were already calibrated in Hachisu & Kato (2010), i.e., we know the constant C in Equation (B4). Figure 15(a) shows our model light curves for WDs with 0.8, 0.82, 0.85, and 0.9 $M_\odot$, assuming that $(m-M)_V$ = 13.6. We changed the WD mass first in coarser steps of 0.05 $M_\odot$ and then in finer

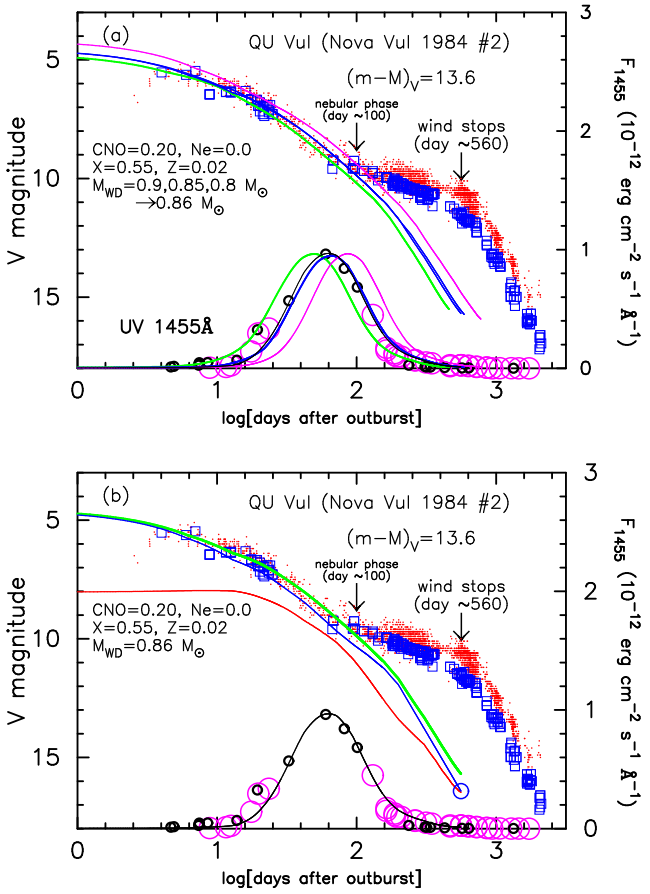

Figure 16. Same as Figure 13, but for CO nova 4. (a) We plot four model light curves of 0.8 $M_\odot$ (magenta solid lines), 0.85 $M_\odot$ (blue solid lines), 0.86 $M_\odot$ (black thin solid lines), and 0.9 $M_\odot$ (green solid lines) WDs. (b) Model light curves of the 0.86 $M_\odot$ WD for $(m-M)_V = 13.6$. Optically thick winds stop approximately 560 days after the outburst for the 0.86 $M_\odot$ WD.

steps of 0.01 $M_\odot$. In Figure 15(a), the 0.82 $M_\odot$ WD model shows reasonable agreement with the UV 1455 Å observation. However, the V model light curve (black thin solid line) is slightly darker than the V and visual observation in Figure 15(a). Therefore, we must adopt a smaller value for the distance modulus, i.e., $(m-M)_V = 13.4$, to fit the model light curve with the V and visual observation, as shown in Figure 15(b).

In Figure 15(b), we plot three model light curves of the blackbody emission, free-free emission, and total flux. The distance-reddening relation of Equation (1) is plotted by a blue solid line (labeled "$(m-M)_V = 13.4$") in Figure 14(b). We also plot the distance-reddening relation calculated from our UV 1455 Å flux fitting (magenta solid line labeled "UV 1455 Å "), i.e., Equation (2) with $F^{\rm mod}_{\lambda 1455} = 12.0 \times 10^{-12}$ erg cm^{-2} s^{-1} Å^{-1}. The two distance-reddening relations cross each other at $E(B-V) \approx 0.58$ and $d \approx 2.1$ kpc, which deviate slightly from but still consistent with the reddening of $E(B-V) = 0.55 \pm 0.05$ and distance of $d = 2.4 \pm 0.3$ kpc in Section 3.1.

3.3.3. *CO nova 4*

We further consider a relatively low degree of mixing, 25%, i.e., CO nova 4 in Table 2. The absolute magnitudes of the model light curves were already calibrated in Hachisu & Kato (2015). Figure 16(a) shows our model light curves for 0.8, 0.85, 0.86, and 0.9 $M_\odot$ WDs. In this case, we chose a best-fit model of $M_{\rm WD} = 0.86\ M_\odot$. The UV 1455 Å flux and total (free-free plus blackbody) emission of the 0.86 $M_\odot$ WD agree well with the observational data. Assuming that $(m-M)_V = 13.6$, we plot three model light curves of the blackbody emission, free-free emission, and total flux for the 0.86 $M_\odot$ WD in Figure 16(b).

The distance-reddening relation of Equation (1) is plotted by a blue solid line (labeled "$(m-M)_V = 13.6$") in Figure 14(c). We also plot the distance-reddening relation calculated from our UV 1455 Å flux fitting (magenta solid line labeled "UV 1455 Å "), i.e., Equation (2) with $F^{\rm mod}_{\lambda 1455} = 11.0 \times 10^{-12}$ erg cm^{-2} s^{-1} Å^{-1}. Note that $F^{\rm obs}_{\lambda 1455}$ is the same as $F^{\rm obs}_{1455} = 3.0 \times 10^{-12}$ erg cm^{-2} s^{-1} Å^{-1} in Section 3.3.2. The two distance-reddening relations cross each other at $E(B-V) \approx 0.55$ and $d \approx 2.4$ kpc. These two values are consistent with our estimates in Section 3.1.

3.3.4. *Ne nova 3*

Figure 17(a) shows light curve fittings of our model UV 1455 Å flux with the *IUE* data and our free-free emission flux with the optical data for 0.9, 0.95, 0.96, and 1.0 $M_\odot$ WDs. We chose the $M_{\rm WD} = 0.96\ M_\odot$ model as the best-fit model for a fine mass-grid in steps of 0.01 $M_\odot$ because our model light curve for this WD fits the UV 1455 Å observation well. The free-free model light curves are arbitrarily shifted in the vertical direction, and their absolute magnitudes are determined below.

We plot the distance-reddening relation calculated from our UV 1455 Å flux fitting (magenta solid line labeled "UV 1455 Å "), i.e., Equation (2) with $F^{\rm mod}_{\lambda 1455} = 11.7 \times 10^{-12}$ erg cm^{-2} s^{-1} Å^{-1}, as the calculated model flux for the upper bound of Figure 17(a). This distance-reddening relation crosses the vertical line of $E(B-V) = 0.55$ at a distance of $d \approx 2.4$ kpc in Figure 14(d), which is consistent with the distance estimate of $d = 2.4$ kpc in Section 3.1.

Unlike the UV 1455 Å blackbody flux, our free-free model light curves of Ne Nova 3 composition are not yet calibrated. The V light curves in Figure 17(a) are shifted up and down to fit them with the observed V because the proportionality constant C in Equation (B4) is not yet determined for Ne nova 3. We determine the absolute magnitude of each light curve from the distance modulus of QU Vul as follows.

First, we calculate the 0.96 $M_\odot$ WD model and obtain the blackbody light curve in the V band (red solid line labeled "BB"), as shown in Figure 17(b). Here, we adopt a distance modulus of $(m-M)_V = 13.6$. With a trial value of C, we obtain the absolute magnitude of the free-free model light curve (blue solid line labeled "FF"). The total flux (green solid line labeled "TOTAL") is the sum of these two fluxes. This total V magnitude light curve generally does not fit the observed V. Then, we change the proportionality constant C and calculate the light curve until the total V flux approaches the observed data. Figure 17(b) shows our final model. We obtain $m_{\rm w} = 16.7$ from Figure 17(b), where $m_{\rm w}$ is the apparent magnitude of free-free emission light curve at the end of the wind phase (open circle at the end of the blue solid line labeled "FF"). Then, we obtain $M_{\rm w} = m_{\rm w} - (m-M)_V = 16.7 - 13.6 = 3.1$, where $M_{\rm w}$ is the absolute magnitude of the free-free model light curve at the end of the wind phase. Thus, the proportionality constant can be specified as $M_{\rm w} = 3.1$ for the 0.96 $M_\odot$ WD model of QU Vul.

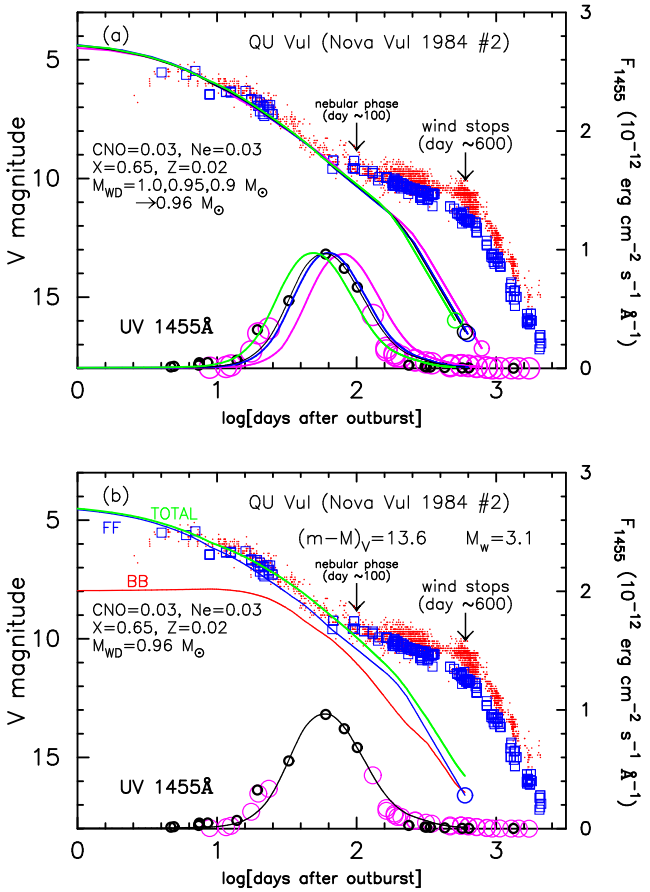

Figure 17. Similar to Figure 13, but for Ne nova 3. (a) We plot four model light curves of 0.9 $M_\odot$ (magenta solid), 0.95 (blue solid), 0.96 (black thin solid), and 1.0 (green solid line) WDs. Optical model light curves are calculated in terms of free-free emission while UV 1455 Å light curves are calculated in terms of blackbody emission. We chose the $M_{\rm WD}$ = 0.96 $M_\odot$ model as the best-fit model for a fine mass-grid in steps of 0.01 $M_\odot$ because our model light curve for this WD fits the UV 1455 Å observation well. The free-free model light curves are arbitrarily shifted in the vertical direction because the absolute magnitudes of free-free model light curves are not yet calibrated for Ne nova 3. (b) We plot three model light curves of blackbody (red solid line labeled "BB"), free-free (blue solid line labeled "FF"), and total flux (green solid line labeled "TOTAL") for the 0.96 $M_\odot$ WD. Assuming that $(m-M)_V$ = 13.6, we calibrated the absolute magnitudes of the free-free emission light curves in such a way that the total V flux fits the observed visual and V light curves well. Then, we obtained the absolute magnitude of $M_{\rm w}$ = 3.1 at the end of the free-free model light curve (open circle at the right end of the blue solid line). Winds end approximately 600 days after the outburst for the 0.96 $M_\odot$ WD.

Using Equation (B11), we obtain the absolute magnitudes of free-free light curves for the other WD masses with the chemical composition of Ne nova 3 (Appendix B). We can specify the absolute magnitude by the value of $M_{\rm w}$ and are listed in Table 4 for 0.7–1.3 $M_\odot$ WDs in steps of 0.05 $M_\odot$. Once the calibrated free-free model light curves are given by the absolute magnitude of $M_{\rm w}$ at the end point of the wind phase, we calculate the absolute magnitudes of the total V flux (free-free plus blackbody emission).

3.4. *Dependence on chemical composition*

Our light curve fittings yield different results for four different chemical compositions. For example, the chemical composition of CO nova 2 (X = 0.35) results in a WD mass of 0.82 $M_\odot$, whereas that of Ne nova 2 (X = 0.55) yields 0.9 $M_\odot$. A nova on a less massive WD generally evolves more slowly. On the other hand, a nova evolves faster at a lower hydrogen content X, even if the WD mass is the same (see Kato & Hachisu 1994; Hachisu & Kato 2001). Thus, a combination of smaller X and smaller WD mass ultimately results in a similar timescale. The distance modulus is affected by the WD mass. The wind mass-loss rate is smaller for a less massive WD (Kato & Hachisu 1994; Hachisu & Kato 2001). Thus, the lower the wind mass-loss rate the fainter the free-free emission. As a result, the fainter the total V light curve. This is the reason that $(m-M)_V$ = 13.4 for CO nova 2 (X = 0.35), i.e., slightly smaller than $(m-M)_V$ = 13.6 for the higher value of X = 0.55.

For the chemical compositions of Ne nova 2 ($X_{\rm CNO}$ = 0.10) and CO nova 4 ($X_{\rm CNO}$ = 0.20), the hydrogen content of X = 0.55 is the same, but the CNO abundance, $X_{\rm CNO}$, is different. The CNO abundance is relevant to the nuclear burning rate, and a lower value of $X_{\rm CNO}$ = 0.10 makes the evolution slower. This requires a more massive WD (0.9 $M_\odot$) than the 0.86 $M_\odot$ WD of CO nova 4, as shown in Figures 13 and 16. A more massive WD generally blows stronger winds, resulting in a brighter free-free emission and a brighter total V light curve. However, the wind mass loss rate of the 0.9 $M_\odot$ WD for Ne nova 2 is very similar to that of the 0.86 $M_\odot$ WD for CO nova 4. This is partly because the larger carbon content contributes to the opacity and accelerates the wind mass loss more strongly for CO nova 4. This is the reason that the value of $(m-M)_V$ = 13.6 is the same for CO nova 4 and Ne nova 2. Note that small enrichment of neon with unchanged hydrogen mass fraction X and CNO mass abundance $X_{\rm CNO}$ affects the nova light curves very little in our model light curves because neon is not relevant to either nuclear burning (the CNO cycle) or the opacity (e.g., Kato & Hachisu 1994; Hachisu & Kato 2006, 2010). In this sense, we cannot distinguish the neon abundance from our light curve analysis.

The consistency between the reddening and the distance could support a lower degree of mixing, $\eta_{\rm mix} \sim 0.25$, i.e., $X \sim 0.55$, rather than a higher degree of mixing, $\eta_{\rm mix} \sim 1.0$, i.e., $X \sim 0.35$, as shown in Figure 14. Schwarz (2002) presented a very low degree of mixing, $X \sim 0.63$, i.e., $\eta_{\rm mix} \sim 0.11$ (11%), as listed in Table 1. We prefer Ne nova 3 among six chemical compositions listed in Table 2.

3.5. *Summary of QU Vul*

To summarize, our model light curves fit the optical V and UV 1455 Å fluxes of QU Vul well. Our fitting results give reasonable values for the distance, d = 2.4 kpc, and the reddening, $E(B-V)$ = 0.55, but give relatively small WD masses of $M_{\rm WD}$ = 0.82 – 0.96 $M_\odot$. The distance estimate is consistent with the arithmetic mean of various estimates based on the expansion parallax method (Section 3.1). As mentioned in Section 1, natal ONe WDs with a CO mantle are more massive than $\sim$ 1.0 $M_\odot$. Such a mass range of 0.82 – 0.96 $M_\odot$ suggests that the WD in QU Vul would have lost a mass of $\sim$ 0.1 $M_\odot$ or more since its birth. Our best-fit model of Ne nova 3 gives $(m-M)_V$ = 13.6, $E(B-V)$ = 0.55, d = 2.4 kpc, $M_{\rm WD}$ = 0.96 $M_\odot$, and $M_{\rm env} = 2.44 \times 10^{-5}$ $M_\odot$ at optical maximum, where $M_{\rm env}$ is the mass of the hydrogen-rich envelope, as summarized in Table 6. The envelope mass at the optical maximum approximately represents the ignition mass of the nova.

We calculated the contribution of photospheric emission to the V magnitude of QU Vul as well as that of free-free emission. Figures 13(b), 15(b) – 17(b) show photospheric emis-

Table 4
Free-free Light Curves of Neon Novae 3[a]

$m_{\rm ff}$ (mag)	$0.7M_\odot$ (day)	$0.75M_\odot$ (day)	$0.8M_\odot$ (day)	$0.85M_\odot$ (day)	$0.9M_\odot$ (day)	$0.95M_\odot$ (day)	$1.0M_\odot$ (day)	$1.05M_\odot$ (day)	$1.1M_\odot$ (day)	$1.15M_\odot$ (day)	$1.2M_\odot$ (day)	$1.25M_\odot$ (day)	$1.3M_\odot$ (day)
3.000	0.0	0.0	0.0	0.0	0.0	0.0	0.0	0.0	0.0	0.0	0.0	0.0	0.0
3.250	3.180	2.570	2.110	1.550	1.310	1.148	0.9900	0.8280	0.7320	0.6630	0.5970	0.6520	0.5580
3.500	6.390	5.500	4.220	3.250	2.660	2.320	2.010	1.681	1.468	1.311	1.191	1.362	1.119
3.750	9.650	9.050	6.610	5.370	4.200	3.577	3.060	2.555	2.228	1.970	1.770	2.162	1.694
4.000	14.30	13.37	9.080	7.490	5.840	4.929	4.140	3.454	2.992	2.645	2.368	2.952	2.300
4.250	21.59	18.65	12.65	9.910	7.530	6.324	5.310	4.384	3.778	3.321	2.987	3.632	2.945
4.500	30.51	24.36	16.99	12.39	9.270	7.762	6.570	5.444	4.613	4.020	3.620	4.352	3.593
4.750	42.18	30.92	21.80	15.60	11.79	9.817	7.870	6.604	5.605	4.796	4.352	5.172	4.294
5.000	54.67	38.87	26.98	19.26	14.74	12.11	9.420	7.814	6.697	5.830	5.211	6.052	5.024
5.250	68.18	48.77	33.15	23.41	17.89	14.56	11.48	9.304	7.867	6.870	6.087	6.962	5.724
5.500	84.88	59.67	40.32	28.13	21.25	17.28	13.66	10.97	9.115	7.900	6.959	7.932	6.414
5.750	103.1	72.33	48.06	34.01	24.84	20.16	15.97	12.76	10.46	8.950	7.869	8.972	7.134
6.000	123.1	86.68	57.12	40.51	29.61	23.44	18.44	14.69	11.93	10.08	8.839	10.06	7.904
6.250	145.1	102.9	68.08	47.65	34.80	27.42	21.19	16.79	13.56	11.34	9.879	11.22	8.714
6.500	168.5	118.8	79.98	55.82	40.47	31.77	24.37	19.20	15.36	12.75	10.97	12.45	9.574
6.750	191.1	135.9	92.60	64.87	46.71	36.59	27.85	21.89	17.33	14.32	12.13	13.75	10.48
7.000	215.8	153.7	104.6	74.78	53.65	41.87	31.74	24.83	19.53	16.06	13.41	15.13	11.44
7.250	244.3	172.6	117.7	84.16	61.27	47.74	36.08	27.89	21.89	17.88	14.85	16.58	12.47
7.500	278.3	193.4	132.9	94.16	68.74	54.06	40.84	31.26	24.43	19.72	16.41	18.13	13.55
7.750	316.5	219.9	149.8	106.0	76.73	60.26	45.88	34.93	27.22	21.72	18.00	19.76	14.70
8.000	357.2	250.4	168.8	119.5	86.38	67.04	51.14	38.94	30.24	23.93	19.68	21.50	15.92
8.250	403.0	282.8	190.6	134.6	97.58	75.70	56.87	43.30	33.51	26.51	21.60	23.33	17.20
8.500	455.4	316.2	215.3	152.5	110.3	85.49	64.26	48.49	37.35	29.42	23.97	25.28	18.57
8.750	509.7	354.5	240.9	172.6	124.8	96.65	72.72	54.93	42.13	33.06	26.68	27.34	20.01
9.000	566.7	395.7	269.6	193.9	141.2	109.3	82.25	62.15	47.45	37.32	29.95	29.52	21.54
9.250	622.9	430.3	302.3	217.4	158.7	123.4	92.97	70.31	53.63	42.09	33.61	31.83	23.16
9.500	679.8	470.0	336.8	244.1	178.4	139.3	105.0	79.44	60.58	47.43	37.94	34.28	24.88
9.750	744.4	515.2	375.2	267.3	200.7	157.3	118.3	89.79	68.43	53.39	42.75	36.87	26.70
10.00	792.7	566.5	405.6	289.7	221.9	175.7	133.3	101.5	77.44	60.53	48.17	39.62	28.63
10.25	841.1	612.5	436.4	315.1	244.8	189.9	149.3	114.6	87.50	68.51	54.30	42.53	30.67
10.50	892.3	649.5	470.8	343.6	263.0	205.6	164.1	126.2	97.41	76.51	61.02	45.61	32.83
10.75	946.6	688.7	499.8	375.4	281.7	223.1	179.3	138.8	107.1	82.96	67.43	48.88	35.12
11.00	1004.	730.3	530.5	399.3	302.4	242.5	191.9	149.1	116.4	89.97	73.00	52.33	37.55
11.25	1065.	774.3	563.1	423.9	321.3	261.6	205.7	159.8	124.8	97.52	78.94	56.00	40.11
11.50	1130.	820.9	597.6	449.9	341.3	277.2	220.0	171.4	133.9	105.7	85.33	59.88	42.84
11.75	1198.	870.2	634.2	477.6	362.5	293.7	233.8	182.0	142.9	114.0	91.96	63.99	45.72
12.00	1270.	922.5	672.9	506.8	384.9	311.3	248.4	193.3	151.9	121.0	97.97	68.35	48.77
12.25	1347.	977.9	714.0	537.8	408.7	329.8	263.9	205.2	161.7	128.5	104.0	72.96	52.01
12.50	1428.	1037.	757.4	570.6	433.9	349.5	280.3	217.7	172.3	136.4	110.4	77.85	55.43
12.75	1514.	1099.	803.5	605.4	460.6	370.3	297.7	231.1	183.5	144.8	117.1	83.02	59.07
13.00	1606.	1165.	852.2	642.2	488.8	392.4	316.1	245.2	194.4	153.7	124.3	88.50	62.91
13.25	1702.	1234.	903.8	681.2	518.7	415.7	335.6	260.2	206.0	163.1	131.8	94.30	66.98
13.50	1804.	1308.	958.6	722.5	550.4	440.5	356.3	276.0	218.3	173.1	139.9	100.5	71.29
13.75	1913.	1387.	1017.	766.3	584.0	466.7	378.1	292.8	231.2	183.6	148.3	107.0	75.87
14.00	2027.	1469.	1078.	812.7	619.6	494.4	401.3	310.6	245.0	194.8	157.3	113.9	80.71
14.25	2149.	1557.	1143.	861.8	657.2	523.8	425.8	329.5	259.6	206.7	166.9	121.2	85.83
14.50	2278.	1650.	1212.	913.8	697.2	555.0	451.8	349.4	275.0	219.2	176.9	128.9	91.26
14.75	2414.	1749.	1285.	968.9	739.4	588.0	479.4	370.6	291.4	232.5	187.6	137.1	96.98
15.00	2559.	1853.	1362.	1027.	784.2	623.0	508.5	393.0	308.7	246.6	199.0	145.8	103.1
X-ray[b]	7229	5205	3791	2715	1958	1468	1090	749	511	346	233	136	71.5
$\log f_{\rm s}$[c]	0.55	0.44	0.33	0.22	0.12	0.02	–0.06	–0.18	–0.28	–0.40	–0.49	–0.62	–0.78
$M_{\rm w}$[d]	5.5	4.9	4.4	3.9	3.5	3.1	2.7	2.3	1.9	1.6	1.3	1.0	0.7

[a] Chemical composition of the envelope is assumed to be that of Ne nova 3 in Table 2.
[b] Duration of supersoft X-ray phase in units of days.
[c] Stretching factor against QU Vul UV 1455 Å observation in Figure 54.
[d] Absolute magnitudes at the bottom point in Figure 57 by assuming $(m-M)_V = 13.6$ (QU Vul).

sion light curves, which are calculated on the basis of the blackbody emission at the pseudophotosphere. The blackbody emission flux is always smaller than the free-free emission flux, but it contributes to the total brightness by 0.4 – 0.8 mag at most. The overall features and shape of the total V light curves are essentially the same as those of the free-free light curve.

3.6. *Comparison with previous results*

Wanajo et al. (1999) presented yields of nuclear burning on the ONe core and estimated the WD mass from fitting their results with the abundance pattern observed by Saizar et al. (1992). They suggested the WD mass of 1.05–1.1 $M_\odot$. Downen et al. (2013) also estimated the WD mass of QU Vul by comparing their theoretical yields of nuclear burning (abundance ratio) with the observed ones. They obtained $M_{\rm WD} < 1.2\ M_\odot$ for QU Vel. Downen et al.'s value is consistent with our new estimate of $0.96\ M_\odot$ for the chemical composition of Ne nova 3, but Wanajo et al.'s value is ~ 0.1–$0.2\ M_\odot$ more massive than ours. It should be noted that, however, Wanajo et al.'s model is based on a one-zone model of a hydrogen-rich envelope and this is too simplified to correctly predict the abundance ratio.

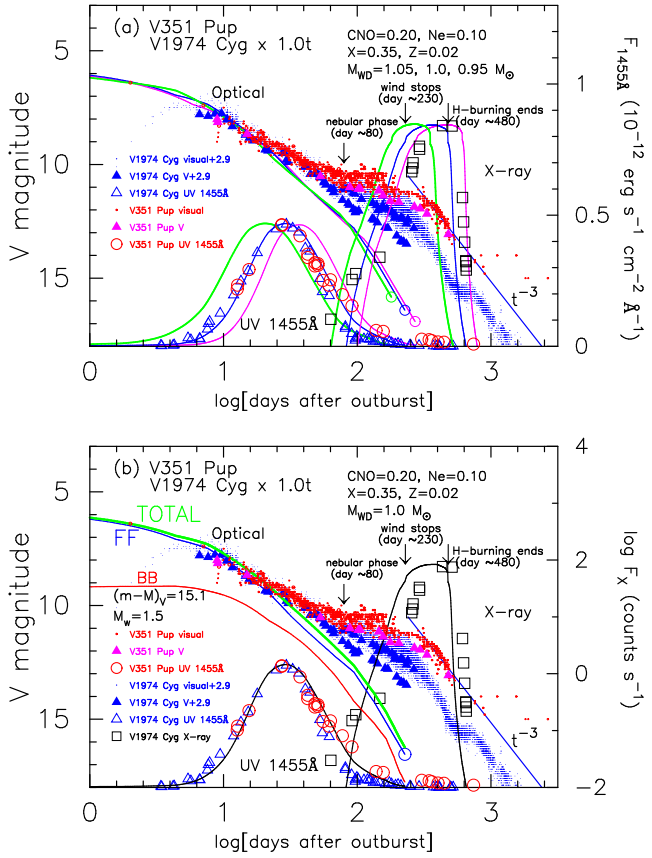

Figure 18. Same as Figure 17, but for V351 Pup. (a) Model light curves of 0.95 $M_\odot$ (magenta solid lines), 1.0 $M_\odot$ (blue solid lines), and 1.05 $M_\odot$ (green solid lines) WDs with the chemical composition of Ne Nova 1 as well as visual (small red open circles), V (magenta filled triangles), and UV 1455 Å (large red open circles) light curves of V351 Pup. We also added V (small blue dots) and UV 1455 Å (large open blue triangles), and X-ray (large black open squares) light curves of V1974 Cyg, because the timescale of V1974 Cyg is almost the same as that of V351 Pup. Optical model light curves are calculated in terms of free-free emission while UV 1455 Å and X-ray light curves are calculated in terms of blackbody emission. We chose the 1.0 $M_\odot$ WD as the best-fit model because the UV 1455 Å model light curve fits the observation very well. The free-free model light curves are arbitrarily shifted in the vertical direction because the absolute magnitudes of free-free model light curves are not yet calibrated for Ne nova 1. (b) Assuming that $(m-M)_V$ = 15.1 and M_w = 1.5 mag for the 1.0 $M_\odot$ free-free emission model light curve, we plot three model light curves of the blackbody (red solid line), free-free (blue solid), and total flux (green solid) of free-free plus blackbody. The UV 1455 Å and X-ray model light curves (black solid lines) are also added.

4. V351 PUP 1991

V351 Pup was discovered on UT 1991 December 27 by P. Camilleri near maximum (Camilleri et al. 1992). It reached m_v = 6.4 at optical maximum (e.g., Downes & Duerbeck 2000). The light curves of V351 Pup are shown in Figure 18 together with those of V1974 Cyg. Optical data are poor, and no V magnitude data were reported around the maximum. Its decline rates were estimated to be t_2 = 10 and t_3 = 26 days by Downes & Duerbeck (2000), so V351 Pup belongs to the fast nova class. Saizar et al. (1996) reported that V351 Pup shows a pattern of enhanced abundances (see Table 1) consistent with an ONe WD whose mass is close to the Chandrasekhar limit. An orbital period of $P_{\rm orb}$ = 2.83 hr was obtained by Woudt & Warner (2001).

4.1. *Reddening and distance*

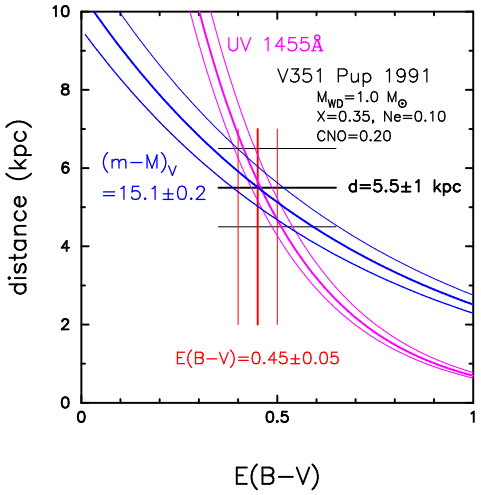

Figure 19. Various distance-reddening relations toward V351 Pup, whose galactic coordinates are (l,b) = (252.°7225, −0.°7329). The blue solid line flanking two thin solid lines shows the distance-reddening relation calculated from Equation (1) with $(m-M)_V = 15.1 \pm 0.2$. The red vertical solid line flanking two thin solid lines shows the reddening estimate of $E(B-V) = 0.45 \pm 0.05$. The black horizontal solid line flanking two thin solid lines show the distance estimate of $d = 5.5 \pm 1$ kpc. We also add another distance-reddening relation of V351 Pup for the UV 1455 Å flux fitting of a 1.0 $M_\odot$ WD with Ne nova 1, that is, the magenta solid lines calculated from Equation (2). See text for more detail.

The reddening toward V351 Pup was estimated as $E(B-V) = 0.3 \pm 0.1$ by Orio et al. (1996) from the Balmer decrement observed in 1994 March and as $E(B-V) = 0.72 \pm 0.10$ by Saizar et al. (1996) from the line ratio of He II λ4686/He II λ1640. These two values are very different, and their arithmetic mean is $E(B-V) = 0.51 \pm 0.1$. In Figure 11(b) (see also Section 8.2), we obtain $E(B-V) = 0.45 \pm 0.05$ using the UBV color-color evolution method proposed by Hachisu & Kato (2014). This value is consistent with the above arithmetic mean. Therefore, we adopt $E(B-V) = 0.45 \pm 0.05$ in this paper.

The distance toward V351 Pup was estimated from the nebular expansion parallax method by Downes & Duerbeck (2000) to be $d = 2.7 \pm 0.10$ kpc with an expansion velocity of 1200 km s^{-1} and by Orio et al. (1996) to be $d = 4.7 \pm 0.6$ kpc with an expansion velocity of 2000 km s^{-1}. A distance modulus in the V band of $(m-M)_{V,\rm V351\ Pup} = 15.1 \pm 0.2$ is obtained using the time-stretching method of nova light curves (Hachisu & Kato 2010) described in Appendix A. Figure 19 shows various distance-reddening relations toward V351 Pup. Red vertical lines denote the reddening estimate of $E(B-V) = 0.45 \pm 0.05$. Blue lines show Equation (1) with $(m-M)_V = 15.1 \pm 0.2$. The two trends cross at $E(B-V) \sim 0.45$ and $d \sim 5.5$ kpc. Our distance estimate is close to that given by Orio et al. (1996) but twice larger than that by Downes & Duerbeck (2000). In this paper, we adopt $E(B-V) = 0.45 \pm 0.05$ and $d = 5.5 \pm 1.0$ kpc. In Section 8.3, we will discuss the nova outburst track in the color-magnitude diagram and show that the track of V351 Pup almost overlaps that of a similar type of nova, V1974 Cyg, which supports the set of $E(B-V) = 0.45$ and $(m-M)_V = 15.1$ for V351 Pup.

4.2. *Light curve fitting for various chemical compositions*

Saizar et al. (1996) estimated the chemical composition of the ejecta from the *IUE* spectra, i.e., X = 0.37, Y = 0.24, $X_{\rm CNO}$ = 0.26, and $X_{\rm Ne}$ = 0.13, as listed in Table 1. This estimate is close to that of our model chemical composition of

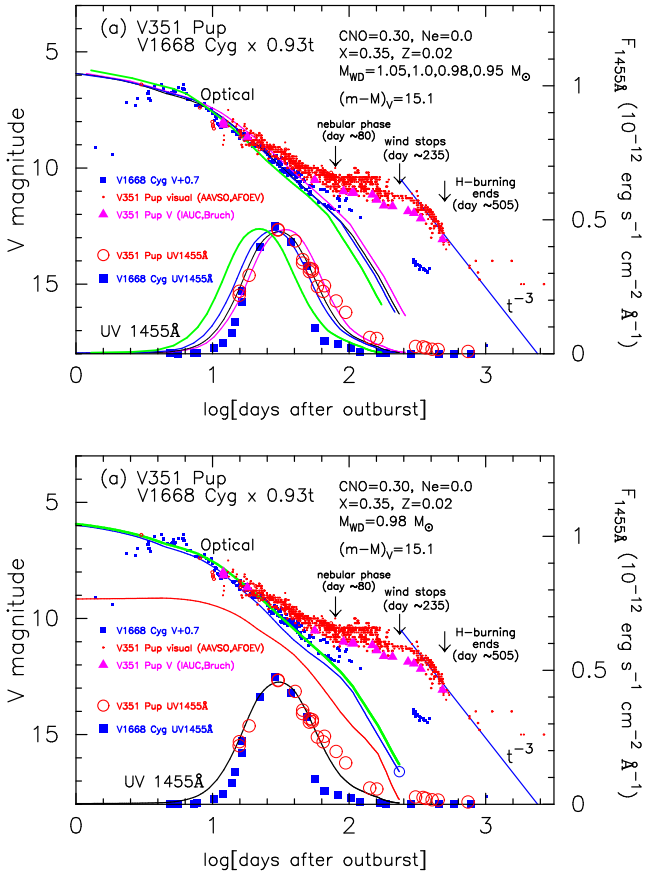

Figure 20. Same as Figure 13, but for V351 Pup and the chemical composition of CO nova 2. (a) Model light curves of 0.95 $M_\odot$ (magenta solid lines), 0.98 $M_\odot$ (black thin solid lines), 1.0 $M_\odot$ (blue solid lines), and 1.05 $M_\odot$ (green solid lines) WDs for $(m-M)_V$ = 15.1. We added V (small blue filled squares) and UV 1455 Å (large blue filled squares) light curves of V1668 Cyg. The timescale of V1668 Cyg is squeezed by a factor of 0.93. We plot the total V flux in optical. (b) Model light curves of the 0.98 $M_\odot$ WD for the same distance modulus of $(m-M)_V$ = 15.1. Optically thick winds and hydrogen shell burning end approximately 235 days and 505 days after the outburst, respectively, for the 0.98 $M_\odot$ WD.

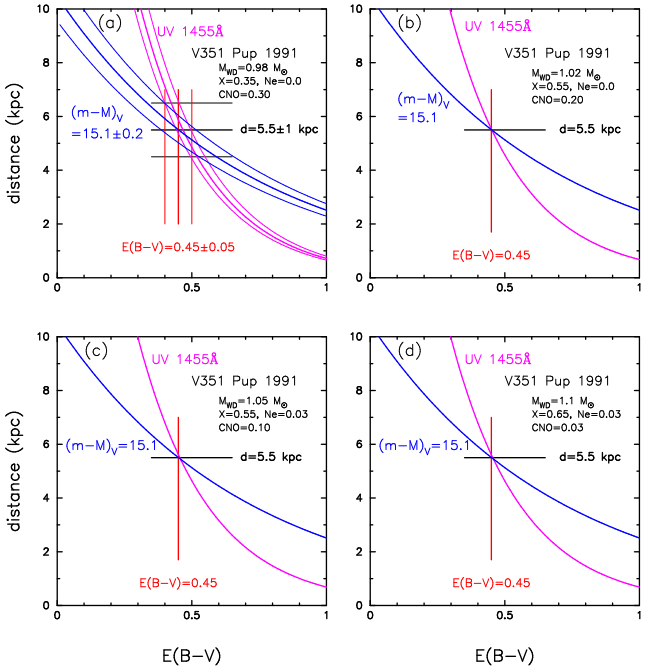

Figure 21. Same as Figure 14, but for V351 Pup. Two distance-reddening relations toward V351 Pup are calculated from the V (blue solid lines) and UV 1455 Å (magenta solid lines) light curve fittings of (a) the 0.98 $M_\odot$ WD model with CO nova 2, (b) 1.02 $M_\odot$ WD model with CO nova 4, (c) 1.05 $M_\odot$ WD model with Ne nova 2, and (d) 1.1 $M_\odot$ WD model with Ne nova 3. Two other constraints are also plotted: one is the distance estimate of d = 5.5 ± 1 kpc and the other is the reddening estimate of $E(B-V) = 0.45 \pm 0.05$.

Ne nova 1 and is also close to that of CO nova 2, except for the neon abundance of $X_{\rm Ne}$ = 0.13. We found no other estimates for V351 Pup in the literature. Therefore, we examine first the light curves of Ne nova 1 and then those of CO nova 2, CO nova 4, Ne nova 2, and Ne nova 3 in this order, in Figures 18, 20 – 24 together with the light curves of V1974 Cyg, V1668 Cyg, PW Vul, V1974 Cyg, and QU Vul, respectively, which reflects the order of the degree of mixing, because the nova chemical composition values estimated by various authors usually have a large scatter, as shown in Table 1. Note again that enrichment of neon with unchanged hydrogen and CNO mass fractions affects the nova light curves very little in our model light curves because neon is not relevant to nuclear burning (the CNO cycle) or increasing the opacity (e.g., Kato & Hachisu 1994; Hachisu & Kato 2006, 2010). Therefore, our model light curves could follow the observation well even for the chemical composition of the same X and $X_{\rm CNO}$ but different $X_{\rm Ne}$ with $Y + X_{\rm Ne}$ being the same.

4.2.1. *Ne nova 1*

Figure 18(a) shows our model UV 1455 Å flux and free-free emission flux, in addition to the visual, V, and UV 1455 Å light curves of V351 Pup. It also shows observational data for V1974 Cyg, whose WD mass is estimated to be similar to that of V351 Pup. For the V351 Pup data, the visual magnitudes are taken from the archives of AAVSO and Association Française des Observateurs d'Étoiles Variables; the V magnitudes are from IAU Circ. Nos. 5422, 5427, 5430, 5455, 5483, 5493, 5527, 5538, 5552, 5566, 5628, 5655, 5666, and 5781, and from Bruch (1992). The UV 1455 Å fluxes are compiled from the INES archive data (Cassatella et al. 2002). We chose the $M_{\rm WD}$ = 1.0 $M_\odot$ model as the best-fit model because our model light curve for the 1.0 $M_\odot$ WD fits the UV 1455 Å observation in Figure 18(a) well. Optically thick winds and hydrogen shell burning end approximately 230 days and 480 days after the outburst, respectively, for the 1.0 $M_\odot$ WD. We have no absolute magnitude calibration of the free-free model light curves for the chemical composition of Ne nova 1, so we tentatively shift the free-free model light curves up and down to fit them with the optical observation in Figure 18(a).

From our UV 1455 Å flux fitting in Figure 18(a), we obtain $F^{\rm mod}_{\lambda 1455} = 4.6 \times 10^{-12}$ erg cm^{-2} s^{-1} Å^{-1} and $F^{\rm obs}_{\lambda 1455} = (4.6 \pm 0.49) \times 10^{-13}$ erg cm^{-2} s^{-1} Å^{-1} at the UV 1455 Å flux maximum. Substituting these values into Equation (2), we plot the distance-reddening relation (magenta solid line) in Figure 19. This line crosses the blue solid line of $(m-M)_V$ = 15.1 at a reddening of $E(B-V)$ = 0.46 and a distance of $d \approx 5.4$ kpc, which is consistent with our estimates of $E(B-V) = 0.45 \pm 0.05$ and $d = 5.5 \pm 1$ kpc in Section 4.1. This may support our choice of these two values.

Our free-free emission model light curves are not yet calibrated for the chemical composition of Ne nova 1. In the same way as in Sections 2 and 3, we determine the absolute magnitude of the free-free emission model light curve for the 1.0 $M_\odot$ WD. The total V magnitudes are calculated as the sum

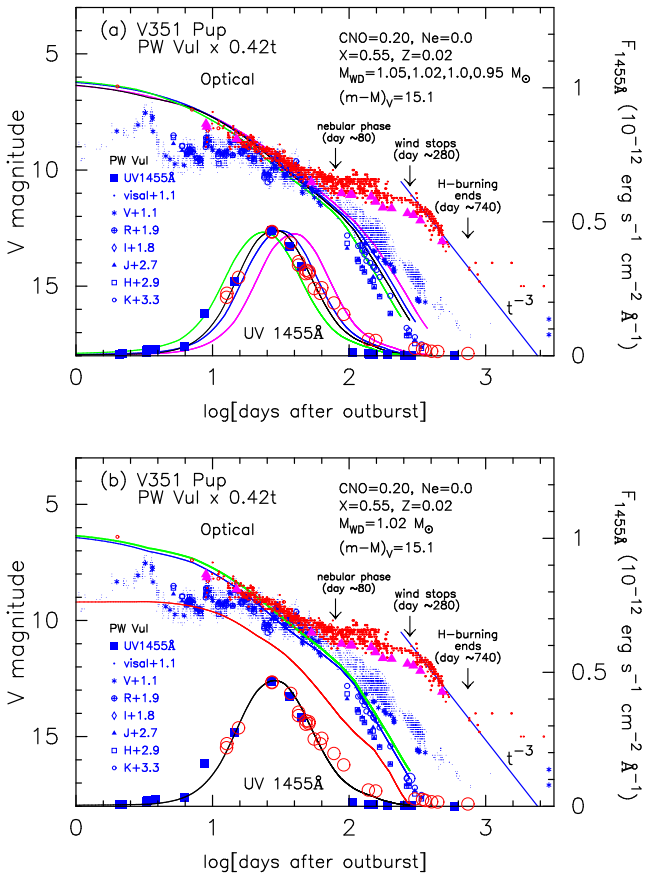

Figure 22. Same as Figure 20, but for CO nova 4. (a) Assuming that $(m-M)_V$ = 15.1, we plot four model light curves of 0.95 $M_\odot$ (magenta solid line), 1.0 $M_\odot$ (blue solid line), 1.02 $M_\odot$ (black thin solid line), and 1.05 $M_\odot$ (green solid line) WDs. We added the V (blue asterisks) and UV 1455 Å (large blue filled squares) light curves of PW Vul. The timescale of PW Vul is squeezed by a factor of 0.42. (b) Assuming again that $(m-M)_V$ = 15.1, we plot the blackbody emission (red solid line), free-free emission (blue solid line), and total emission (green thick solid line) light curves of 1.02 $M_\odot$ WD. Optically thick winds and hydrogen shell burning end approximately 280 days and 740 days after the outburst, respectively, for the 1.02 $M_\odot$ WD.

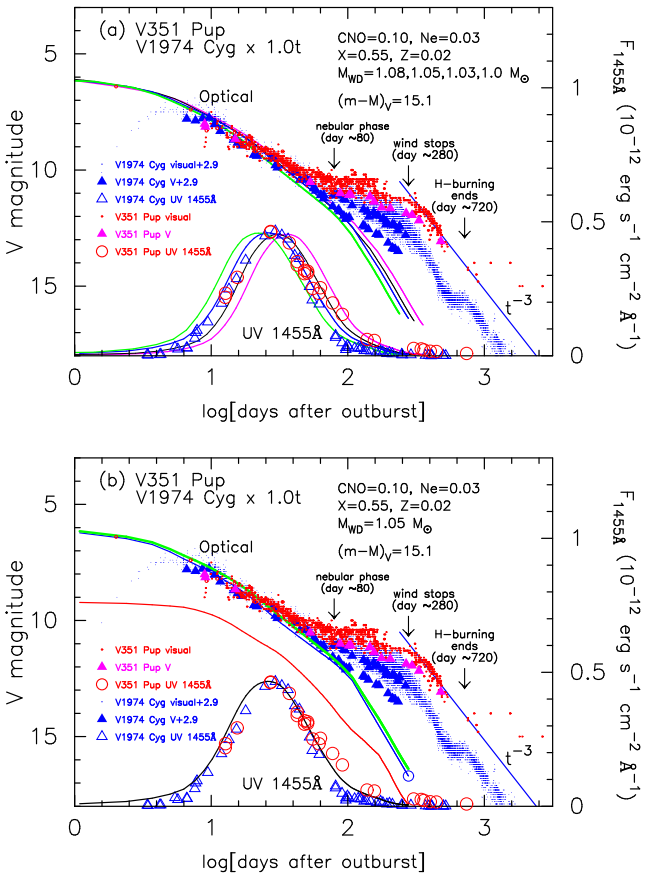

Figure 23. Same as Figure 20, but for Ne nova 2. (a) Assuming that $(m-M)_V$ = 15.1, we plot four model light curves of 1.0 $M_\odot$ (magenta solid line), 1.03 $M_\odot$ (black thin solid line), 1.05 $M_\odot$ (blue solid line), and 1.08 $M_\odot$ (green solid line) WDs. We added the V (blue asterisks) and UV 1455 Å (large blue filled squares) light curves of V1974 Cyg. The timescale of V1974 Cyg is the same as that of V351 Pup. (b) Assuming that $(m-M)_V$ = 15.1, we plot the blackbody emission (red solid line), free-free emission (blue solid line), and total emission (green thick solid line) light curves of 1.05 $M_\odot$ WD. Optically thick winds and hydrogen shell burning end approximately 280 days and 720 days after the outburst, respectively, for the 1.05 $M_\odot$ WD.

of the free-free and blackbody emission, which are shown in Figure 18(b). We directly read $m_{\rm w}$ = 16.6 from Figure 18(b) and obtain $M_{\rm w} = m_{\rm w} - (m-M)_V$ = 16.6 − 15.1 = 1.5. Thus, the proportionality constant is specified by $M_{\rm w}$ = 1.5 for the 1.0 $M_\odot$ WD with the Ne nova 1 composition. Using Equation (B11), we obtain the absolute magnitudes of the free-free model light curves for the other WD masses with the chemical composition of Ne nova 1, which are listed in Table 5.

Our model light curve fits the early V and visual light curves but deviates from the V and visual observation in the later phase, that is, in the nebular phase (Williams et al. 1994; Saizar et al. 1996), as shown in Figure 18. In the figure, we suppose that V351 Pup entered the nebular phase at $m_V \approx 11.0$, about 80 days after the outburst. This is because strong emission lines such as [O III] contribute to the V magnitude but our model light curves do not include such emission lines as discussed in Section 2.1.

4.2.2. *CO nova 2*

Figure 20 shows our model light curve fittings for the chemical composition of CO nova 2. The absolute magnitudes of the model light curves for this chemical composition were already calibrated in Hachisu & Kato (2010). Assuming that $(m-M)_V$ = 15.1, we obtain the 0.98 $M_\odot$ WD as the best-fit model, as shown in Figure 20(a), from the UV 1455 Å light curve fitting. We plot the total, free-free emission, and blackbody emission fluxes for the 0.98 $M_\odot$ WD model in Figure 20(b).

Optically thick winds and hydrogen shell burning end approximately 235 days and 505 days after the outburst, respectively, for the 0.98 $M_\odot$ WD. For $(m-M)_V$ = 15.1, the total V flux light curve follows the observed V magnitudes of V351 Pup reasonably well in the early decline phase. It deviates from the observed V in the middle and later phases, mainly because strong emission lines dominate the spectrum in the nebular phase that started on day $\sim$ 80. These strong emission lines are not included in our light curve model.

We obtain two distance-reddening relations from the V and UV 1455 Å light curve fittings of the 0.98 $M_\odot$ WD, i.e., Equation (1) together with $(m-M)_V$ = 15.1 and Equation (2) together with $F^{\rm mod}_{\lambda 1455} = 5.0\times10^{-12}$ erg cm^{-2} s^{-1} Å^{-1} and $F^{\rm obs}_{\lambda 1455} = (4.6\pm0.49)\times10^{-13}$ erg cm^{-2} s^{-1} Å^{-1} at the UV 1455 Å flux maximum in Figure 20(b). The two distance-reddening relations are plotted in Figure 21(a); they cross each other at $E(B-V) \approx 0.48$ and $d \approx 5.3$ kpc, which are consistent with

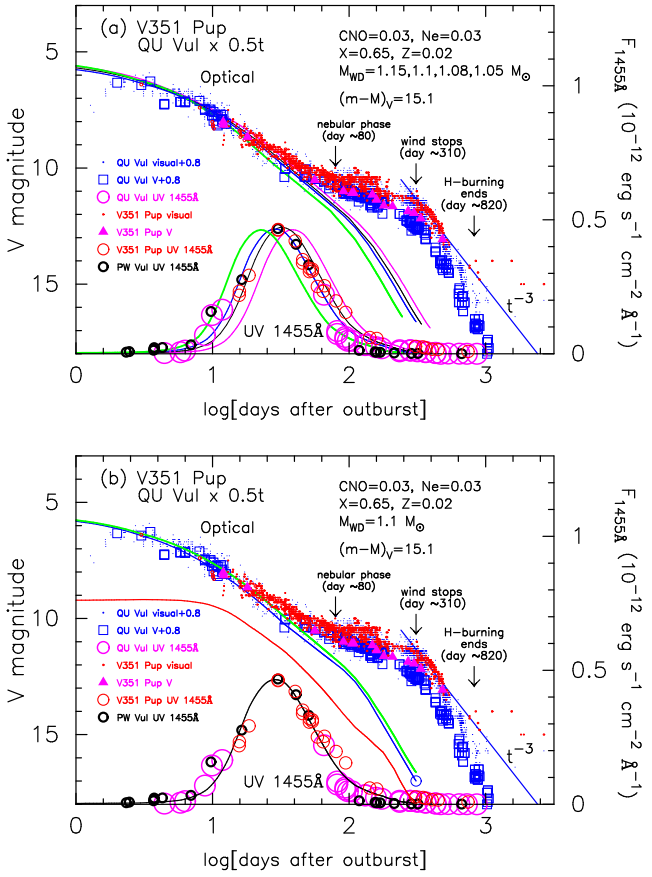

Figure 24. Same as Figure 20, but for Ne nova 3. (a) Assuming that $(m-M)_V = 15.1$, we plot four model light curves of 1.05 $M_\odot$ (magenta solid line), 1.08 $M_\odot$ (thin black solid line), 1.1 $M_\odot$ (blue solid line), and 1.15 $M_\odot$ (green solid line) WDs. We added the V (blue open squares), visual (blue dots), and UV 1455 Å (large magenta open circles) light curves of QU Vul. The timescale of QU Vul is squeezed by a factor of 0.5. We also added the UV 1455 Å (black open circles) light curve of PW Vul, the same as that in Figure 22. (b) Assuming that $(m-M)_V = 15.1$, we plot the blackbody emission (red solid line), free-free emission (blue solid line), and total emission (green thick solid line) light curves of the 1.1 $M_\odot$ WD. Optically thick winds and hydrogen shell burning end approximately 310 days and 820 days after the outburst, respectively, for the 1.1 $M_\odot$ WD.

our estimates of $E(B-V) = 0.45 \pm 0.05$ and $d = 5.5 \pm 1$ kpc in Section 4.1.

4.2.3. *CO nova 4*

Figure 22(a) shows that the 1.02 $M_\odot$ WD model is the best-fit model because of its agreement with the UV 1455 Å observed fluxes. The absolute magnitudes of the free-free model light curves were already calibrated in Hachisu & Kato (2015). We plot the total, free-free emission, and blackbody emission fluxes of the 1.02 $M_\odot$ WD model in Figure 22(b). In this case, optically thick winds and hydrogen shell burning end approximately 280 days and 740 days after the outburst, respectively. For $(m-M)_V = 15.1$, the total V flux light curve follows the observed V magnitudes of V351 Pup reasonably well in the early decline phase.

We obtain two distance-reddening relations from the V and UV 1455 Å light curve fittings of the 1.02 $M_\odot$ WD, i.e., Equation (1) with $(m-M)_V = 15.1$ and Equation (2) with $F^{\rm mod}_{\lambda 1455} = 4.4 \times 10^{-12}$ erg cm^{-2} s^{-1} Å^{-1} and $F^{\rm obs}_{\lambda 1455} = 4.6 \times 10^{-13}$ erg cm^{-2} s^{-1} Å^{-1} at the UV 1455 Å flux maximum in Figure 22(b). The two distance-reddening relations are plotted in Figure 21(b); they cross each other at $E(B-V) \approx 0.45$ and $d \approx 5.5$ kpc. These values are consistent with our estimates of $E(B-V) = 0.45 \pm 0.05$ and $d = 5.5 \pm 1$ kpc in Section 4.1.

4.2.4. *Ne nova 2*

Figure 23(a) shows that the 1.05 $M_\odot$ WD model is the best-fit model because of its agreement with the UV 1455 Å observed fluxes. The absolute magnitudes of the free-free model light curves were published in Hachisu & Kato (2010). We plot the total, free-free emission, and blackbody emission fluxes of the 1.05 $M_\odot$ WD model in Figure 23(b). Optically thick winds and hydrogen shell burning end approximately 280 days and 720 days after the outburst, respectively, for the 1.05 $M_\odot$ WD. For $(m-M)_V = 15.1$, the total V flux light curve follows the observed V magnitudes of V351 Pup reasonably well in the early decline phase.

We obtain two distance-reddening relations from the V and UV 1455 Å light curve fittings of the 1.05 $M_\odot$ WD, i.e., Equation (1) with $(m-M)_V = 15.1$ and Equation (2) with $F^{\rm mod}_{\lambda 1455} = 4.6 \times 10^{-12}$ erg cm^{-2} s^{-1} Å^{-1} and $F^{\rm obs}_{\lambda 1455} = 4.6 \times 10^{-13}$ erg cm^{-2} s^{-1} Å^{-1} at the UV 1455 Å flux maximum in Figure 23(b). The two distance-reddening relations are plotted in Figure 21(c); they cross each other at $E(B-V) \approx 0.46$ and $d \approx 5.4$ kpc. These values are consistent with our estimates of $E(B-V) = 0.45 \pm 0.05$ and $d = 5.5 \pm 1$ kpc in Section 4.1.

4.2.5. *Ne nova 3*

Figure 24(a) shows that the 1.1 $M_\odot$ WD model is the best-fit model because of its agreement with the UV 1455 Å observed fluxes. The absolute magnitudes of the free-free model light curves are determined in Section 3. We plot the total, free-free emission, and blackbody emission fluxes for the 1.1 $M_\odot$ WD model in Figure 24(b). Optically thick winds and hydrogen shell burning end approximately 310 days and 820 days after the outburst, respectively. For $(m-M)_V = 15.1$, the total V flux light curve follows the observed V magnitudes of V351 Pup reasonably well in the early decline phase.

We obtain two distance-reddening relations from the V and UV 1455 Å light curve fittings of the 1.1 $M_\odot$ WD, i.e., Equation (1) with $(m-M)_V = 15.1$ and Equation (2) with $F^{\rm mod}_{\lambda 1455} = 4.55 \times 10^{-12}$ erg cm^{-2} s^{-1} Å^{-1} and $F^{\rm obs}_{\lambda 1455} = 4.6 \times 10^{-13}$ erg cm^{-2} s^{-1} Å^{-1} at the UV 1455 Å flux maximum in Figure 24(b). The two distance-reddening relations are plotted in Figure 21(d); they cross each other at $E(B-V) \approx 0.46$ and $d \approx 5.4$ kpc. These values are consistent with our estimates of $E(B-V) = 0.45 \pm 0.05$ and $d = 5.5 \pm 1$ kpc in Section 4.1.

4.3. *Summary of V351 Pup*

Our model light curves fit the optical V and UV 1455 Å fluxes of V351 Pup well and give a reasonable set of the distance, $d = 5.5$ kpc, and the reddening, $E(B-V) = 0.45$. Our best-fit models give relatively small WD masses of 0.98 – 1.1 $M_\odot$ as an ONe WD. As mentioned in Section 1, the WD should be a naked ONe WD because the ejecta are enriched with neon. A natal ONe WD had a CO mantle. Therefore, this WD may have lost a mass of ~ 0.1 $M_\odot$ CO mantle before the naked ONe core was revealed. If we adopt Ne nova 1 for the chemical composition of V351 Pup, we can summarize the results of our light curve fittings (see also Table 6) as follows:

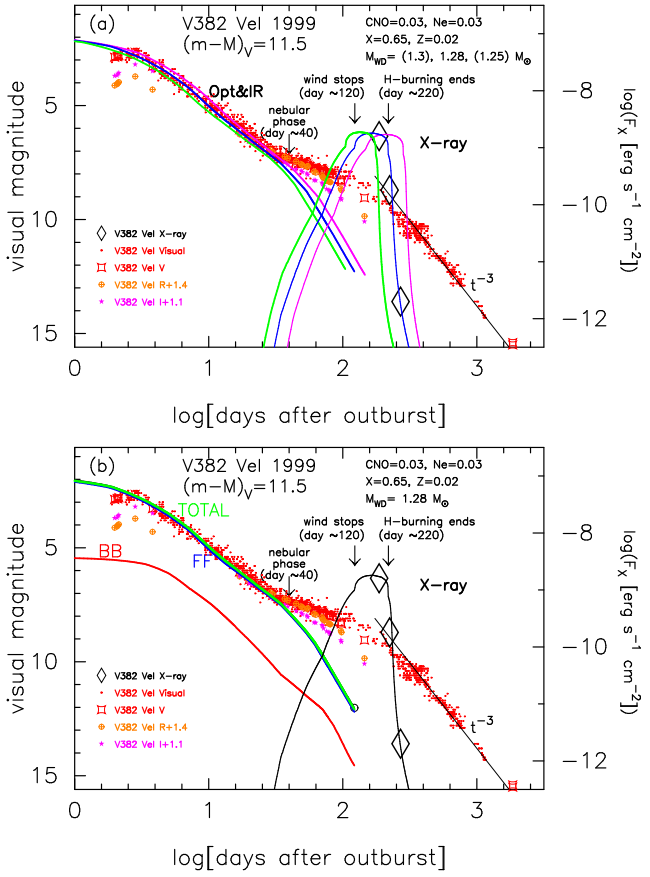

Figure 25. (a) Model light curves of 1.25 $M_\odot$ (magenta solid lines), 1.28 $M_\odot$ (blue solid), and 1.3 $M_\odot$ (green solid) WDs for Ne nova 3 as well as visual (small red dots), V (red boxes with sharp corners), R (orange encircled pluses), near infrared I (magenta filled star marks), and supersoft X-ray (black large open diamonds) light curves of V382 Vel. Assuming that $(m-M)_V$ = 11.5, we plot the V model light curves. (b) Assuming also that $(m-M)_V$ = 11.5, we plot three V model light curves for the 1.28 $M_\odot$ WD: the green, blue, and red solid lines show the total, free-free emission, and blackbody emission V fluxes, respectively. The black solid line denotes the supersoft X-ray fluxes. Optically thick winds and hydrogen shell burning end approximately 120 days and 220 days after the outburst, respectively, for the 1.28$M_\odot$ WD. The nebular phase starts $\sim$ 40 days after the outburst (della Valle et al. 2002). See text for the sources of the observed data.

$(m-M)_V = 15.1$, $E(B-V) = 0.45$, $d = 5.5$ kpc, $M_{\rm WD} = 1.0\,M_\odot$, and $M_{\rm env} = 1.98\times10^{-5}\,M_\odot$ at optical maximum.

4.4. *Comparison with previous results*

Wanajo et al. (1999) estimated the WD mass from fitting their abundance pattern model with that observed by Saizar et al. (1996) and suggested $M_{\rm WD} \gtrsim 1.25\,M_\odot$. Kato & Hachisu (2007) estimated the WD mass and distance of V351 Pup to be 1.0 $M_\odot$ and 2.1 kpc, respectively, based on their optically thick wind model (Kato & Hachisu 1994). They fitted their UV 1455Å model light curves with the observation. Because the timescale of the nova evolution is the same between their models and ours, the obtained WD mass is the same. However, they determined the distance only from the UV 1455Å fitting. They adopted the reddening of $E(B-V) = 0.72$ (Saizar et al. 1996) and obtained the distance of 2.1 kpc, which is much shorter than our new estimate of 5.5 kpc.

5. V382 VEL 1999

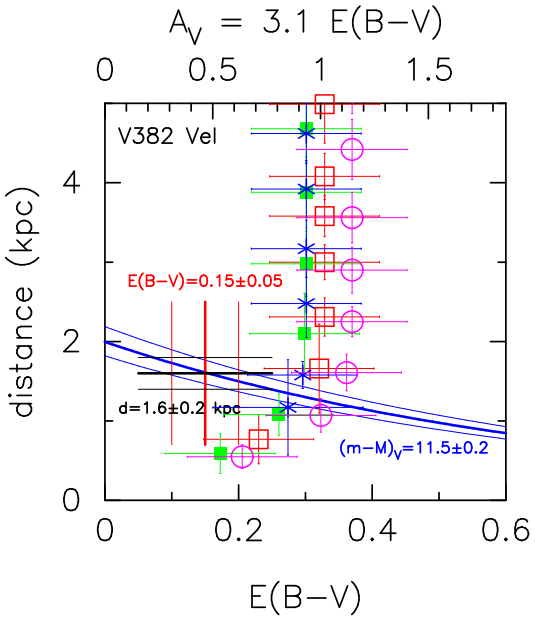

Figure 26. Various distance-reddening relations toward V382 Vel. We plot Equation (1) with $(m-M)_V = 11.5 \pm 0.2$ (blue solid lines) from our time-stretching method in Appendix A, $E(B-V) = 0.15 \pm 0.05$ (red thick solid lines) from our color-color diagram method in Section 8.2, $d = 1.6 \pm 0.2$ kpc (black solid lines), and four Marshall et al.'s (2006) distance-reddening relations toward $(l, b) = (284.^\circ00, +5.^\circ75)$ (red open squares), $(284.^\circ25, +5.^\circ75)$ (green filled squares), $(284.^\circ00, +6.^\circ00)$ (blue asterisks), and $(284.^\circ25, +6.^\circ00)$ (magenta open circles), which are four directions close to V382 Vel, $(l, b) = (284.^\circ1674, +5.^\circ7715)$.

V382 Vel is a very fast nova identified as a neon nova (Woodward et al. 1999). The optical and NIR light curves and supersoft X-ray count rates are plotted in Figure 25. The nova reached $m_V = 2.7$ at maximum on UT 1999 May 23. Supersoft X-rays were detected by *BeppoSAX* (Orio et al. 2002) about six months after the outburst, followed by a rapid decline, as shown in Figure 25. *Chandra* observations by Burwitz et al. (2002) and Ness et al. (2005) suggest that hydrogen shell burning ended approximately 220 days after the outburst. We have already analyzed the light curves of V382 Vel in Hachisu & Kato (2010) on the basis of our optical free-free emission and X-ray model light curves, but not included the effect of photospheric emission. Here, we calculate the total V flux model light curves and compare them with the optical observations.

5.1. *Reddening and distance*

The reddening toward V382 Vel was estimated as $E(B-V) = 0.20$ by Shore et al. (2003), and as $E(B-V) = 0.05$–0.099 by della Valle et al. (2002) from various line ratios and the Na I D interstellar absorption features. Hachisu & Kato (2014) obtained $E(B-V) = 0.15 \pm 0.05$ by the UBV color-color diagram fitting. We again plot the color-color diagram of V382 Vel in Figure 11(c). Mukai & Ishida (2001) obtained a hydrogen column density toward V382 Vel of $N_{\rm H} = (1.01 \pm 0.05) \times 10^{21}$ from early hard X-ray spectrum fittings. This value can be converted to $E(B-V) = N_{\rm H}/5.8\times10^{21} \approx 0.2$ (Bohlin et al. 1978), $E(B-V) = N_{\rm H}/6.8\times10^{21} \approx 0.15$ (Güver & Özel 2009), or $E(B-V) = N_{\rm H}/8.3\times10^{21} \approx 0.12$ (Liszt 2014), which are consistent with Hachisu & Kato's value of $E(B-V) = 0.15 \pm 0.05$. Therefore, we adopt $E(B-V) = 0.15 \pm 0.05$ in this paper.

The distance of V382 Vel was also estimated to be d =

Table 5
Free-free Light Curves of Neon Novae 1[a]

$m_{\rm ff}$ (mag)	$0.7M_\odot$ (day)	$0.75M_\odot$ (day)	$0.8M_\odot$ (day)	$0.85M_\odot$ (day)	$0.9M_\odot$ (day)	$0.95M_\odot$ (day)	$1.0M_\odot$ (day)	$1.05M_\odot$ (day)	$1.1M_\odot$ (day)	$1.15M_\odot$ (day)	$1.2M_\odot$ (day)	$1.25M_\odot$ (day)	$1.3M_\odot$ (day)
3.500	0.0	0.0	0.0	0.0	0.0	0.0	0.0	0.0	0.0	0.0	0.0	0.0	0.0
3.750	1.704	1.540	1.320	1.050	0.940	0.838	0.776	0.699	0.620	0.583	0.557	0.510	0.511
4.000	3.446	3.330	2.670	2.130	1.880	1.683	1.549	1.395	1.241	1.161	1.089	1.030	0.993
4.250	5.849	5.160	4.040	3.260	2.870	2.546	2.327	2.077	1.862	1.727	1.627	1.540	1.473
4.500	8.850	7.050	5.590	4.460	3.890	3.416	3.122	2.767	2.482	2.297	2.162	2.050	1.948
4.750	11.93	8.970	7.320	5.680	4.920	4.296	3.922	3.489	3.117	2.890	2.710	2.560	2.428
5.000	15.12	12.21	9.120	7.050	6.030	5.266	4.772	4.231	3.777	3.507	3.290	3.080	2.898
5.250	19.01	15.80	10.98	8.800	7.220	6.306	5.742	5.129	4.447	4.134	3.874	3.600	3.398
5.500	25.07	19.62	14.65	10.61	8.600	7.376	6.752	6.086	5.317	5.043	4.634	4.160	3.978
5.750	31.59	24.06	18.70	12.90	10.63	8.996	8.202	7.336	6.277	6.004	5.604	4.830	4.738
6.000	38.10	28.73	22.03	16.21	13.03	11.00	10.22	9.106	7.477	7.084	6.514	5.750	5.478
6.250	44.82	33.82	25.47	19.28	15.46	12.81	11.66	10.29	8.957	8.164	7.424	6.730	6.248
6.500	52.06	39.37	29.18	21.96	17.78	14.64	13.04	11.40	9.797	8.864	8.094	7.360	6.828
6.750	60.05	45.31	33.65	24.83	20.02	16.51	14.54	12.61	10.67	9.614	8.704	7.850	7.208
7.000	69.13	51.76	38.51	28.26	22.43	18.44	16.20	13.90	11.63	10.42	9.354	8.350	7.598
7.250	78.94	58.74	43.75	32.14	25.35	20.51	18.00	15.31	12.71	11.29	10.05	8.870	8.008
7.500	89.61	66.33	49.10	36.37	28.57	22.92	20.05	16.88	13.89	12.25	10.80	9.410	8.418
7.750	99.71	74.54	54.89	40.49	32.00	25.57	22.29	18.58	15.20	13.24	11.61	9.980	8.858
8.000	110.1	82.59	61.14	44.87	35.26	28.44	24.72	20.46	16.57	14.33	12.45	10.59	9.298
8.250	121.3	90.77	67.67	49.59	38.77	31.23	26.94	22.23	17.93	15.49	13.29	11.20	9.718
8.500	133.8	99.47	74.19	54.68	42.54	34.22	29.31	24.14	19.37	16.63	14.15	11.81	10.15
8.750	147.5	110.5	81.23	59.98	46.61	37.33	31.87	26.17	20.83	17.86	15.05	12.42	10.58
9.000	162.7	122.4	89.70	65.64	51.25	40.66	34.63	28.35	22.41	19.18	16.09	13.06	11.01
9.250	180.1	135.2	99.20	72.25	56.27	44.54	38.09	31.11	24.22	20.62	17.25	13.80	11.52
9.500	199.5	149.3	109.7	80.18	61.87	48.76	41.89	34.19	26.34	22.53	18.62	14.67	12.12
9.750	220.1	164.8	121.3	88.87	68.70	53.87	46.28	37.75	28.90	24.62	20.21	15.68	12.83
10.00	243.2	182.4	134.2	98.17	76.14	59.70	51.21	41.76	31.87	27.01	22.01	16.85	13.64
10.25	269.4	202.6	148.9	108.6	84.29	66.12	56.76	46.29	35.18	29.63	24.10	18.18	14.55
10.50	293.1	225.5	166.0	120.3	93.24	73.26	63.09	51.64	38.96	32.84	26.42	19.72	15.61
10.75	314.4	246.9	185.5	134.5	103.8	81.11	70.04	57.42	43.37	36.65	29.49	21.42	16.77
11.00	338.5	269.5	200.2	150.5	116.3	90.57	78.34	64.19	48.22	40.84	32.84	23.76	18.41
11.25	365.8	286.5	213.8	165.7	130.3	101.4	87.68	71.78	54.61	45.61	36.93	26.33	20.24
11.50	396.5	303.9	228.9	180.0	139.6	113.5	97.74	79.95	60.57	50.83	40.92	29.32	22.31
11.75	421.1	323.0	245.7	192.4	148.9	122.8	104.1	86.11	66.49	55.74	44.83	32.31	24.43
12.00	446.2	338.6	264.3	203.0	158.4	132.8	111.0	92.76	71.85	59.67	48.10	35.21	26.51
12.25	472.8	355.0	277.9	214.6	168.4	141.2	118.4	98.29	77.06	63.49	51.45	37.75	28.33
12.50	501.0	373.1	290.6	225.8	178.9	150.0	126.0	103.9	82.04	67.52	54.78	40.26	30.10
12.75	530.8	393.7	304.5	236.4	190.1	159.3	133.9	109.9	87.31	71.80	58.21	42.83	31.96
13.00	562.4	417.7	323.0	251.4	202.0	169.1	142.3	115.9	92.89	76.33	62.05	45.37	34.33
13.25	595.8	443.2	342.8	267.2	214.6	179.5	151.1	122.1	98.77	81.12	66.12	47.98	36.84
13.50	631.3	470.1	363.8	284.0	227.9	190.6	160.6	129.6	105.1	86.20	70.43	51.69	39.50
13.75	668.9	498.7	386.1	301.7	242.0	202.3	170.5	137.5	111.7	91.59	74.99	55.65	42.32
14.00	708.7	528.9	409.6	320.5	257.0	214.7	181.1	145.9	118.8	97.27	79.82	59.86	45.31
14.25	750.8	561.0	434.6	340.5	272.8	227.8	192.2	154.9	126.2	103.4	84.95	64.30	48.47
14.50	795.4	594.9	461.0	361.6	289.5	241.8	204.1	164.3	134.1	109.8	90.37	69.01	51.82
14.75	842.7	630.9	489.0	384.0	307.3	256.5	216.6	174.3	142.5	116.5	96.10	74.00	55.37
15.00	892.8	669.0	518.6	407.6	326.1	272.1	229.9	184.9	151.3	123.7	102.2	79.29	59.13
X-ray[b]	1734	1250	900	645	457	338	248	170	114	78	52	30.5	16.3
log $f_{\rm s}$[c]	0.56	0.46	0.35	0.25	0.16	0.08	0.0	–0.10	–0.19	–0.29	–0.385	–0.50	–0.65
$M_{\rm w}$[d]	3.8	3.3	2.8	2.4	2.0	1.8	1.5	1.3	1.0	0.7	0.5	0.2	0.0

[a] Chemical composition of the envelope is assumed to be that of Ne nova 1 in Table 2.
[b] Duration of supersoft X-ray phase in units of days.
[c] Stretching factor against V351 Pup UV 1455 Å observation in Figure 55.
[d] Absolute magnitudes at the bottom point in Figure 58 by assuming $(m-M)_V$ = 15.1 (V351 Pup).

1.66 ± 0.11 kpc by della Valle et al. (2002) from the maximum magnitude versus rate of decline (MMRD) relation whereas Shore et al. (2003) obtained a larger distance of d = 2.5 kpc, assuming that the UV fluxes of V382 Vel and V1974 Cyg are the same. Shore et al. (2003) assumed a distance of d = 3.1 kpc to V1974 Cyg, but this value is much larger than the reasonable one of d = 1.8 kpc, as shown in Section 7 (see also, e.g., Chochol et al. 1997a; Hachisu & Kato 2010, 2014). If we take d = 1.8 kpc instead of 3.1 kpc to V1974 Cyg, Shore et al.'s method gives a much shorter distance of 1.5 kpc to V382 Vel, which is consistent with della Valle et al.'s value. Hachisu & Kato (2010) estimated the distance modulus of V382 Vel to be $(m-M)_V = 11.5 \pm 0.1$ using four different methods, including the free-free emission model light curve fitting method based on the chemical composition Ne nova 2. If we adopt $E(B-V) = 0.15 \pm 0.05$, the distance of V382 Vel is calculated to be $d = 1.6 \pm 0.2$ kpc from Equation (1). These values are all consistent with each other. Therefore, we adopt $d = 1.6 \pm 0.2$ kpc in this paper. In Figure 26, we plot these three constraints of the distance, reddening, and distance modulus in the V band as well as Marshall et al.'s (2006) distance-reddening relations.

Marshall et al.'s relation suggests an extinction of as large as $E(B-V)$ = 0.3–0.4 at the distance of 1.6 kpc. The NASA/IPAC galactic dust absorption map also gives $E(B-V) = 0.385 \pm 0.01$ in the direction of V382 Vel, whose galac-

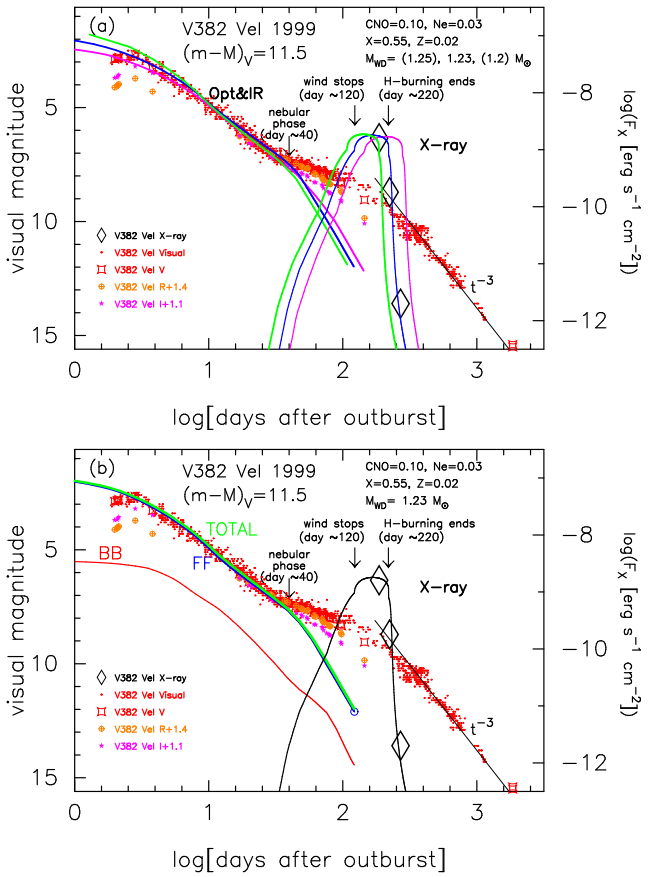

Figure 27. Same as Figure 25, but for Ne nova 2. (a) Model light curves of 1.2 $M_\odot$ (magenta solid lines), 1.23 $M_\odot$ (blue solid lines), and 1.25 $M_\odot$ (green solid lines) WDs. Assuming that $(m-M)_V$ = 11.5, we plot the V model light curves. (b) Assuming also that $(m-M)_V$ = 11.5, we plot three V model light curves of the 1.23 $M_\odot$ WD. Optically thick winds and hydrogen shell burning end approximately 120 days and 220 days after the outburst, respectively, for the 1.23$M_\odot$ WD.

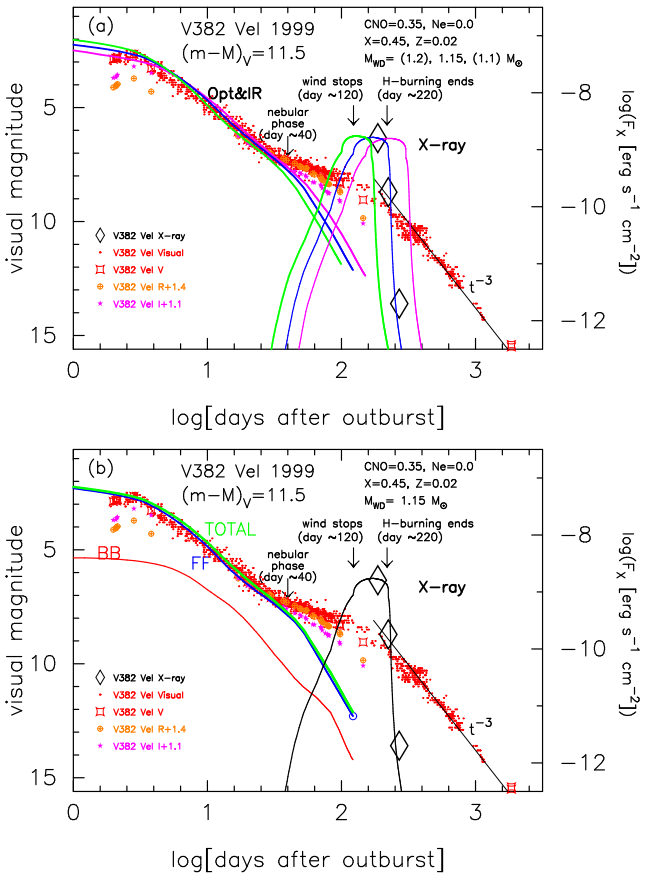

Figure 28. Same as Figure 25, but for CO nova 3. (a) Model light curves of 1.1 $M_\odot$ (magenta solid lines), 1.15 $M_\odot$ (blue solid lines), and 1.2 $M_\odot$ (green solid lines) WDs. Assuming that $(m-M)_V$ = 11.5, we plot the V model light curves. (b) Assuming also that $(m-M)_V$ = 11.5, we plot three V model light curves of the 1.15 $M_\odot$ WD. Optically thick winds and hydrogen shell burning end approximately 120 days and 220 days after the outburst, respectively, for the 1.15$M_\odot$ WD.

tic coordinates are (l,b) = (284.°1674, +05.°7715). These two extinctions are consistent with each other, but disagree with our obtained value of $E(B-V) = 0.15 \pm 0.05$. Because various estimates on the absorption toward V382 Vel are consistent with $E(B-V) = 0.15 \pm 0.05$ as mentioned above, this disagreement between the pin-point extinction toward V382 Vel ($E(B-V) \sim 0.15$) and Marshall et al.'s relation ($E(B-V) \sim$ 0.3–0.4 at 1.6 kpc) suggests a low extinction hole in front of V382 Vel.

5.2. *Light curve fitting of V382 Vel*

The chemical composition of V382 Vel was obtained as $X = 0.47$, $X_{\rm CNO} = 0.018$, and $X_{\rm Ne} = 0.0099$ by Augusto & Diaz (2003), and as $X = 0.66$, $X_{\rm CNO} = 0.043$, and $X_{\rm Ne} = 0.027$ by Shore et al. (2003) (see Table 1). Shore et al.'s estimate is close to that for Ne nova 3. We first examine the chemical composition of Ne nova 3, then those of Ne nova 2, CO nova 3, and finally Ne nova 1 in order of the degree of mixing. The absolute magnitudes of the free-free emission model light curves are already calibrated for Ne nova 1 in Section 4, for CO nova 3 in Section 2, for Ne nova 2 in Hachisu & Kato (2010), and for Ne nova 3 in Section 3. Our fitting results are shown in Figures 25, 27 – 29. In these figures, the visual magnitudes are taken from the AAVSO archive. The V, R, and I data are taken from IAU Circular Nos. 7176, 7179, 7196, 7209, 7216, 7226, 7232, 7238, and 7277. The faintest observational V magnitudes at day $\sim$ 1850 are taken from Woudt et al. (2005). The X-ray data are taken from Orio et al. (2002) and Burwitz et al. (2002).

5.2.1. *Ne nova 3*

Figure 25(a) shows that the 1.28 $M_\odot$ WD model is the best-fit model, especially because of its agreement with the X-ray light curves. We plot the total, free-free emission, and blackbody emission fluxes of the 1.28 $M_\odot$ WD model in Figure 25(b). Optically thick winds and hydrogen shell burning end approximately 120 days and 220 days after the outburst, respectively, for the 1.28 $M_\odot$ WD. For $(m-M)_V$ = 11.5, the total V flux light curve follows the observed V magnitudes of V382 Vel reasonably well in the early decline phase. We have obtained a hydrogen-rich envelope mass of $M_{\rm env} = 0.46 \times 10^{-5} M_\odot$ at optical maximum, which corresponds approximately to the ignition mass.

Our model light curve fits the early V and visual light curves but deviates from the V and visual observation in the later phase, that is, in the nebular phase. V382 Vel entered the nebular phase at least by the end of June 1999, that is, at $m_V \approx 7.4$ and $\sim$ 40 days after the the optical maximum (della Valle et al. 2002), as shown in Figure 25. This is because strong emission lines such as [O III] contribute to the V magnitude but our model light curves do not include such emission lines as discussed in Section 2.1.

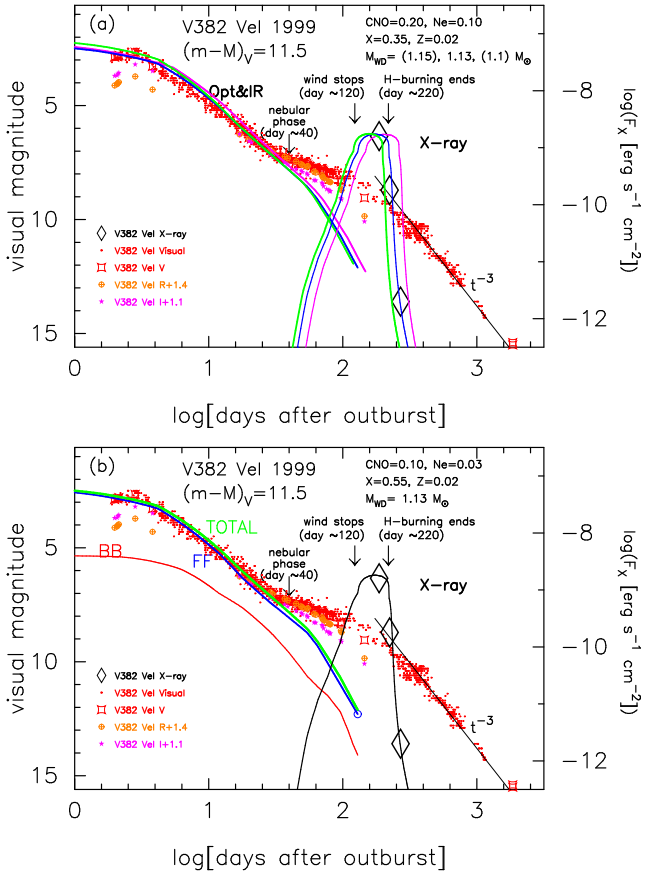

Figure 29. Same as Figure 25, but for Ne Nova 1. (a) Model light curves of 1.1 $M_\odot$ (magenta solid lines), 1.13 $M_\odot$ (blue solid lines), and 1.15 $M_\odot$ (green solid lines) WDs with the chemical composition of "Ne Nova 1." Assuming that $(m-M)_V = 11.5$, we plot the V model light curves. (b) Assuming also that $(m-M)_V = 11.5$, we plot three V model light curves of the 1.13 $M_\odot$ WD. Optically thick winds and hydrogen shell burning end approximately 120 days and 220 days after the outburst, respectively, for the 1.13$M_\odot$ WD.

5.2.2. *Ne nova 2*

Figure 27(a) shows that the 1.23 $M_\odot$ WD model is the best-fit model from the X-ray light curve fitting. We plot the total, free-free emission, and blackbody emission fluxes of the 1.23 $M_\odot$ WD model in Figure 27(b). Optically thick winds and hydrogen shell burning end approximately 120 days and 220 days after the outburst, respectively. For $(m-M)_V = 11.5$, the total V flux light curve follows the observed V magnitudes of V382 Vel reasonably well in the early decline phase. We have obtained a hydrogen-rich envelope mass of $M_{\rm env} = 0.48 \times 10^{-5} M_\odot$ at optical maximum.

5.2.3. *CO nova 3*

Figure 28(a) shows that the 1.15 $M_\odot$ WD model is the best-fit model from the X-ray light curve fitting. We plot the total, free-free emission, and blackbody emission fluxes of the 1.15 $M_\odot$ WD model in Figure 28(b). Optically thick winds and hydrogen shell burning end approximately 120 days and 220 days after the outburst, respectively. For $(m-M)_V = 11.5$, the total V flux light curve follows the observed V magnitudes of V382 Vel reasonably well in the early decline phase. We have obtained a hydrogen-rich envelope mass of $M_{\rm env} = 0.70 \times 10^{-5} M_\odot$ at optical maximum.

5.2.4. *Ne nova 1*

Figure 29(a) shows that the 1.13 $M_\odot$ WD model is the best-fit model from the X-ray light curve fitting. We plot the total, free-free emission, and blackbody emission fluxes of the 1.13 $M_\odot$ WD model in Figure 29(b). Optically thick winds and hydrogen shell burning end approximately 120 days and 220 days after the outburst, respectively. For $(m-M)_V = 11.5$, the total V flux light curve follows the observed V magnitudes of V382 Vel reasonably well in the early decline phase. We have obtained a hydrogen-rich envelope mass of $M_{\rm env} = 0.85 \times 10^{-5} M_\odot$ at optical maximum.

5.3. *Summary of V382 Vel*

Our model light curve fittings of Ne nova 3, Ne nova 2, CO nova 3, and Ne nova 1 give WD masses of 1.28, 1.23, 1.15, and 1.13 $M_\odot$, respectively, with a distance modulus of $(m-M)_V = 11.5$. Here, we adopt Ne nova 2 for the chemical composition of V382 Vel because it is close to the arithmetic mean of $X = 0.47$ (Augusto & Diaz 2003) and $X = 0.66$ (Shore et al. 2003), i.e., $X = 0.56$. We summarize the results of our light curve fittings (see also Table 6) as follows: $(m-M)_V = 11.5$, $E(B-V) = 0.15$, $d = 1.6$ kpc, $M_{\rm WD} = 1.23\,M_\odot$, and $M_{\rm env} = 0.48 \times 10^{-5}\,M_\odot$ at optical maximum. The effect of photospheric emission is rather small and it affects the light curve fitting very little. Therefore, we can reproduce the optical light curves of V382 Vel using only the free-free emission light curves. The reddening and distance are consistent with the previous estimates mentioned in Section 5.1, but deviate from the distance-reddening relation given by Marshall et al. (2006).

5.4. *Comparison with previous results*

Using the time-stretching method of the universal decline law, Hachisu & Kato (2010) obtained the absolute magnitude of their free-free emission model light curves and applied their light curve model to V382 Vel. They obtained the distance modulus in the V band of $(m-M)_V = 11.5 \pm 0.1$ and the WD mass of $1.23 \pm 0.05\,M_\odot$. Downen et al. (2013) estimated the WD mass of V382 Vel by comparing their model elemental abundance with the observed ratios. They obtained 1.18–1.21 $M_\odot$. Our new estimate of 1.23 $M_\odot$ is close to their upper value.

6. V693 CRA 1981

V693 CrA is a very fast nova identified as a neon nova (Williams et al. 1985). The optical and *IUE* UV light curves are plotted in Figure 30. The nova had already reached 7.0 mag at discovery by M. Honda (Kozai et al. 1981) on UT 1981 April 2.75. The discovery magnitude was later revised by M. Honda to 6.5 mag (see Caldwell 1982). V693 CrA declined with $t_2 = 5.8$ and $t_3 = 12$ days (see, e.g., Table 5.2 of Warner 1995).

6.1. *Reddening and distance*

The reddening toward V693 CrA was estimated as $E(B-V) = A_V/3.1 = 1.7/3.1 = 0.55$ by Brosch (1981) from the Balmer decrement. Miroshnichenko (1993) gave $E(B-V) = A_V/3.1 = (1.65 \pm 0.05)/3.1 = 0.53 \pm 0.02$ toward V693 CrA. On the other hand, Vanlandingham et al. (1997) obtained $E(B-V) = 0.2 \pm 0.1$ using several independent methods, each of which has a large uncertainty, as noted in their paper. The Galactic dust absorption map of NASA/IPAC gives $E(B-V) = 0.099 \pm 0.001$ in the direction toward V693 CrA, $(l, b) = (357.^\circ8299, -14.^\circ3912)$. We prefer a very small value

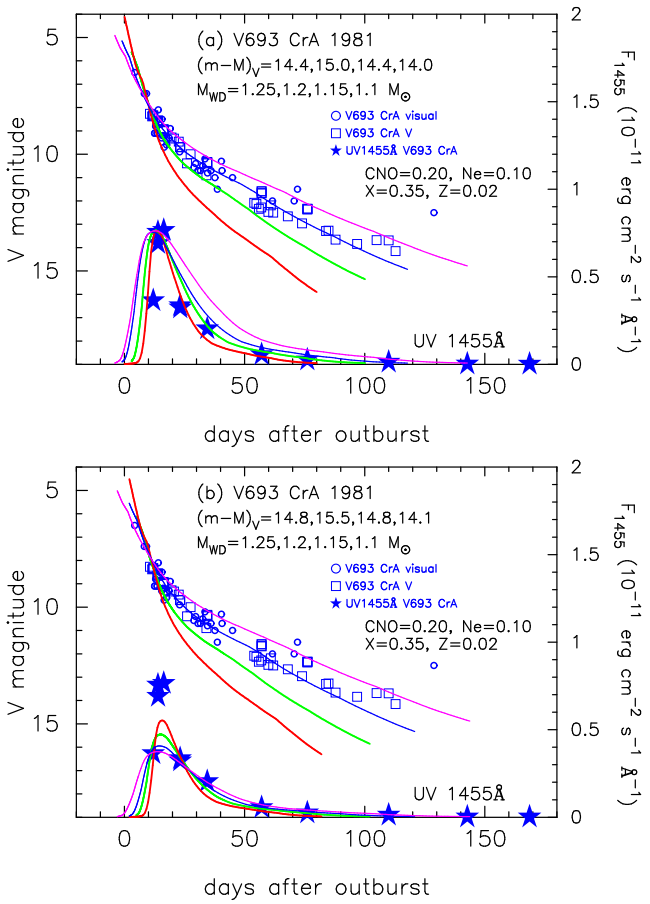

Figure 30. (a) Model light curves of 1.1 $M_\odot$ (magenta solid lines), 1.15 $M_\odot$ (blue solid lines), 1.2 $M_\odot$ (green solid lines), and 1.25 $M_\odot$ (red solid lines) WDs with the chemical composition of Ne Nova 1 as well as V band (blue open squares), visual (blue open circles), and UV 1455 Å (large blue filled star-marks) light curves of V693 CrA. We place the UV 1455Å model light curves to run through the observed peak. (b) We place the UV 1455Å model light curves to skip the observed peak (three star-marks near the peak) but follow the other observations. See text for details.

of $E(B-V)$ because the undreddened UBV color-color evolution of V693 CrA is close to the general track of the UBV evolution, as shown in Figure 11(d). Therefore, we adopted $E(B-V) = 0.05 \pm 0.05$ in this paper.

The distance of V693 CrA was estimated using the MMRD relations: Caldwell (1981) derived d = 7.9–8.5 kpc, whereas Brosch (1982) revised it to d = 12 kpc using $m_{v,\max} = 6.5$. It is well known that the MMRD relations do not give an accurate estimate of the distance for a single nova because of the large scatter of each MMRD value (e.g., Downes & Duerbeck 2000). Instead, we adopted the distance modulus of $(m-M)_V = 14.4 \pm 0.2$ obtained by the time-stretching method (Hachisu & Kato 2010) described in Appendix A. Using Equation (1) with $E(B-V) = 0.05 \pm 0.05$, we obtain a distance of $d = 7.1 \pm 0.7$ kpc. We plot these constraints in Figures 31 and 32.

6.2. *Light curve fitting of V693 CrA*

The chemical composition of the ejecta was estimated by four groups (Williams et al. 1985; Andreä et al. 1994; Arkhipova et al. 1997; Vanlandingham et al. 1997) and their values are summarized in Table 1. There is a large scatter for each value, i.e., X = 0.16 – 0.40, $X_{\rm CNO}$ = 0.14 – 0.36, and $X_{\rm Ne}$ = 0.17 – 0.26. We obtain X = 0.29, $X_{\rm CNO}$ = 0.24, and

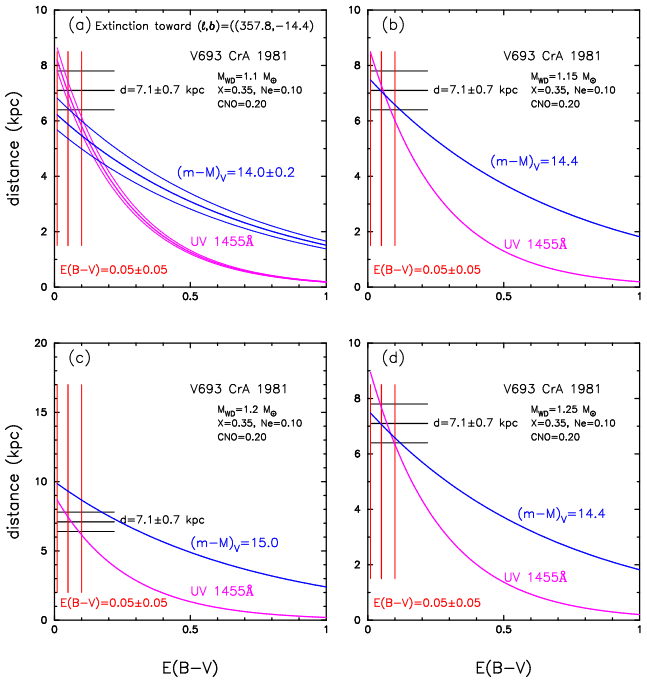

Figure 31. Various distance-reddening relations toward V693 CrA for various WD masses with the chemical composition of Ne nova 1. In panel (a), we plot the results of 1.1 $M_\odot$ WD obtained from Equation (1) with $(m-M)_V = 14.0 \pm 0.2$ from our model V light curve fitting and Equation (2) with our UV 1455Å fitting in Figure 30(a). Two other constraints are also plotted, $E(B-V) = 0.05 \pm 0.05$ and $d = 7.1 \pm 0.7$ kpc. In panel (b), the results of 1.15 $M_\odot$ WD. In panel (c), the results of 1.2 $M_\odot$ WD. In panel (d), the results of 1.25 $M_\odot$ WD. See text for details.

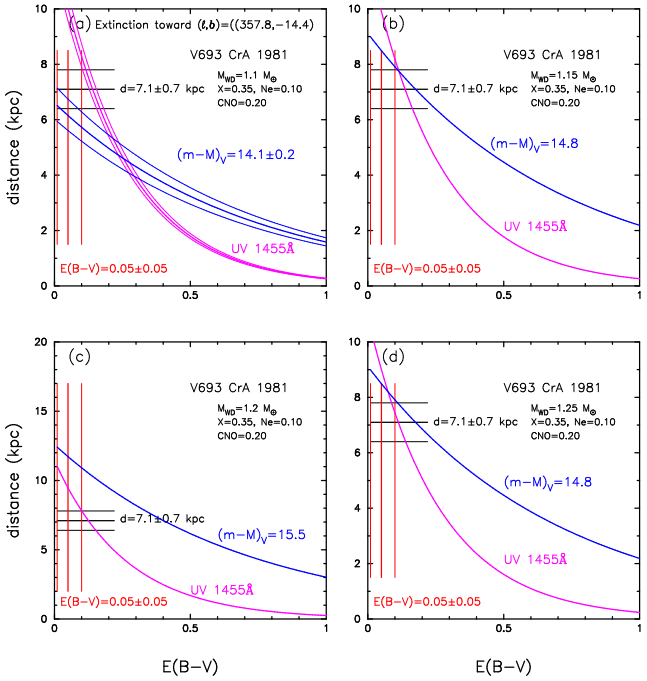

Figure 32. Same as Figure 31, but for the fittings in Figure 30(b). See text for details.

$X_{\rm Ne}$ = 0.21 as an arithmetic average. We first examine the chemical composition of Ne nova 1, then those of CO nova 3, Ne nova 2, and finally Ne nova 3 in the order of the degree of mixing. Our light curve fittings are shown in Figures 30, 33 – 36. In these figures, the data of visual magnitudes are

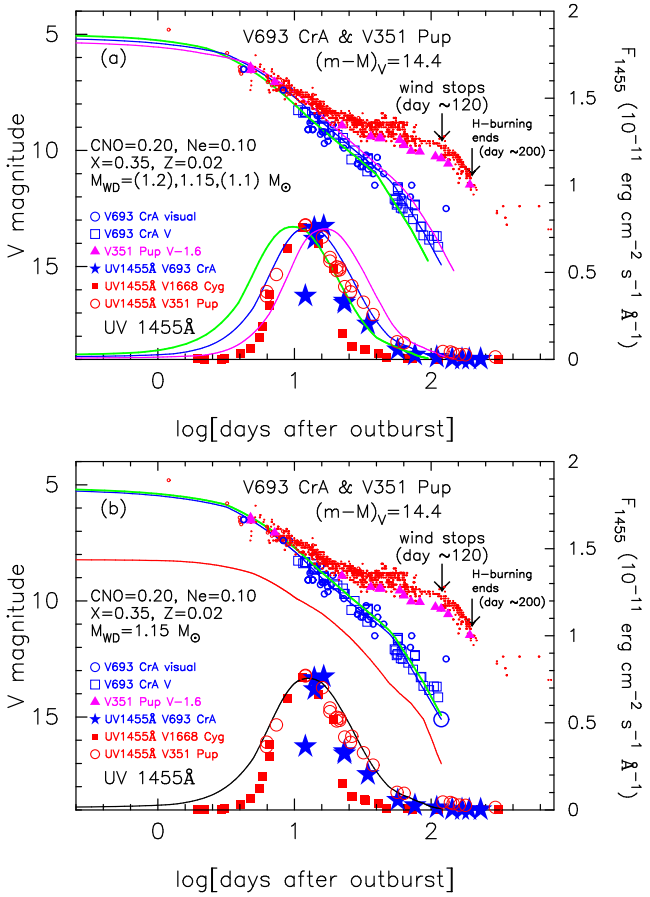

Figure 33. Same as Figure 20, but for V693 CrA. (a) Model light curves of 1.1 $M_\odot$ (magenta solid lines), 1.15 $M_\odot$ (blue solid lines), and 1.2 $M_\odot$ (green solid lines) WDs with Ne Nova 1 as well as visual (small blue open circles), V (blue open sqaures), and UV 1455 Å (blue star marks) light curves of V693 CrA. We added the visual (red small dots), V (magenta filled triangles), UV 1455 Å (red open circles) light curves of V351 Pup. The timescale of V351 Pup is squeezed by a factor of $f_s = 0.40$. We also added the UV 1455 Å (large red filled squares) light curve of V1668 Cyg. The timescale of V1668 Cyg is squeezed by a factor of $f_s = 0.37$. Assuming that $(m-M)_V = 14.4$, we plot the V model light curves. (b) Assuming also that $(m-M)_V = 14.4$, we plot three V model light curves of the 1.15 $M_\odot$ WD. Optically thick winds end $\sim$ 120 days and hydrogen shell-burning stops $\sim$ 200 days after the outburst for the 1.15 $M_\odot$ WD.

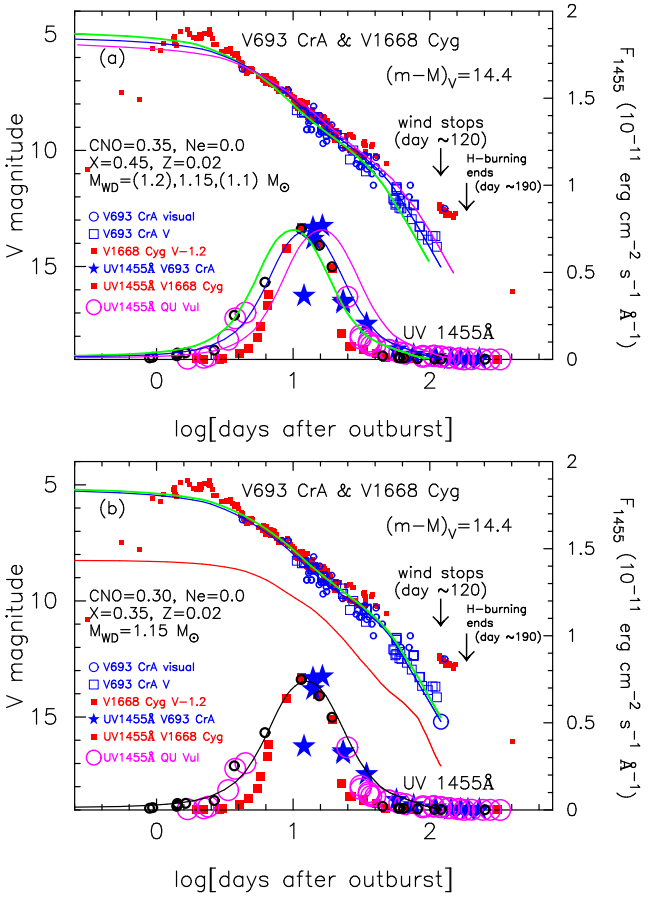

Figure 34. Same as Figure 33, but for CO nova 3. We added the V light curve (red filled squares) of V1668 Cyg. The timescale of V1668 Cyg is squeezed by a factor of $f_s = 0.37$. We also added the UV 1455 Å light curve (magenta large open circles) of QU Vul. The timescale of QU Vul is squeezed by a factor of $f_s = 0.19$. (a) We plot three model light curves of 1.1 $M_\odot$ (magenta solid lines), 1.15 $M_\odot$ (blue solid lines), and 1.2 $M_\odot$ (green solid lines) WDs. Assuming that $(m-M)_V = 14.4$, we plot the V model light curves. (b) Assuming also that $(m-M)_V = 14.4$, we plot three V model light curves of the 1.15 $M_\odot$ WD. Optically thick winds end $\sim$ 120 days and hydrogen shell-burning stops $\sim$ 190 days after the outburst for the 1.15 $M_\odot$ WD.

taken from IAU Circ. Nos. 3590, 3594 and the archive of AAVSO. The V magnitudes are taken from Caldwell (1981), Walker & Marino (1982), IAU Circ. No. 3604, and the *IUE* VFES archive. The UV 1455 Å fluxes are taken from the *IUE* archive (see, e.g., Cassatella et al. 2002).

6.2.1. *Ne nova 1*

Figure 30 shows model light curves of the chemical composition of Ne nova 1 for four different WD masses, i.e., 1.1 (magenta), 1.15 (blue), 1.2 (green), and 1.25 $M_\odot$ (red), as well as observational data. The absolute magnitudes of the free-free emission model light curves are already calibrated in Section 4. Note that we plot the light curve in a linear timescale. In Figure 30(a), we place the UV 1455Å model light curves to run through the observational peak (three blue filled star-marks). The total V model light curve of 1.15 $M_\odot$ WD reasonably fits to the V and visual data, but the UV 1455Å model light curve does deviate largely from the first observational point.

Although we successfully obtained light curve models for V1668 Cyg, QU Vul, V351 Pup, and V1974 Cyg, it seems difficult for V693 CrA to obtain a model that reasonably reproduce both optical and UV 1455Å light curves. In our experience of GQ Mus, we saw that the UV 1455Å light curve sometimes shows sharp pulses above a smooth light curve (see Hachisu et al. 2008). If this UV peak in Figure 30(a) is in such a pulse phase, we may ignore the points and fit our model light curve with other points. Figure 30(b) shows such fittings with the same models as in Figure 30(a). In this figure, we skip the three peak points (three filled star-marks) but adopt the other data.

Now we examine which model is the best from the distance-reddening relations in Figures 31 and 32. The absolute magnitudes of model light curves are already calibrated in Section 4 for Ne Nova 1. Therefore, we directly obtain the distance modulus in V band from fitting between our model light curve and the observation, which are shown in Figure 30, in the order of the WD mass. Equation (1) is plotted in Figures 31 and 32 by blue solid lines. On the other hand, the fitting with the UV 1455Å data gives a relation of Equation (2), which are also plotted in Figures 31 and 32 by magenta solid lines. The

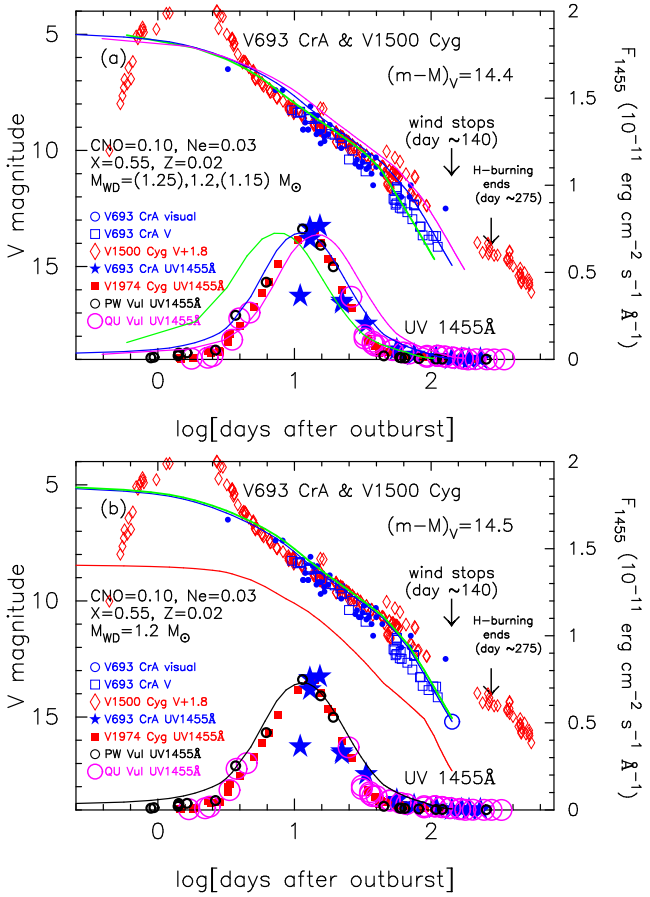

Figure 35. Same as Figure 34, but for Ne nova 2. We added the V (red open diamonds) light curve of V1500 Cyg. The timescale of V1500 Cyg is squeezed by a factor of $f_s = 0.79$. (a) We plot model light curves of 1.15 $M_\odot$ (magenta solid lines), 1.2 $M_\odot$ (blue solid lines), and 1.25 $M_\odot$ (green solid lines) WDs. Assuming that $(m-M)_V = 14.4$, we plot the V model light curves. (b) Assuming that $(m-M)_V = 14.5$, slightly larger than that in Figure 34, we plot three V model light curves of the 1.2 $M_\odot$ WD. Optically thick winds end $\sim$ 140 days and hydrogen shell-burning stops $\sim$ 275 days after the outburst for the 1.2 $M_\odot$ WD.

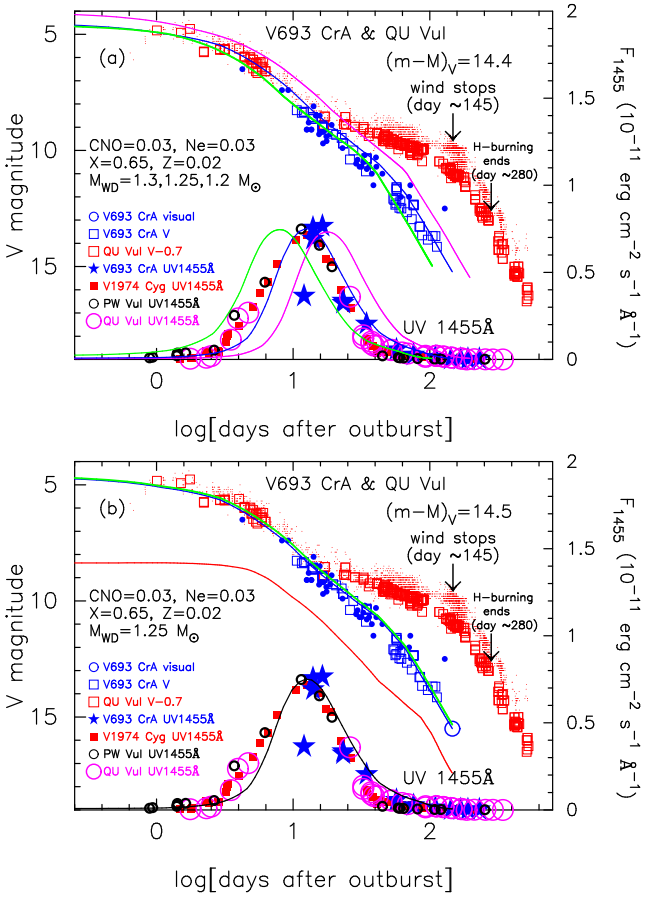

Figure 36. Same as Figure 35, but for Ne nova 3. We added the V (red open squares), visual (red dots), and UV 1455 Å (large magenta open circles) light curves of QU Vul. The timescale of QU Vul is squeezed by a factor of $f_s = 0.25$. (a) We plot three model light curves of 1.2 $M_\odot$ (magenta solid lines), 1.25 $M_\odot$ (blue solid lines), and 1.3 $M_\odot$ (green solid lines) WDs. Assuming that $(m-M)_V = 14.4$, we plot the V model light curves. (b) Assuming that $(m-M)_V = 14.5$, we plot three model light curves of the 1.25 $M_\odot$ WD. Optically thick winds end $\sim$ 145 days and hydrogen shell-burning stops $\sim$ 280 days after the outburst for the 1.25 $M_\odot$ WD.

intersection of these two distance-reddening relations gives a set of (distance, reddening) for V693 CrA. As mentioned in Section 6.1, we obtain a constraint of $E(B-V) = 0.05 \pm 0.05$ and $d = 7.1 \pm 0.7$ kpc. The 1.15 $M_\odot$ WD model can satisfy this constraint both in Figures 31 and 32. Although the intersects for the 1.25 $M_\odot$ WD reasonably satisfy our constraint, its V light curve decays too fast to be comparable with the observation. So, we exclude the 1.25 $M_\odot$ WD. We also exclude the two models of 1.1 and 1.2 $M_\odot$ WDs, because they do not result in a good agreement in Figures 31 and 32. Among the model fittings of the 1.15 $M_\odot$ WD, Figure 30(b) results in a distance modulus of $(m-M)_V = 14.8$, which is larger than $(m-M)_V = 14.4 \pm 0.2$ obtained from the time-stretching method. Therefore, we adopt the 1.15 $M_\odot$ model in Figure 30(a). Our UV 1455Å model light curve runs through the observational peak but skip the first observational point. In what follows, we adopt a similar way, that is, we do not include the first observational point in our UV 1455Å fitting process of V693 CrA but regard the subsequent three points as the peak of UV 1455Å flux.

Figure 33(a) shows V693 CrA as well as other novae which we will discuss later. We plot the light curves in a logarithmic timescale. We see that the 1.15 $M_\odot$ model is the best-fit model among the 1.1, 1.15, and 1.2 $M_\odot$ WD models. In Figure 33(b), we plot the total, free-free emission, and blackbody emission fluxes of the 1.15 $M_\odot$ WD model. Optically thick winds end $\sim$ 120 days and hydrogen shell-burning stops $\sim$ 200 days after the outburst for the 1.15 $M_\odot$ WD. For $(m-M)_V = 14.4$, the total V flux light curve follows the observed V magnitudes of V693 CrA reasonably well. We have obtained a hydrogen-rich envelope mass of $M_{\rm env} = 0.71 \times 10^{-5} M_\odot$ at optical maximum, which corresponds approximately to the ignition mass.

6.2.2. *CO nova 3*

Figure 34(a) shows that the 1.15 $M_\odot$ model is the best-fit model among the 1.1, 1.15, and 1.2 $M_\odot$ WD models. We plot the total, free-free emission, and blackbody emission fluxes of the 1.15 $M_\odot$ WD model in Figure 34(b). Optically thick winds end approximately 120 days and hydrogen shell-burning stops $\sim$ 190 days after the outburst for the 1.15 $M_\odot$ WD. For $(m-M)_V = 14.4$, the total V flux light curve follows the observed V magnitudes of V693 CrA reasonably well. We have obtained a hydrogen-rich envelope mass of $M_{\rm env} = 0.59 \times 10^{-5} M_\odot$ at optical maximum.

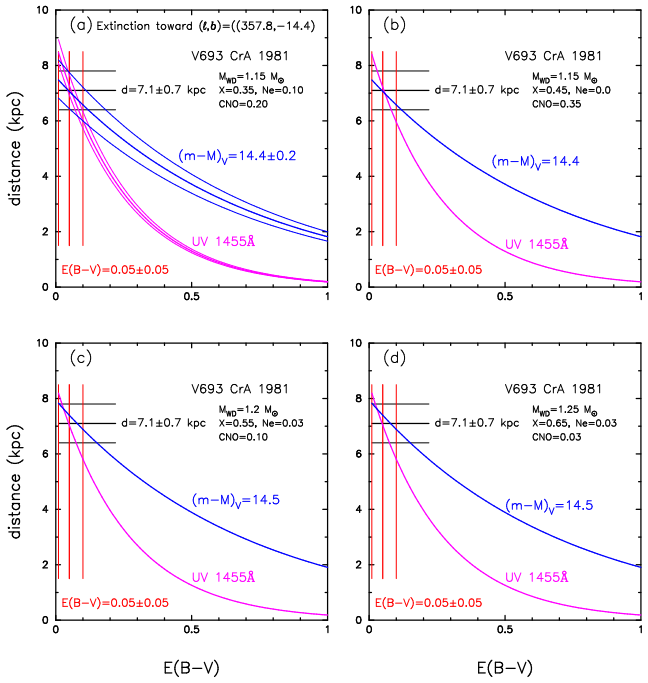

Figure 37. Various distance-reddening relations toward V693 CrA. We plot distance-reddening relations for the chemical composition of (a) Ne nova 1, (b) CO nova 3, (c) Ne nova 2, and (d) Ne nova 3. In panel (a), we plot the results obtained from Equation (1) with $(m-M)_V = 14.4 \pm 0.2$ from our model V light curve fitting and Equation (2) with $F_{1455}^{\rm mod} = 1.55 \times 10^{-11}$ erg cm^{-2} s^{-1} Å^{-1} as the calculated model flux of the upper bound of Figure 33(b) at the distance of 10 kpc and $F_{1455}^{\rm obs} = (2.0 \pm 0.2) \times 10^{-11}$ erg cm^{-2} s^{-1} Å^{-1} as the observed flux corresponding to that of the upper bound in Figure 33(b) from our UV 1455 Å flux fitting. Two other constraints are also plotted, $E(B-V) = 0.05 \pm 0.05$ and $d = 7.1 \pm 0.7$ kpc. See Figures 34(b), 35(b), and 36(b) for model fittings in panels (b), (c), and (d), respectively.

6.2.3. *Ne nova 2*

Figure 35(a) shows that the 1.2 $M_\odot$ model is the best-fit model among the 1.15, 1.2, and 1.25 $M_\odot$ WD models. We plot the total, free-free emission, and blackbody emission fluxes of the 1.2 $M_\odot$ WD model in Figure 35(b). Optically thick winds end approximately 140 days and hydrogen shell-burning stops $\sim$ 275 days after the outburst for the 1.2 $M_\odot$ WD. For $(m-M)_V = 14.5$, the total V flux light curve follows the observed V magnitudes of V693 CrA reasonably well. We have obtained a hydrogen-rich envelope mass of $M_{\rm env} = 0.53 \times 10^{-5} M_\odot$ at optical maximum.

6.2.4. *Ne nova 3*

Figure 36(a) shows that the 1.25 $M_\odot$ model is the best-fit model among the 1.2, 1.25, and 1.3 $M_\odot$ WD models. We plot the total, free-free emission, and blackbody emission fluxes of the 1.25 $M_\odot$ WD model in Figure 36(b). Optically thick winds end approximately 145 days and hydrogen shell-burning stops $\sim$ 280 days after the outburst for the 1.25 $M_\odot$ WD. For $(m-M)_V = 14.5$, the total V flux light curve follows the observed V magnitudes of V693 CrA reasonably well. We have obtained a hydrogen-rich envelope mass of $M_{\rm env} = 0.58 \times 10^{-5} M_\odot$ at optical maximum.

6.3. *Summary of V693 CrA*

Our model light curve fittings give a reasonable set of distance and reddening, $(m-M)_V = 11.4$, $E(B-V) = 0.05$, and $d = 7.1$ kpc, for Ne nova 1 and CO nova 3, but the other two compositions, Ne nova 2 and Ne nova 3, result in a slightly larger distance modulus of $(m-M)_V = 14.5$, as shown in Figure 37, but still consistent with $(m-M)_V = 11.4 \pm 0.2$ and $E(B-V) = 0.05 \pm 0.05$. Because the chemical composition of Ne nova 1 is close to the arithmetic average of the four groups' values mentioned above, we adopt Ne nova 1 for the chemical composition of V693 CrA. Thus, we summarize the results of our light curve fittings as follows (see also Table 6): $(m-M)_V = 14.4$, $E(B-V) = 0.05$, $d = 7.1$ kpc, $M_{\rm WD} = 1.15\ M_\odot$, and $M_{\rm env} = 0.71 \times 10^{-5}\ M_\odot$ at optical maximum. The contribution of photospheric emission is rather small, and it affects the light curve fitting very little. Therefore, we can reproduce the optical light curves of V693 CrA using only the free-free emission light curves.

6.4. *Comparison with previous results*

Wanajo et al. (1999) estimated the WD mass from fitting their nuclear synthesis results with the abundance pattern determined by Vanlandingham et al. (1997). They suggested the WD mass of 1.05 $M_\odot$. Downen et al. (2013) estimated the WD mass of V693 CrA to be $M_{\rm WD} < 1.3\ M_\odot$ from the abundance analysis similar to Wanajo et al. (1999).

Kato & Hachisu (2007) estimated the WD mass and distance of V693 CrA to be 1.3 $M_\odot$ and 4.4 kpc based on the optically thick wind model. They fitted their UV 1455Å model light curves with the observation. Because they adopted a super-Eddington luminosity model of artificially reduced effective opacity (based on an assumption of porous structure of hydrogen-rich envelope), the early timescale of the nova evolution is not the same between their models and ours. This is the reason that they adopted the 1.3 $M_\odot$ WD, which is much larger than our new estimate of 1.15 $M_\odot$. They adopted the reddening of $E(B-V) = 0.20$ and obtained the distance of 4.4 kpc, which is shorter than our new estimate of 7.1 kpc.

7. V1974 CYG 1992

We reanalyzed the light curves of V1974 Cyg including the effect of photospheric emission, which is not considered in Hachisu & Kato (2006, 2010, 2014). We obtained a distance modulus of $(m-M)_V = 12.2 \pm 0.1$ for V1974 Cyg using our time-stretching method (see Appendix A) and other estimates cited in Hachisu & Kato (2014). In the following analyses, we assume that $(m-M)_V = 12.2$. The chemical composition of V1974 Cyg was estimated by Austin et al. (1996), Hayward et al. (1996), Arkhipova et al. (1997), and Vanlandingham et al. (2005) to be $X = 0.19$ – 0.55 and $X_{\rm CNO} = 0.12$ – 0.375 (see Table 1). Because these values are so scattered, we use all six of the chemical compositions in Table 2, i.e., Ne nova 1, Ne nova 2, Ne nova 3, CO nova 2, CO nova 3, and CO nova 4.

7.1. *Light curve fittings of V1974 Cyg*

Figures 18, 23, 38, 39, 40, 41, and 42 show our model light curve fittings for six chemical compositions. In Figures 38 – 42, the visual (red small dots) data are taken from the AAVSO archive; the V magnitudes (blue open circles) are from Chochol et al. (1993); the supersoft X-ray data (green filled squares) are from Krautter et al. (1996); the UV 1455 Å data (red filled squares) are from Cassatella et al. (2002). The supersoft X-ray phase started $\sim$ 250 days after the outburst and that is identified to be the epoch when optically

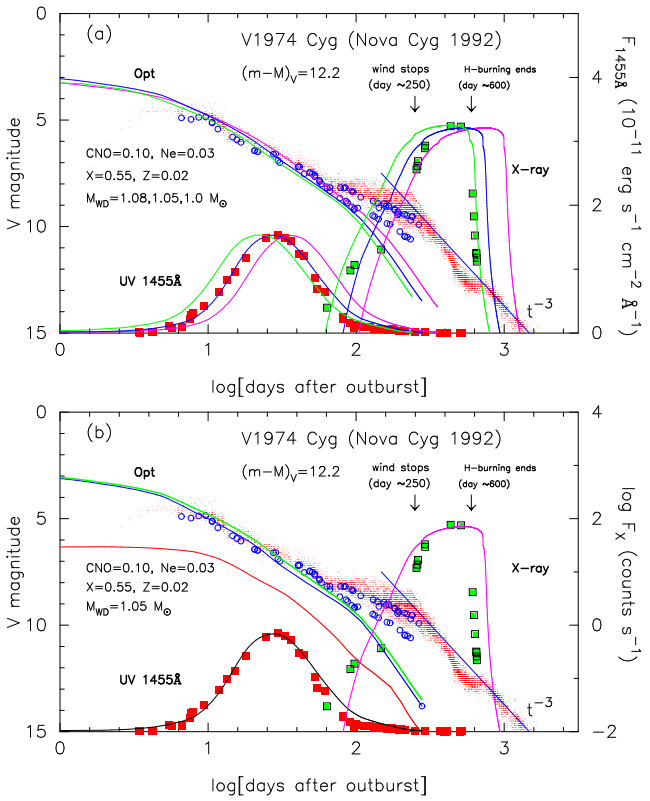

Figure 38. Same as Figure 13, but for V1974 Cyg. (a) Model light curves of 1.0 $M_\odot$ (magenta solid lines), 1.05 $M_\odot$ (blue solid lines), and 1.08 $M_\odot$ (green solid lines) WDs with Ne nova 2. We indicate two epochs, which are observationally suggested, by large downward arrows: the end of optically thick winds and the end of hydrogen shell-burning. Assuming that $(m-M)_V$ = 12.2, we plot the V model light curves. (b) Assuming also that $(m-M)_V$ = 12.2, we plot three model light curves of the 1.05 $M_\odot$ WD. The end of hydrogen shell-burning of the 1.05 $M_\odot$ WD model is not consistent with the observation ($\sim$ 600 days).

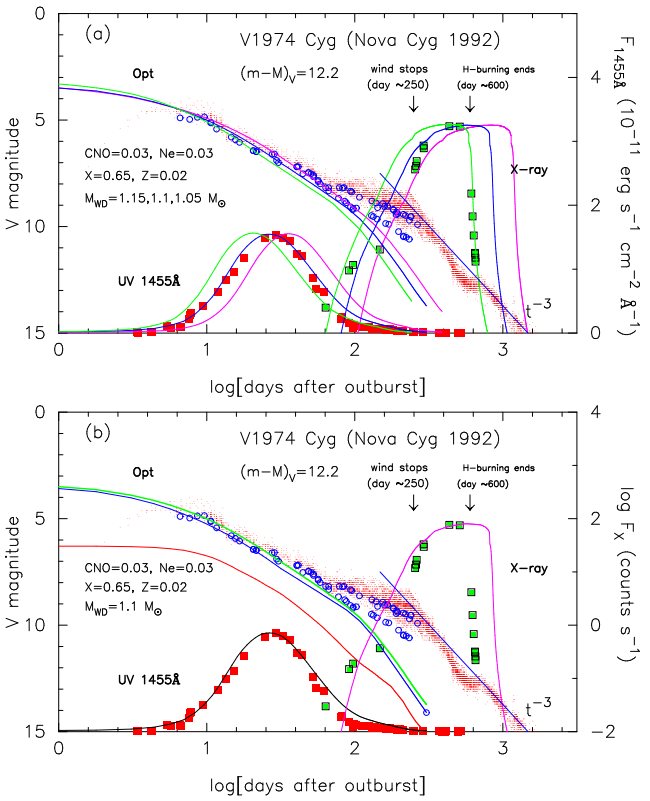

Figure 39. Same as Figure 38, but for Ne nova 3. (a) Model light curves of 1.05 $M_\odot$ (magenta solid lines), 1.1 $M_\odot$ (blue solid lines), and 1.15 $M_\odot$ (green solid lines) WDs. Assuming that $(m-M)_V$ = 12.2, we plot the V model light curves. (b) Assuming also that $(m-M)_V$ = 12.2, we plot three model light curves of the 1.1 $M_\odot$ WD. The end of hydrogen shell-burning is not consistent with the observation.

thick winds stop (Hachisu & Kato 2006, 2010). The hydrogen shell-burning ended $\sim$ 600 days after the outburst, corresponding to the sharp decay of supersoft X-ray flux.

Figure 18(a) shows that the timescale of V1974 Cyg is almost the same as that of V351 Pup and we chose the 1.0 $M_\odot$ WD model as the best-fit model from the UV 1455 Å fitting (Ne nova 1). However, Figure 18(b) shows that the hydrogen shell-burning on the 1.0 $M_\odot$ WD model ended too earlier than the observation. Therefore, we examine other cases of the chemical composition.

Figure 38(a) shows that the 1.05 $M_\odot$ WD model is the best-fit model from the UV 1455 Å model light curve fitting (Ne nova 2). The total V light curve model agrees well with the V magnitude observation, and the shape of UV 1455 Å light curve model fits the observation well. In this case, however, the end of hydrogen shell burning is not consistent with the observation as shown in Figure 38(b).

Figure 39(a) suggests that the 1.1 $M_\odot$ WD model is the best-fit model from the UV 1455 Å model light curve fitting (Ne nova 3). In this case, too, the end of hydrogen shell burning is not consistent with the observation as shown in Figure 39(b).

Figure 40(a) shows that the 0.95 $M_\odot$ WD model is the best-fit model from the UV 1455 Å light curve fitting (CO nova 2). Figure 40(b) shows that optically thick winds and hydrogen shell burning end approximately 250 days and 600 days after the outburst, respectively, which is consistent with the X-ray decay time. The total V light curve model agrees well with the V magnitude observation, and the shape of the UV 1455 Å light curve model fits the observation reasonably well.

Figure 41(a) shows that the 0.98 $M_\odot$ WD model is the best-fit model from the UV 1455 Å model light curve fitting (CO nova 3). Figure 41(b) shows that the V magnitude observation and the shape of the UV 1455 Å light curve model fit the observation well. The two epochs are consistent with the X-ray observation; that is, optically thick winds and hydrogen shell burning end approximately 250 days and 600 days after the outburst, respectively.

Figure 42(a) shows that the 1.0 $M_\odot$ WD model is the best-fit model from the UV 1455 Å model light curve fitting (CO nova 4). Figure 42(b) shows that the total V light curve model agrees well with the V magnitude observation, and the shape of the UV 1455 Å light curve model fits the observation well. In this case, however, the end of hydrogen shell burning is not consistent with the observation as shown in Figure 42(b).

It should be noted that our UV 1455Å light curve represents the early phase development of the pseudophotosphere while the X-ray light curve constrains the later phase development. Therefore, if the X-ray data as well as UV 1455Å data are available, we could select a better model to constrain the abundance.

7.2. *Distance and reddening toward V1974 Cyg*

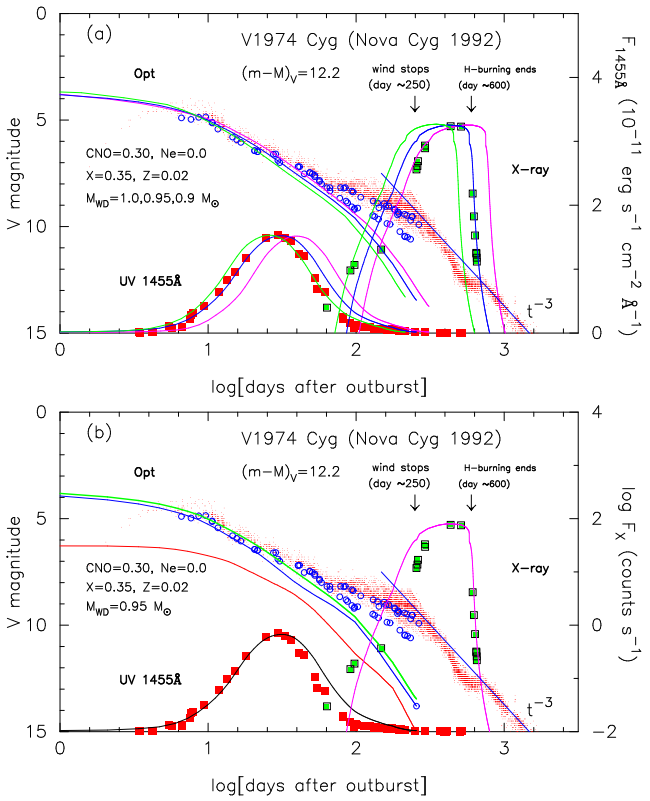

Figure 40. Same as Figure 38, but for CO nova 2. (a) Model light curves of 0.9 $M_\odot$ (magenta solid lines), 0.95 $M_\odot$ (blue solid lines), and 1.0 $M_\odot$ (green solid lines) WDs. Assuming that $(m-M)_V$ = 12.2, we plot the V model light curves. (b) Assuming also that $(m-M)_V$ = 12.2, we plot three model light curves of the 0.95 $M_\odot$ WD. Optically thick winds and hydrogen shell-burning end approximately 250 days and 600 days after the outburst, respectively, for the 0.95 $M_\odot$ WD, which are both consistent with the observation.

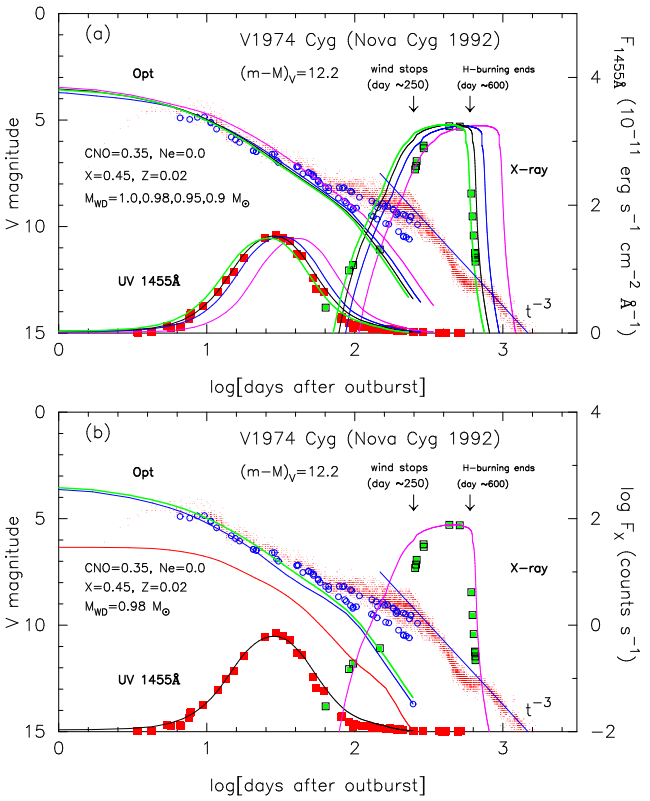

Figure 41. Same as Figure 38, but for CO Nova 3. (a) Model light curves of 0.9 $M_\odot$ (magenta solid lines), 0.95 $M_\odot$ (blue solid lines), 0.98 $M_\odot$ (black thin solid lines), and 1.0 $M_\odot$ (green solid lines) WDs. Assuming that $(m-M)_V$ = 12.2, we plot the V model light curves. (b) Assuming also that $(m-M)_V$ = 12.2, we plot three model light curves of the 0.98 $M_\odot$ WD. In this case, the two epochs are consistent with the observation.

We obtain two distance-reddening relations to V1974 Cyg from the two model light curve fittings (V and UV 1455 Å), which are plotted in Figures 43 and 44. The thick blue solid line shows the result obtained using Equation (1) with $(m-M)_V = 12.2 \pm 0.1$. The thick magenta solid line shows the result obtained using Equation (2) with $F_{1455}^{\rm mod} = 1.53 \times 10^{-11}$ erg cm^{-2} s^{-1} Å^{-1} as the upper bound of Figure 18(b) at a distance of 10 kpc and $F_{1455}^{\rm obs} = (5.0 \pm 0.3) \times 10^{-11}$ erg cm^{-2} s^{-1} Å^{-1} as the corresponding observed flux. These two relations are indicated in Figure 43(a) by flanking thin solid lines.

Figure 43(a) shows another distance-reddening relation toward V1974 Cyg: that given by Marshall et al. (2006), where the galactic coordinates of V1974 Cyg are (l,b) = (89.°1338, 7.°8193). The four sets of data points with error bars correspond to the distance-reddening relations in four directions close to V1974 Cyg: (l,b) = (89.°00, 7.°75) (red open squares), (89.°25, 7.°75) (green filled squares), (89.°00, 8.°00) (blue asterisks), and (89.°25, 8.°00) (magenta open circles), the data for which are taken from Marshall et al. (2006). We also add Green et al.'s (2015) relation (black thick solid line). These trends are consistent with the cross at $d \approx 1.8$ kpc and $E(B-V) \approx 0.30$.

Chochol et al. (1997a) estimated the distance to V1974 Cyg as $d = 1.77 \pm 0.11$ kpc from an expansion parallax method. Here, we adopted $d = 1.8 \pm 0.1$ kpc (black horizontal solid line flanked by thin solid lines) after Chochol et al. The reddening was also estimated by many researchers. Austin et al. (1996) obtained the reddening toward V1974 Cyg mainly on the basis of the UV and optical line ratios for days 200 through 500, i.e., $E(B-V) = 0.3 \pm 0.1$. The NASA/IPAC galactic dust absorption map gives $E(B-V) = 0.35 \pm 0.01$ in the direction toward V1974 Cyg. These are all consistent with the above observational estimates, that is, $d = 1.8 \pm 0.1$ kpc and $E(B-V) = 0.3 \pm 0.05$.

For Ne nova 2, Ne nova 3, CO nova 2, CO nova 3, and CO nova 4, we obtain a reasonable set of $d \sim 1.8$ kpc and $E(B-V) \sim 0.30$, as shown in Figures 43(b), 43(c), 44(a), 44(b), and 44(c), respectively.

7.3. *Summary of V1974 Cyg*

Our light curve fittings of the V and UV 1455 Å fluxes give a reasonable set of (distance, reddening)=$(d, E(B-V))$ = $(1.8 \pm 0.1$ kpc$, 0.30 \pm 0.05)$ for all six chemical compositions. The reddening and distance are consistent with the results presented in the previous subsection (Section 7.2). We obtain a chemical composition close to that of CO nova 2 or CO nova 3 from X-ray flux fittings because the two epochs of the model light curve are consistent with the X-ray observation; that is, optically thick winds and hydrogen shell burning end approximately 250 days and 600 days after the outburst, respectively. It should be noted again that enrichment of neon with unchanged hydrogen and CNO mass fractions affects the nova model light curves very little. Therefore, we cannot select the best-fit $X_{\rm Ne}$ only from our model light curve analysis.

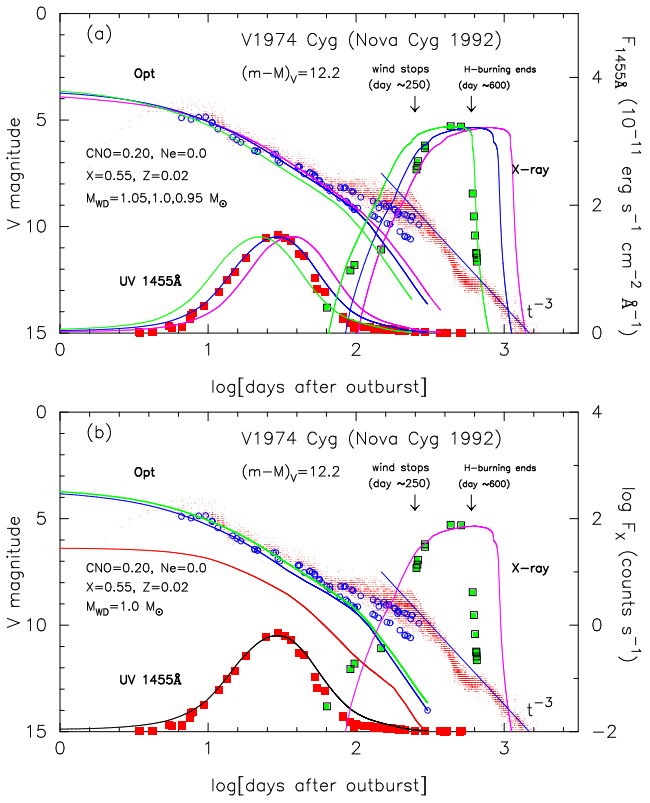

Figure 42. Same as Figure 38, but for CO nova 4. (a) Model light curves of 0.95 $M_\odot$ (magenta solid lines), 1.0 $M_\odot$ (blue solid lines), and 1.05 $M_\odot$ (green solid lines) WDs. Assuming that $(m-M)_V = 12.2$, we plot the V model light curves. (b) Assuming also that $(m-M)_V = 12.2$, we plot three model light curves of the 1.0 $M_\odot$ WD. In this case, however, the end of hydrogen shell-burning is not consistent with the observation.

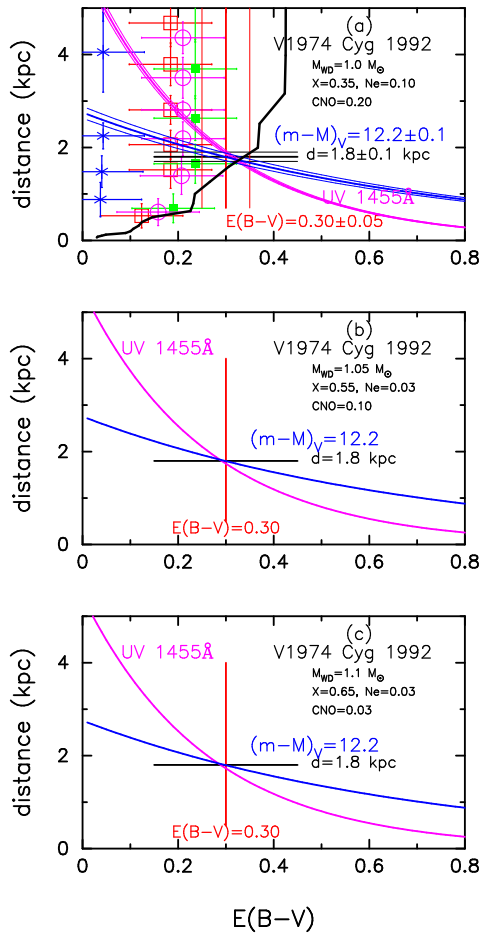

Figure 43. Distance-reddening relations toward V1974 Cyg calculated from the V (blue solid lines) and UV 1455Å (magenta solid lines) light curve fittings: (a) 1.0 $M_\odot$ WD with the chemical composition of Ne nova 1, (b) 1.05 $M_\odot$ WD with Ne nova 2, and (c) 1.1 $M_\odot$ WD with Ne nova 3. The red vertical solid lines show the reddening estimate of $E(B-V) = 0.3 \pm 0.05$, whereas the black horizontal solid lines correspond to the distance estimate of $d = 1.8 \pm 0.1$ kpc. Panel (a) also shows the distance-reddening relations in four directions close to V1974 Cyg, $(l,b) = (89.^\circ1338, 7.^\circ8193)$: $(l,b) = (89.^\circ00, 7.^\circ75)$ (red open squares), $(89.^\circ25, 7.^\circ75)$ (green filled squares), $(89.^\circ00, 8.^\circ00)$ (blue asterisks), and $(89.^\circ25, 8.^\circ00)$ (magenta open circles), the data for which are taken from Marshall et al. (2006). We also add Green et al.'s (2015) relation (black solid line). See text for more detail.

We suppose that our model light curves do follow the observation well for other chemical compositions, for example, of $X = 0.35$, $X_{\rm CNO} = 0.30$, $Y = 0.33 - X_{\rm Ne}$, $Z = 0.02$ (CO nova 2 type), and any $X_{\rm Ne} \approx 0.0$–0.1, or of $X = 0.45$, $X_{\rm CNO} = 0.35$, $Y = 0.18 - X_{\rm Ne}$, $Z = 0.02$ (CO nova 3 type), and any $X_{\rm Ne} \approx 0.0$–0.1. If we adopt the composition of CO nova 3 type, we obtain $M_{\rm WD} = 0.98\ M_\odot$ and $M_{\rm env} = 1.28 \times 10^{-5}\ M_\odot$ at optical maximum (see Table 6).

7.4. *Comparison with previous results*

Several groups tried to estimate the WD mass of V1974 Cyg. Paresce et al. (1995) presented a result of $0.75 - 1.1\ M_\odot$ from various empirical relations on novae. Retter et al. (1997) also obtained a mass range of $M_{\rm WD} = 0.75 - 1.07\ M_\odot$ based on the precessing disk model of superhump phenomenon. Wanajo et al. (1999) presented nuclear burning yields on the ONe core and compared them with the observed pattern by Austin et al. (1996). They suggested the WD mass of $M_{\rm WD} \lesssim 1.15\ M_\odot$.

Sala & Hernanz (2005) calculated static sequences of hydrogen shell-burning and compared them with the evolutional speed of post-wind phase for V1974 Cyg. They suggested that the WD mass is 0.9 $M_\odot$ for 50% mixing of a solar composition envelope with an ONe core (i.e., $X = 0.35$, $X_{\rm CNO} = 0.25$, and $X_{\rm Ne} = 0.16$), or 1.0 $M_\odot$ for 25% mixing (i.e., $X = 0.53$, $X_{\rm CNO} = 0.13$, and $X_{\rm Ne} = 0.08$). Their two cases resemble our Ne nova 1 and Ne nova 2, respectively. These WD masses are consistent with our new estimates.

Hachisu & Kato (2006) proposed the free-free emission model for optical light curves and applied to the V1974 Cyg light curve. They obtained the WD mass of 0.95 $M_\odot$ based on the UV 1455Å and supersoft X-ray light curve fittings. They could not fix the proportionality constant C in their models and did not estimate the distance modulus. Instead, they adopted the distance of 1.8 kpc and the reddening of $E(B-V) = 0.32$, taken from Chochol et al. (1997a).

Kato & Hachisu (2007) estimated the WD mass and distance of V1974 Cyg to be 1.05 $M_\odot$ and 1.8 kpc, respectively, based on the optically thick wind model. They fitted their UV 1455Å model light curves with the observation. Because they adopted a super-Eddington luminosity model of reduced effective opacity, the early timescale of the nova evolution is not the same between their models and ours as explained in Section 6.4. This is the reason that they adopted the 1.05 $M_\odot$ WD, which is slightly larger than our new estimate of 0.98 $M_\odot$. They adopted the reddening of $E(B-V) = 0.32$ and obtained the distance of 1.8 kpc.

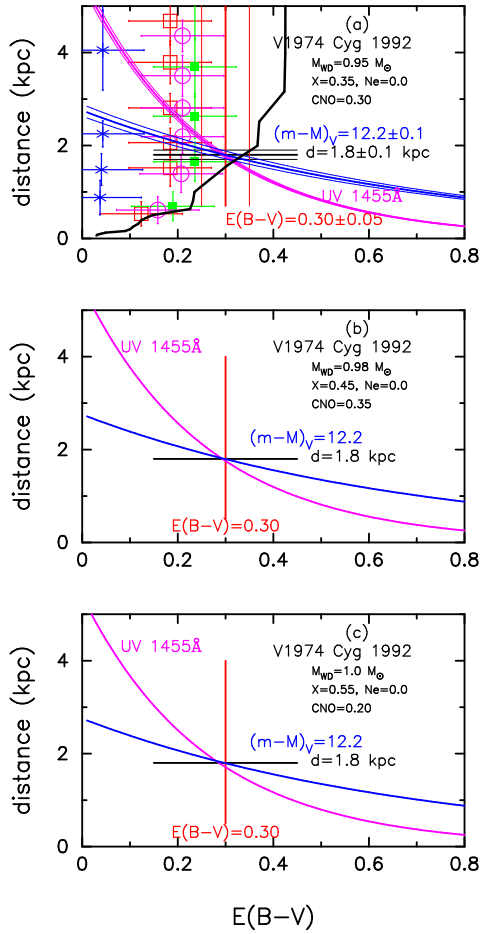

Figure 44. Same as Figure 43, but for (a) 0.95 $M_\odot$ WD with CO Nova 2, (b) 0.98 $M_\odot$ WD with CO Nova 3, and (c) 1.0 $M_\odot$ WD with CO Nova 4.

Using the time-stretching method of the universal decline law, Hachisu & Kato (2010) obtained the absolute magnitude of their free-free emission model light curves and applied their light curve model to V1974 Cyg and obtained the distance modulus in the V band as $(m-M)_V = 12.2$ and the WD mass of 0.95 $M_\odot$. Introducing the effect of photospheric emission as well as free-free emission in the present paper, we reanalyzed the optical light curve of V1974 Cyg and fixed $M_{\rm WD} = 0.98\ M_\odot$ and $(m-M)_V = 12.2$ for the chemical composition of CO nova 3.

8. DISCUSSION

8.1. *White dwarf masses of neon novae*

We obtained the WD masses of neon novae, i.e., $M_{\rm WD}$ = 0.82 – 0.96 $M_\odot$ for QU Vul in Section 3, $M_{\rm WD}$ = 0.98 – 1.1 $M_\odot$ for V351 Pup in Section 4, $M_{\rm WD} = 1.13 - 1.28\ M_\odot$ for V382 Vel in Section 5, $M_{\rm WD} = 1.15 - 1.25\ M_\odot$ for V693 CrA in Section 6, and $M_{\rm WD} = 0.95 - 1.1\ M_\odot$ for V1974 Cyg in Section 7. On the other hand, a lower mass bound of $\sim 1.07\ M_\odot$ for natal ONe WDs with a CO-rich mantle (as well as a thin helium-rich layer on the CO mantle) was obtained by Umeda et al. (1999) from their evolution calculation. A different estimate, $\sim 1.0\ M_\odot$, was also obtained by Weidemann (2000) from discussion on the initial/final mass relation of remnants in open clusters. Gil-Pons et al. (2003) presented their evolution calculations showing that a CO-rich mantle is more massive for lower-mass ONe cores, i.e., as massive as $\sim 0.1\ M_\odot$ for a 1.1 $M_\odot$ WD. Therefore, we suppose that the lower mass bound for natal pure ONe cores without a CO-rich mantle is $\sim 1.0\ M_\odot$. So we conclude that the WD mass of QU Vul, 0.82 – 0.96 $M_\odot$, is smaller than the minimum mass of ONe core. This suggests that the WD in QU Vul has lost at least $\sim 0.1\ M_\odot$ of mass since its birth.

The WD masses of V351 Pup and V1974 Cyg are close to this lower bound of natal pure ONe cores, whereas those of V382 Vel and V693 CrA are much above this lower bound. The WD mass of V1668 Cyg (not a neon nova) was also estimated in Section 2 to be $M_{\rm WD} = 0.98 - 1.1\ M_\odot$, which is on the lower mass bound of natal pure ONe cores. We point out two possibilities. One is that at its birth, the WD mass was close to the upper mass bound of natal CO cores, $< 1.07\ M_\odot$ (e.g., Umeda et al. 1999), and it decreased to the present value. The other is that at its birth, the WD mass was above 1.07 $M_\odot$, and it decreased to the present value, but the CO-rich mantle is still surrounding the ONe core.

Note that strong neon emission lines were also observed in the very slow nova V723 Cas, although it was not identified as a neon nova. Iijima (2006) estimated its neon mass fraction to be $X_{\rm Ne} = 0.052$, which is comparable to the values of 0.06 for V1974 Cyg (Vanlandingham et al. 2005), 0.03–0.038 for V838 Her (Vanlandingham et al. 1997; Schwarz et al. 2007), 0.043 for V382 Vel (Shore et al. 2003), and 0.032–0.040 for QU Vul (Saizar et al. 1992; Schwarz 2002) as listed in Table 1. Unlike that of the above novae, the WD mass of V723 Cas was estimated to be as small as $M_{\rm WD}$ = 0.5–0.55 $M_\odot$ from optical, UV 1455 Å, and X-ray light curve fittings (Hachisu & Kato 2015). It could be a CO WD, if the strong neon emission lines are not direct evidence of an ONe core.

Livio & Truran (1994) proposed an explanation of modest neon enrichments for such low mass WDs. They grouped the 18 classical novae into three classes on the basis of the abundance characteristics: class 1 that show a modest enrichment in heavy elements but a large enrichment in helium; class 2 that show a high enrichment in CNO nuclei and sometimes a modest enrichment in neon; class 3 which show quite extreme enrichments in both neon and heavier elements (than neon). Class 3 includes V693 CrA, V1370 Aql, and QU Vul. They identified these class 3 novae unambiguously as "the neon novae," which require dredge-up from an underlying ONe WD. Class 2 includes DQ Her, V1500 Cyg, V1668 Cyg, GQ Mus, PW Vul, V842 Cen, V827 Her, and V2214 Oph. These systems show considerable CNO enrichment and sometimes a modest enrichment in neon and a range in helium concentration from approximately solar to twice solar. Class 1 includes T Aur, RR Pic, HR Del, V977 Sco, V443 Sct, and LMC 1990#1. These show a modest enrichment in CNO nuclei but a large enrichment in helium, and a modest enrichment in neon appears in some of these novae. For class 1 and class 2 novae, Livio & Truran (1994) discussed that their modest neon enrichment can be explained by a concentration of ^{22}Ne in the underlying CO core. In the pre-nova evolution, intermediate mass stars convert most of the initial carbon, nitrogen, and oxygen isotopes into ^{14}N in the CNO cycle during their main-sequence period. During the ensuing helium burning phase, some of this ^{14}N is transformed into ^{22}Ne by $^{14}{\rm N}(\alpha,\gamma)^{18}{\rm F}(e^+\nu)^{18}{\rm O}(\alpha,\gamma)^{22}{\rm Ne}$. Dredge-up of the CO core material could accompany enrichment of ^{22}Ne. We suppose that V723 Cas belongs to the class 1 defined by Livio & Truran, because the optical light curve of V723 Cas is very sim-

Table 6
Nova parameters

object name	$E(B-V)$	$(m-M)_V$	distance (kpc)	WD mass ($M_\odot$)	envelope mass[a] ($10^{-5}M_\odot$)	best-fit abundance
V1668 Cyg	0.30	14.6	5.4	0.98	1.38	CO nova 3
V1974 Cyg	0.30	12.3	1.8	0.98	1.28	CO nova 3[b]
QU Vul	0.55	13.6	2.4	0.96	2.44	Ne nova 3
V351 Pup	0.45	15.1	5.5	1.0	1.98	Ne nova 1
V382 Vel	0.15	11.5	1.6	1.23	0.48	Ne nova 2
V693 CrA	0.05	14.4	7.1	1.15	0.71	Ne nova 1

[a] Mass of the hydrogen-rich envelope at optical maximum calculated from each nova model.
[b] V1974 Cyg was identified as a neon nova. Note, however, that enrichment of neon with unchanged hydrogen and CNO mass fractions affects the nova light curves very little in our model light curves because neon is not relevant to either nuclear burning (the CNO cycle) or the opacity.

Table 7
Extinctions and Distances of Selected Novae

Object	Year	$E(B-V)$	$(m-M)_V$	distance (kpc)	reference[a]
OS And	1986	0.15	14.7	7.0	1
V603 Aql	1918	0.07	7.2	0.25	2,3
V1370 Aql	1982	0.35	15.2	6.7	1
V1419 Aql	1993	0.50	14.6	4.1	1
V705 Cas	1993	0.45	13.4	2.5	4
V723 Cas	1995	0.35	14.0	3.85	4,5
IV Cep	1971	0.70	14.7	3.2	1
V693 CrA	1981	0.05	14.4	7.1	6
V1500 Cyg	1975	0.45	12.3	1.5	1
V1668 Cyg	1978	0.30	14.6	5.4	6
V1974 Cyg	1992	0.30	12.2	1.8	1,6,7
V2274 Cyg	2001#1	1.35	18.7	8.0	1
HR Del	1967	0.15	10.4	0.97	1,4,8
DQ Her	1934	0.10	8.2	0.39	3,9
V446 Her	1960	0.40	11.7	1.2	1
V533 Her	1963	0.05	10.8	1.3	1
GQ Mus	1983	0.45	15.7	7.3	4
RS Oph	1958	0.65	12.8	1.4	1
GK Per	1901	0.30	9.3	0.48	3,10
RR Pic	1925	0.04	8.7	0.52	3
V351 Pup	1991	0.45	15.1	5.5	6
T Pyx	1966	0.25	14.2	4.8	1,12
V443 Sct	1989	0.40	15.5	7.1	1
V475 Sct	2003	0.55	15.6	6.0	1
FH Ser	1970	0.60	11.7	0.93	1
V5114 Sgr	2004	0.45	16.5	10.5	1
V5558 Sgr	2007	0.70	13.9	2.2	1
V382 Vel	1999	0.15	11.5	1.6	6
LV Vul	1968#1	0.60	11.9	1.0	1
NQ Vul	1976	1.00	13.6	1.3	1
PU Vul	1979	0.30	14.3	4.7	1,11
PW Vul	1984#1	0.55	13.0	1.8	4
QU Vul	1984#2	0.55	13.6	2.4	6
QV Vul	1987	0.60	14.0	2.7	1

[a] 1–Hachisu & Kato (2014), 2–Gallagher & Holm (1974), 3–Harrison et al. (2013), 4–Hachisu & Kato (2015), 5–Lyke & Campbell (2009), 6–Present paper, 7–Chochol et al. (1997a), 8–Harman & O'Brien (2003), 9–Verbunt (1987), 10–Wu et al. (1989), 11–Kato et al. (2012), 12–Sokoloski et al. (2013).

ilar to those of RR Pic and HR Del (e.g., Hachisu & Kato 2015).

8.2. *Color-color diagram of nova outbursts*

Hachisu & Kato (2014) proposed a new method of determining the reddening of classical novae. They identified a general course of the color evolution track in the $(B-V)_0$-$(U-B)_0$ diagram and determined the reddening of novae by comparing the track of a target nova with the general course. Our target neon novae also show a similarity in the $B-V$ and $U-B$ color evolutions. We made the color-color diagrams of our five neon novae in Figure 11, that is, 11(a) for QU Vul, 11(b) for V351 Pup and V1974 Cyg, 11(c) for V382 Vel, and 11(d) for V693 CrA.

Hachisu & Kato (2014) showed that novae evolve along the nova-giant sequence in the pre-maximum and near-maximum phases. This sequence is parallel to but $\Delta(U-B) \approx$ –0.2 mag bluer than the supergiant sequence, as indicated by green solid lines in Figure 11. After optical maximum, a nova quickly comes back blueward along the nova-giant sequence and reaches the point of free-free emission ($(B-V)_0$ = –0.03, $(U-B)_0$ = –0.97; this point is denoted by a black open diamond), which coincides with the intersection of the blackbody sequence and the nova-giant sequence, and remains there for a while. Then the color evolves leftward (blueward in $B-V$ but almost constant in $U-B$), owing mainly to the development of strong emission lines.

Figure 11(a) shows the color-color evolution of QU Vul. The data are taken from Bergner et al. (1988) (red filled circles) and Rosino et al. (1992) (blue open circles). We obtained $E(B-V) = 0.55 \pm 0.05$.

Figure 11(b) shows that of V351 Pup and V1974 Cyg. We plot the data for V351 Pup taken from Bruch (1992) (large red filled circles) and IAU Circulars (blue open circles), as well as the data for V1974 Cyg (small magenta dots), which are taken from Chochol et al. (1993). The track of V351 Pup is similar to that of V1974 Cyg. We obtained $E(B-V) = 0.45 \pm 0.05$ for V351 Pup as well as $E(B-V) = 0.30 \pm 0.05$ for V1974 Cyg (Hachisu & Kato 2014).

Figure 11(c) shows that of V382 Vel. The color data for V382 Vel are taken from IAU Circulars (red filled circles). We obtained $E(B-V) = 0.15 \pm 0.05$.

Figure 11(d) shows that of V693 CrA. The data for V693 CrA are taken from Caldwell (1981) (red filled circles), Walker & Marino (1982) (magenta open diamond), and IAU Circulars (blue open circle). We obtained $E(B-V) = 0.05 \pm 0.05$.

These reddening values of $E(B-V)$ are very consistent with those obtained in the previous sections.

8.3. *Color-magnitude diagram of nova outbursts*

Figure 45 summarizes the color-magnitude diagrams for six well-observed novae. The figure is similar to Figure 39 of Hachisu & Kato (2014), but we added the track of V1974 Cyg assuming that $(m-M)_V$ = 12.2 and $E(B-V)$ = 0.30. We revised the distance modulus of $(m-M)_V$ = 14.6 and the color excess of $E(B-V)$ = 0.30 for V1668 Cyg, as obtained in Section 2. The other four novae are the same as those in Figure 39 of Hachisu & Kato (2014), i.e., $(m-M)_V$ = 12.3

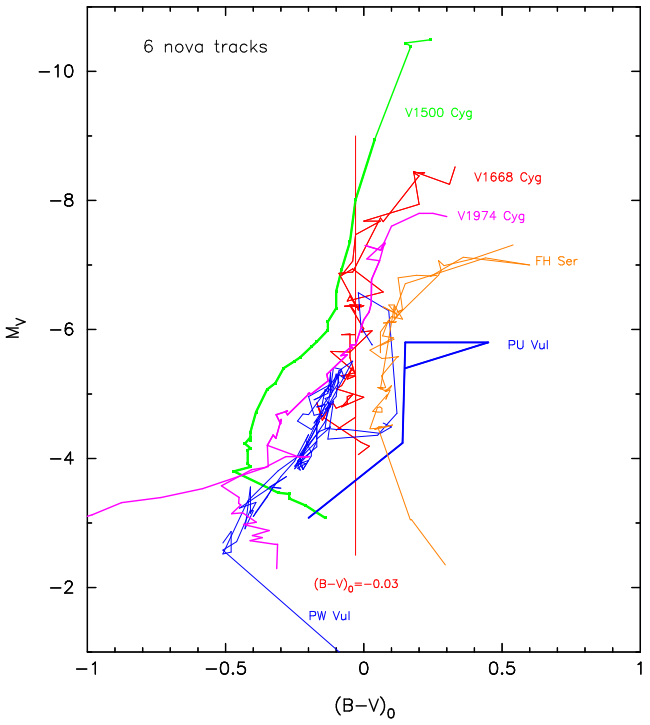

Figure 45. Color-magnitude diagrams of six well-observed novae in outburst, i.e., V1500 Cyg, V1668 Cyg, V1974 Cyg, PW Vul, FH Ser, and PU Vul, in the order of the nova speed class. Here, $(B-V)_0$ is the dereddened color of $B-V$, and M_V is the absolute V magnitude. The red vertical line of $(B-V)_0 = -0.03$ indicates the color of optically thick free-free emission. The figure is a similar one to Figure 39 of Hachisu & Kato (2014), but the tracks of V1974 Cyg and V1668 Cyg are revised. See text for more detail. The sources of these six nova data were the same as those cited in Hachisu & Kato (2014). We adopt $E(B-V)$ = 0.45, 0.30, 0.30, 0.55, 0.60, 0.30, and $(m-M)_V$ = 12.3, 14.6, 12.2, 13.0, 11.7, 14.3, for V1500 Cyg, V1668 Cyg, V1974 Cyg, PW Vul, FH Ser, and PU Vul, respectively.

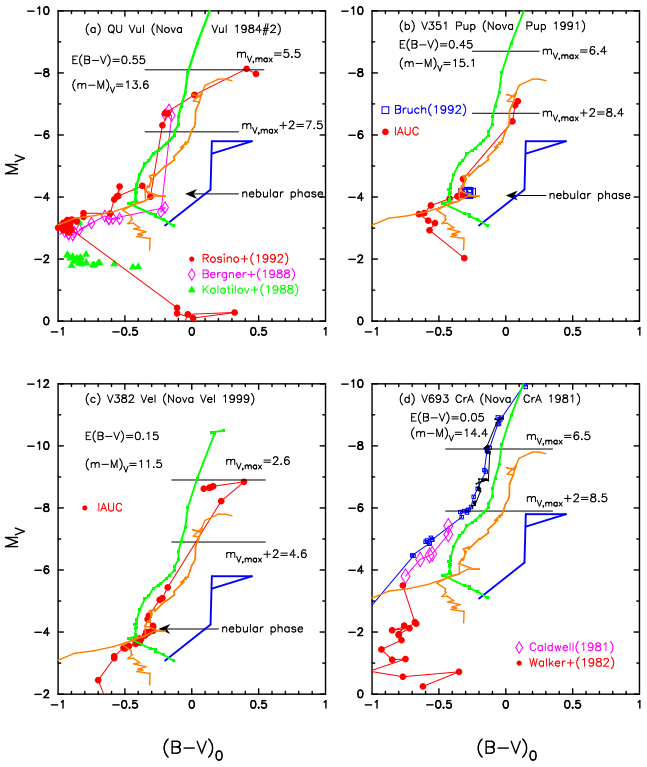

Figure 46. Color-magnitude diagrams of four neon novae in outburst as well as the tracks of V1500 Cyg (green thick solid line), V1974 Cyg (orange thick solid line), and PU Vul (blue thick solid line). The data of V1500 Cyg, V1974 Cyg, and PU Vul are the same as those in Figure 45. (a) QU Vul for $(m-M)_V$ = 13.6 and $E(B-V)$ = 0.55. The data of QU Vul are taken from Bergner et al. (1988), Kolotilov (1988), and Rosino et al. (1992). (b) V351 Pup for $(m-M)_V$ = 15.1 and $E(B-V)$ = 0.45. The data of V351 Pup are taken from Bruch (1992) and IAU Circulars. (c) V382 Vel for $(m-M)_V$ = 11.5 and $E(B-V)$ = 0.15. The data of V382 Vel are taken from IAU Circulars. (d) V693 CrA for $(m-M)_V$ = 14.4 and $E(B-V)$ = 0.05. The data of V693 CrA are taken from Caldwell (1981) and Walker & Marino (1982). Other color-magnitude data of V1500 Cyg are added to show different observed colors, i.e., taken from Pfau (1976, small blue squares connected by blue thin solid line) and Lindgren (1979, small filled black circles connected by black thin solid line).

and $E(B-V)$ = 0.45 for V1500 Cyg, $(m-M)_V$ = 13.0 and $E(B-V)$ = 0.55 for PW Vul, $(m-M)_V$ = 11.7 and $E(B-V)$ = 0.60 for FH Ser, $(m-M)_V$ = 14.3 and $E(B-V)$ = 0.30 for PU Vul. The sources of these color-magnitude data are cited in Hachisu & Kato (2014). A vertical straight line of $(B-V)_0 = -0.03$ indicates the intrinsic $B-V$ color of optically thick free-free emission (Hachisu & Kato 2014). If optically thick free-free emission dominates the spectrum of a nova, its track follows this straight line of $(B-V)_0 = -0.03$.

van den Bergh & Younger (1987) derived two general trends of color evolution in nova light curves, i.e., $(B-V)_{0,\max} = 0.23 \pm 0.06$ at maximum and $(B-V)_{0,t2} = -0.02 \pm 0.04$ at day t_2. However, the color at maximum, $(B-V)_{0,\max}$, is not the same for all the novae, as clearly shown in Figure 45. A nova rises to the peak magnitude (top of each line) and then descends along each line. V1500 Cyg, V1668 Cyg, and V1974 Cyg show colors consistent with $(B-V)_{0,\max} = 0.23 \pm 0.06$. In this way, many fast and very fast novae are consistent with van den Bergh & Younger's $(B-V)_{0,\max} = 0.23 \pm 0.06$. The other types of novae, e.g., FH Ser and PU Vul, are not consistent with this, because their long journeys along the nova-giant sequence in the color-color diagram reach $(B-V)_0 \sim 0.6$ (see Figures 4 and 16 of Hachisu & Kato 2014), far beyond $(B-V)_0 = 0.23$. Thus, van den Bergh and Younger's law of $(B-V)_{0,\max} = 0.23 \pm 0.06$ is usually not applicable to slow/very slow novae.

The second law of van den Bergh & Younger's, $(B-V)_{0,t2} = -0.02 \pm 0.04$ at day t_2, shows good agreement with the fast novae, V1500 Cyg, V1668 Cyg, and V1974 Cyg, but is not consistent with the slow novae, FH Ser and PU Vul. Their value of $(B-V)_{0,t2} = -0.02 \pm 0.04$ is very close to the value of $(B-V)_0 = -0.03$ for optically thick free-free emission. This is because fast novae usually remain at the point of the open diamond in Figure 11 for a while when free-free emission dominates the spectrum (Hachisu & Kato 2014). However, some very slow novae, e.g., PU Vul, V5558 Sgr, V723 Cas, and HR Del, remain at a different point of $(B-V)_0 = +0.13$ and $(U-B)_0 = -0.82$ in the color-color diagram for a while, as shown by Hachisu & Kato (2014); the color is not consistent with $(B-V)_{0,t2} = -0.02 \pm 0.04$. Thus, the PU Vul and FH Ser type tracks show much redder colors at day t_2. This is because photospheric emission rather than free-free emission dominates the spectra of slow/very slow novae (Hachisu & Kato 2015).

Figure 46 shows the color-magnitude diagrams of four neon novae in outburst. Figure 46(a) is that of QU Vul 1984#2, assuming $(m-M)_V$ = 13.6 and $E(B-V)$ = 0.55, as well as the tracks of V1500 Cyg (thick green solid line), V1974 Cyg (orange solid line), and PU Vul (blue solid line). The thick solid lines for V1500 Cyg, V1974 Cyg, and PU Vul are the same as those in Figure 45. The data for QU Vul are taken from

Bergner et al. (1988), Kolotilov (1988), and Rosino et al. (1992). The $B-V$ colors of Rosino et al. (1992) are systematically ~ 0.2 mag bluer than those of Bergner et al. (1988), so that we shifted them rightward (redward) by 0.2 mag. Although the color data of QU Vul are scattered between the two groups, i.e., Bergner et al. (1988) and Rosino et al. (1992), the track of QU Vul is close to those of V1500 Cyg and V1974 Cyg.

Figure 46(b) is that of V351 Pup 1991 for $(m-M)_V = 15.1$ and $E(B-V) = 0.45$. The data for V351 Pup are taken from Bruch (1992) and IAU Circulars. The track of V351 Pup is very close to that of V1974 Cyg. This may support our estimates of $(m-M)_V = 15.1$ and $E(B-V) = 0.45$.

Figure 46(c) is that of V382 Vel 1999 for $(m-M)_V = 11.5$ and $E(B-V) = 0.15$. The data for V382 Vel are taken from IAU Circulars. The track of V382 Vel is also close to that of V1974 Cyg. This may also support our estimates of $(m-M)_V = 11.5$ and $E(B-V) = 0.15$.

Figure 46(d) is that of V693 CrA 1981 for $(m-M)_V = 14.4$ and $E(B-V) = 0.05$. The data for V693 CrA are taken from Caldwell (1981) and Walker & Marino (1982). It should be noted that the response functions of B and V filters are sometimes slightly different among different observers. If strong emission lines contribute to the edge of the filter, this small difference makes a large difference in the $B-V$ colors. For V1500 Cyg, we added such different data observed by Pfau (1976, small blue squares connected by blue thin solid line) and Lindgren (1979, small filled black circles connected by black thin solid line). These new lines deviate somewhat from the green thick solid line (same as that in Figure 45). The track of V693 CrA is close to that of V1500 Cyg, that is, closer to the color-magnitude tracks of V1500 Cyg taken from Pfau (1976) and Lindgren (1979) rather than that taken from Kiselev & Narizhnaia (1977) (green thick solid line).

8.4. *MMRD relation of neon novae*

The MMRD relations have frequently been used to estimate the distance to a nova. We call the relation between t_3 (or t_2) and $M_{V,\max}$ the MMRD relation. Here, t_3 (t_2) time is defined as the 3 mag (2 mag) decay time from maximum in units of days. On the basis of our nova light curve analyses, we have already calculated theoretical MMRD relations for CO nova 2 and Ne nova 2 in Hachisu & Kato (2010), and for CO nova 4 in Hachisu & Kato (2015). In Appendix B.3, we obtained theoretical MMRD relations for CO nova 3 based on the V1668 Cyg observations, for Ne nova 3 based on QU Vul, and for Ne nova 1 based on V351 Pup.

8.4.1. *MMRD relations based on V1668 Cyg, QU Vul, and V351 Pup*

Using theoretical light curves of free-free emission, we can derive a relation between the maximum magnitude and t_3 time, i.e., the MMRD relation (see Appendix B.3). Figure 47 shows the theoretical MMRD relation calibrated with the data for QU Vul as well as those calibrated with V1668 Cyg and with PW Vul (Hachisu & Kato 2015). Each MMRD relation is a straight line that goes through the calibrated object. The location of three novae are highlighted by large symbols. On the left ordinate, we convert the apparent magnitude to the absolute magnitude using the distance modulus of QU Vul, $(m-M)_V = 13.6$. We also show the stretching factor f_s on the upper axis of the same figure.

For comparison, two empirical MMRD relations are plotted in Figure 47, i.e., the Kaler-Schmidt law (blue solid line

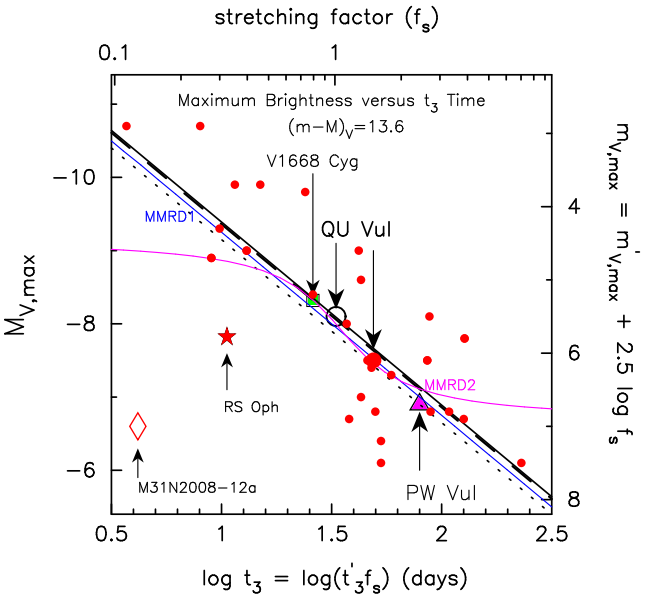

Figure 47. Various MMRD relations on the basis of our free-free emission model light curves. The black solid line shows the theoretical MMRD relation calibrated with QU Vul in Section 3. We also add observational MMRD points ($M_{V,\max}$ vs. t_3) for individual novae (red filled circles), the data for which are taken from Table 5 of Downes & Duerbeck (2000). The black dashed line shows the theoretical MMRD relation calibrated with V1668 Cyg in Section 2. The black dotted line denotes the theoretical MMRD relation calibrated with PW Vul, which is taken from Hachisu & Kato (2015). The blue solid line labeled "MMRD1" represents the Kaler-Schmidt law (Schmidt 1957). The magenta solid line labeled "MMRD2" corresponds to della Valle & Livio's law (1995). The red filled star is the MMRD point of the recurrent nova RS Oph, as an example for a very high mass accretion rate and very short t_3 time (very small f_s). The red open diamond is the MMRD point of the 1-yr recurrence period M31 nova, M31N2008-12a, taken from Darnley et al. (2015), i.e., $M_{V,\max} = -6.6$ and $t_{3,V} \approx 3.8$ days. The large red filed circle is the MMRD point of QU Vul, the data for which are taken from Table 5 of Downes & Duerbeck (2000). The large open black circle is the MMRD point of QU Vul, which is estimated from our free-free model light curve of the 0.96 $M_\odot$ WD. See text for more details.

labeled "MMRD1", Schmidt 1957):

$$M_{V,\max} = -11.75 + 2.5 \log t_3, \tag{3}$$

and della Valle & Livio's law (magenta solid line labeled "MMRD2", della Valle & Livio 1995):

$$M_{V,\max} = -7.92 - 0.81 \arctan\left(\frac{1.32 - \log t_2}{0.23}\right), \tag{4}$$

where we use the relation $t_2 \approx 0.6 \times t_3$ for the optical light curves that follow the free-free model light curves (Hachisu & Kato 2006).

Downes & Duerbeck (2000) also obtained an MMRD relation of

$$M_{V,\max} = (-11.99 \pm 0.56) + (2.54 \pm 0.35) \log t_3, \tag{5}$$

on the basis of their data, although this MMRD relation is not shown in the figure in order to avoid complexity.

Our MMRD relation based on the light curve of QU Vul, i.e., Equation (B16), is consistent with the Kaler-Schmidt law in Equation (3) and Downes & Duerbeck's law of Equation (5), and lies between them. Downes & Duerbeck (2000) estimated a t_3 time of 49 days and $M_{V,\max} = -7.5$ for QU Vul (large red filled circle in Figure 47). Note that we remeasured the t_3 time along our model light curve and obtained $t_3 = 32.7$ days and $M_{V,\max} = -8.1$ for QU Vul (this data point corresponds to

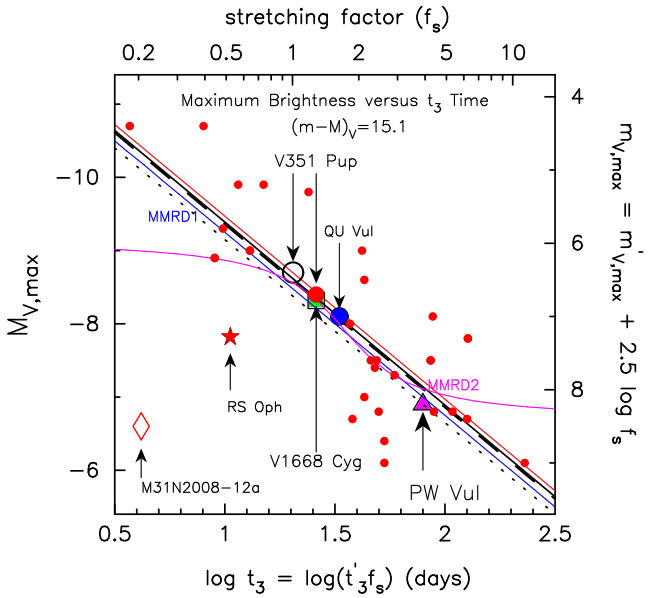

Figure 48. Same as Figure 47, but for the theoretical MMRD relation (red solid line) on the basis of our free-free model light curves calibrated with V351 Pup in Section 4. The large red filled circle denotes the MMRD point of V351 Pup, which is taken from Table 5 of Downes & Duerbeck (2000). The large black open circle is the MMRD point of V351 Pup, which is estimated from our free-free emission model light curve of the 1.0 $M_\odot$ WD with Ne nova 1. The large blue filled circle is the MMRD point for QU Vul, which is the same point as the large black open circle in Figure 47.

a large black open circle above and to the left of Downes & Duerbeck's one).

Figure 48 shows the MMRD relation (red thin solid line with a large black open circle) based on the light curve of V351 Pup, i.e., Equation (B17) in Appendix B.3. This relation is also consistent with the Kaler-Schmidt law of Equation (3) and Downes & Duerbeck's law of Equation (5), and lies between them.

We plot the MMRD relation based on the data of V1668 Cyg in Figures 47 and 48 (black thick dashed line with green filled square). Our MMRD relation, i.e., Equation (B15), is consistent with the Kaler-Schmidt law of Equation (3) and Downes & Duerbeck's law of Equation (5).

Hachisu & Kato (2015) also obtained an MMRD relation based on PW Vul (CO nova 4). This result is also plotted in Figures 47 and 48. The four MMRD relations based on QU Vul (Ne nova 3), V351 Pup (Ne nova 1), V1668 Cyg (CO nova 3), and PW Vul (CO nova 4) are close enough that we may conclude that the theoretical MMRD relations depend very little on the chemical composition.

8.4.2. *Physical properties of MMRD relations*

Figure 49 shows our updated MMRD points (t_3, $M_{V,\rm max}$) as well as Downes & Duerbeck's (2000) and Harrison et al.'s (2013) points. Red large filled triangles represent five novae studied in this work, QU Vul, V351 Pup, V382 Vel, V693 CrA, and V1974 Cyg. The locations of these neon novae in the MMRD diagram are similar to those of other fast novae and have no noteworthy distribution. Black large open circles represent the six novae studied in Hachisu & Kato (2015), PW Vul, V705 Cas, GQ Mus, V5558 Sgr, HR Del, and V723 Cas. Red filled circles are individual novae taken from Table 5 of Downes & Duerbeck (2000). Blue filled squares represent four novae calibrated with the annual parallax method, which are taken from Harrison et al. (2013). Green filled squares depict novae calibrated with the time-stretching method, taken from Table 7 (see Hachisu & Kato 2014). Blue solid line labeled "MMRD1" is the Kaler-Schmidt law (Schmidt 1957) and the blue thin solid lines flanking it are its $\pm$1.5 mag lines (see Equation (3)). Magenta solid line labeled "MMRD2" is della Valle & Livio's (1995) law and is flanked by its $\pm$1.5 mag lines (see Equation (4)). Red filled star is the recurrent nova RS Oph as an example of a very high mass accretion rate and very short timescale t_3 (Hachisu & Kato 2014). Red open diamond is the 1 yr recurrence period M31 nova, M31N2008-12a, taken from Darnley et al. (2015), i.e., $M_{V,\rm max} \approx -6.6 \pm 0.2$ and $t_{3,V} \approx 3.8 \pm 0.2$ days.

The data points are highly scattered evenly both above and below the empirical formulae. This simply means that there is a second (or even a third) parameter that specifies the MMRD relation for individual novae. Hachisu & Kato (2010) proposed that the main parameter is the WD mass represented by the stretching factor f_s, and the second parameter is the initial envelope mass (or the mass accretion rate to the WD). This second parameter can reasonably explain the large scatter of individual novae around the proposed MMRD relation of MMRD1 (see, e.g., Hachisu & Kato 2010, 2015). For a larger envelope mass at ignition, the wind mass loss starts with a large mass-loss rate. Then the nova is bright, as seen in Equation (B2) in Appendix B. For a smaller envelope mass at ignition, the wind mass loss starts with a smaller rate and, as a result, the nova is fainter even if the WD mass is the same.

Hachisu & Kato (2015) further pointed out that the effect of photospheric emission makes t_3 (or t_2) much longer than when free-free emission dominates. This happens in very slow novae such as RR Pic, V723 Cas, HR Del, and V5558 Sgr. These four novae are located far to the right of the line of MMRD1, i.e., Equation (3). This photospheric emission effect could be a third parameter causing deviation from the MMRD relation.

As shown in the previous sections, the photospheric emission contributes slightly to the total V light curve in QU Vul, V351 Pup, and V1974 Cyg, but barely in V382 Vel and V693 CrA. Thus, these five novae distribute evenly above and below the MMRD relation of Equation (3).

It is interesting to place the recurrent nova RS Oph and the 1-yr recurrence period M31 nova, M31N2008-12a, in this diagram. These two recurrent novae are located at the smallest t_3 time and on the underluminous side of the $M_{V,\rm max}$–logt_3 relation. This indicates a relatively small envelope mass at the optical maximum, suggesting that the mass accretion rate to the WD was very high (Kato et al. 2015). Such a situation is very consistent with a preoutburst picture of recurrent novae (see, e.g., Hachisu & Kato 2001, 2010, 2015; Kato et al. 2014, 2015, for more details).

9. CONCLUSIONS

We analyzed five neon novae and reanalyzed a CO nova on the basis of our model light curve fittings and obtained the following results.

1. On the basis of an optically thick wind model (Kato & Hachisu 1994), we made free-free emission model light curves of classical novae for various chemical compositions, including neon enrichment. During the wind phase, our model light curves were calculated from free-free emission of optically thin ejecta outside the photosphere of a nova envelope. The absolute magnitudes of the free-free emission model light curves were calibrated with the known dis-

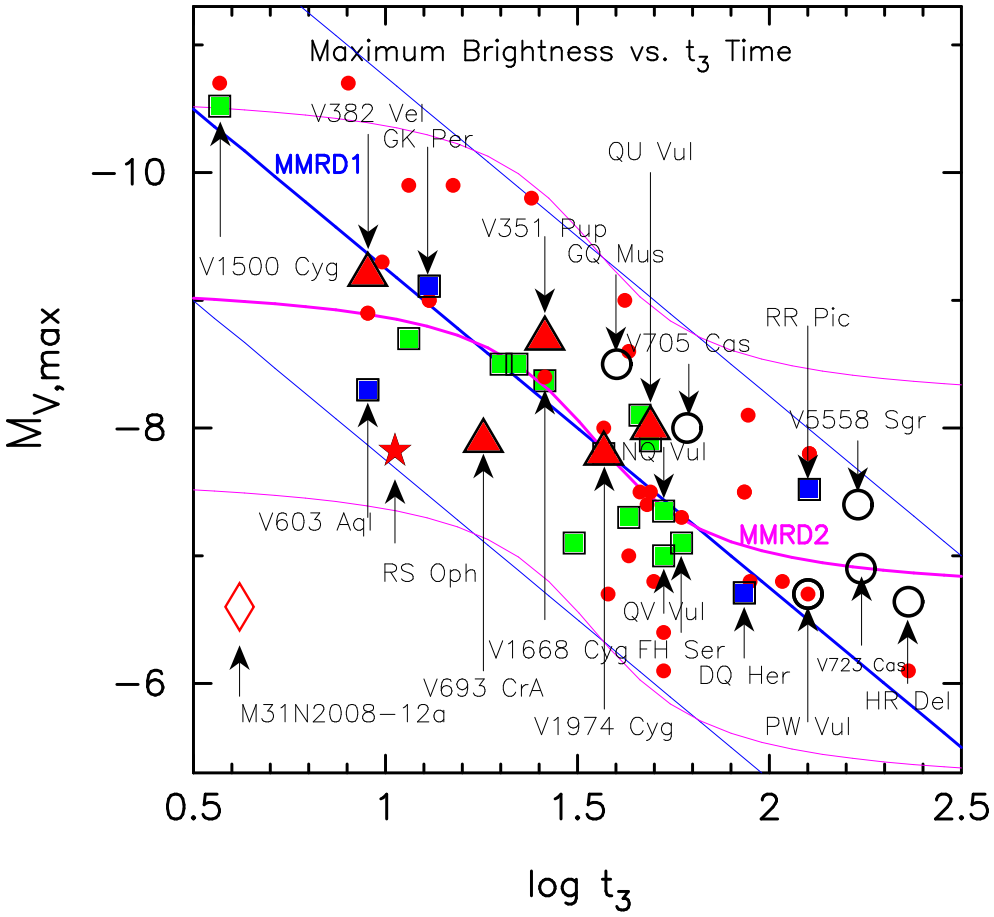

Figure 49. Various MMRD relations, where t_3 is measured on the observational data. The red filled triangles show the five novae studied in the present work, QU Vul, V351 Pup, V382 Vel, V693 CrA, and V1974 Cyg. The black open circles denote the six novae studied in Hachisu & Kato (2015), PW Vul, V705 Cas, GQ Mus, V5558 Sgr, HR Del, and V723 Cas. The blue filled squares correspond to the four novae calibrated with *HST* annual parallaxes, the data for which are taken from Harrison et al. (2013). The green filled squares indicate the novae calibrated with the time-stretching method, the data for which are taken from Hachisu & Kato (2014). The blue solid line labeled "MMRD1" is the Kaler-Schmidt law (Schmidt 1957) and its ±1.5 mag lines (see Equation (3)). The magenta solid line labeled "MMRD2" is della Valle & Livio's law (1995) and its ±1.5 mag lines (see Equation (4)). The other symbols are the same as those in Figures 47 and 48.

tance and reddening of a target nova in the same way as in Hachisu & Kato (2010, 2015). We then calculated the total V flux of free-free emission plus photospheric emission and compared them with the light curves of the novae.

2. With the optical V and UV 1455 Å light curve fittings to QU Vul, we confirmed our basic picture of nova evolution; that is, nova outburst evolution is governed by optically thick winds, and the V light curves can be reproduced well by free-free emission. The photospheric emission contributes to the optical light curve by at most 0.4 – 0.8 mag. This is because QU Vul is relatively slow compared with other fast neon novae, and the wind mass-loss rate is relatively small. We have obtained a consistent set of the distance, $d \sim 2.4$ kpc, and reddening, $E(B-V) \sim 0.55$. The estimated WD mass is in the range of 0.82 – 0.96 $M_\odot$ for various chemical compositions. This small value suggests that the WD has lost a mass of at least $\sim 0.1\ M_\odot$ since its birth if it was born as an ONe WD.

3. In the same way as for QU Vul, we obtained a consistent distance and reddening of $d \sim 5.5$ kpc and $E(B-V) \sim 0.45$ for V351 Pup. The estimated WD mass is in the range of 0.98 – 1.1 $M_\odot$ for various chemical compositions. In this case, the WD could have lost a mass as large as $\sim 0.1\ M_\odot$ or more since its birth if it was born as an ONe WD. The photospheric emission contributes very little to the optical light curve, 0.2 – 0.4 mag at most. This is because V351 Pup is slightly faster than QU Vul, and the wind mass-loss rate is slightly larger than that of QU Vul. These stronger winds produce brighter free-free emission.

4. For V382 Vel, we obtained a consistent set of distance and reddening, $d \sim 1.6$ kpc and $E(B-V) \sim 0.15$. The estimated WD mass is in the range of 1.13 – 1.28 $M_\odot$ for various chemical compositions. In this case, the WD mass is consistent with those of natal ONe WDs. The photospheric emission does not contribute to the optical light curve. This is because V382 Vel is a very fast nova, and the wind mass-loss rate is much larger than that of QU Vul.

5. For V693 CrA, we obtained a consistent set of distance and reddening, $d \sim 7.1$ kpc and $E(B-V) \sim 0.05$. The estimated WD mass is in the range of 1.15 – 1.25 $M_\odot$ for various chemical compositions. In this case, the WD mass is consistent with those of natal ONe WDs. The photospheric emission does not contribute to the optical light curve in the decay phase. This is because V693 CrA is also a very fast nova, and the wind mass-loss rate is much larger than that of QU Vul.

6. For V1974 Cyg, we obtained a consistent set of distance and reddening, $d \sim 1.8$ kpc and $E(B-V) \sim 0.30$. The estimated WD mass is in the range of 0.95 – 1.1 $M_\odot$ for various chemical compositions. The WD could have lost as much

mass as $\sim 0.1\ M_\odot$ or more since its birth if it was born as an ONe WD. The photospheric emission contributes very little to the optical light curve, 0.2 – 0.4 mag at most.

7. For V1668 Cyg, not a neon nova but a carbon-oxygen nova, we reanalyzed light curves including the effect of photospheric emission. We obtained a consistent set of distance and reddening, $d \sim 5.4$ kpc and $E(B-V) \sim 0.30$. The photospheric emission contributes slightly to the optical light curve, 0.2 – 0.4 mag at most. The estimated WD mass is in the range of 0.98 – 1.1 $M_\odot$ for various chemical compositions, which is on the lower mass bound of natal pure ONe cores. We point out two possibilities. One is that at its birth, the WD mass was close to the upper mass bound of natal CO cores, $< 1.07\ M_\odot$ (e.g., Umeda et al. 1999), and it decreased to the present value. The other is that at its birth, the WD mass was above $1.07\ M_\odot$, and it decreased to the present value, but the CO-rich mantle is still surrounding the ONe core.

8. On the basis of the universal decline law, we derived three MMRD relations calibrated with the data of V1668 Cyg, QU Vul, and V351 Pup. These are consistent with other known empirical MMRD relations. The five neon novae studied in the present paper locate evenly above and below the empirical MMRD relations (as well as our theoretically obtained MMRD relations).

9. Additionally, we calibrated the absolute magnitudes of the free-free emission model light curves for the chemical compositions of CO nova 3, Ne nova 3, and Ne nova 1, on the basis of the distances and reddenings of V1668 Cyg, QU Vul, and V351 Pup, respectively. The obtained absolute magnitudes give reasonable fits to the other novae.

We thank the late Angelo Cassatella for providing us with his machine readable UV 1455 Å data of QU Vul, V351 Pup, V382 Vel, V693 CrA, V1974 Cyg, and V1668 Cyg, and also the American Association of Variable Star Observers (AAVSO) and Variable Star Observers League of Japan (VSOLJ) for archival data on novae. We are also grateful to the anonymous referee for useful comments that improved the manuscript. This research was supported in part by Grants-in-Aid for Scientific Research (24540227, 15K05026) from the Japan Society for the Promotion of Science.

APPENDIX

A. DISTANCE MODULUS DETERMINED BY THE TIME-STRETCHING METHOD

Hachisu & Kato (2010, 2014, 2015) developed a method to estimate the distance modulus in the V band on the basis of the time-stretching method (Hachisu & Kato 2010). Nova light curves follow the universal decline law when free-free emission dominates the spectrum in optical and NIR regions (Hachisu & Kato 2010, 2014, 2015). Using this property, Hachisu & Kato (2010) found that, if two nova light curves overlap each other after one of the two is squeezed/stretched by a factor of f_s ($t' = t/f_s$) in the time direction, the brightnesses of the two novae obey the relation of

$$m'_V = m_V - 2.5 \log f_s. \tag{A1}$$

(This equation is essentially the same as Equation (B9) in Appendix B.2.) This means that the light curves of two novae are connected by the simple relation (A1). Thus, if one is a well-studied nova on the distance and reddening, we are able to get information on the distance modulus of the other nova. Applying this property to a target nova, we can estimate the absolute magnitude of the target nova from the calibrated nova with a known distance modulus.

Figure 2 shows time-stretched light curves of QU Vul, PW Vul, and GQ Mus, against V1974 Cyg. This figure is similar to Figure 50 of Hachisu & Kato (2014), but with reanalyzed data. Here, we adopt V1974 Cyg as a well-observed nova and the others are the target novae. The *UBV* data for GQ Mus are taken from Budding (1983) and Whitelock et al. (1984), whereas the V data are from the Fine Error Sensor monitor on board *IUE* and the visual data are those collected by the Royal Astronomical Society of New Zealand and by the AAVSO (see Hachisu et al. 2008, for more details of GQ Mus light curve data). The *UBV* data for PW Vul are taken from Robb & Scarfe (1995) and the V data are the same as those in Figure 8 of Hachisu & Kato (2014). The data for QU Vul and V1974 Cyg are the same as those in Sections 3 and 7.

Figure 2 shows that all four novae well overlap in the UV 1455 Å and V light curves, $B-V$, and $U-B$ color curves. To overlap them, we shift the V light curves up or down by ΔV against that of V1974 Cyg. At the same time, the stretching factors of each nova are obtained to be $f_s = 0.42$ for PW Vul, $f_s = 0.26$ for GQ Mus, and $f_s = 0.42$ for QU Vul, against that of V1974 Cyg. Then, we have relations between the light curves of QU Vul, V1974 Cyg, PW Vul, and GQ Mus,

$$\begin{aligned}(m-M)_{V,\mathrm{V1974\ Cyg}} &= 12.2 \\ &= (m-M)_{V,\mathrm{PW\ Vul}} + \Delta V - 2.5\log 0.42 \\ &\approx 13.0 - 1.8 + 0.95 = 12.15 \\ &= (m-M)_{V,\mathrm{GQ\ Mus}} + \Delta V - 2.5\log 0.26 \\ &\approx 15.7 - 5.0 + 1.46 = 12.16 \\ &= (m-M)_{V,\mathrm{QU\ Vul}} + \Delta V - 2.5\log 0.42 \\ &\approx 13.6 - 2.4 + 0.95 = 12.15, \end{aligned} \tag{A2}$$

where we use the apparent distance moduli of V1974 Cyg, PW Vul, and GQ Mus to be $(m-M)_{V,\mathrm{V1974\ Cyg}} = 12.2$ in Section 7, and both $(m-M)_{V,\mathrm{PW\ Vul}} = 13.0$ and $(m-M)_{V,\mathrm{GQ\ Mus}} = 15.7$ in Hachisu & Kato (2015). All these three are consistent with each other. Considering ambiguity (± 0.2 mag) of fitting accuracy, we obtained $(m-M)_V = 13.6 \pm 0.2$ for QU Vul.

Similarly, for V351 Pup, we obtain

$$\begin{aligned}(m-M)_{V,\mathrm{V351\ Pup}} &= 15.1 \\ &= (m-M)_{V,\mathrm{V1668\ Cyg}} + \Delta V - 2.5\log 0.93 \\ &\approx 14.6 + 0.4 + 0.08 = 15.08 \\ &= (m-M)_{V,\mathrm{PW\ Vul}} + \Delta V - 2.5\log 0.42 \\ &\approx 13.0 + 1.1 + 0.95 = 15.05 \\ &= (m-M)_{V,\mathrm{V1974\ Cyg}} + \Delta V - 2.5\log 1.0 \\ &\approx 12.2 + 2.9 + 0.0 = 15.1 \\ &= (m-M)_{V,\mathrm{QU\ Vul}} + \Delta V - 2.5\log 0.5 \\ &\approx 13.6 + 0.8 + 0.75 = 15.15, \end{aligned} \tag{A3}$$

from Figure 20 (V1668 Cyg), Figure 22 (PW Vul), Figure 23 (V1974 Cyg), and Figure 24 (QU Vul). Here, ΔV is the difference of brightness obtained in Figures 20, 22, 23, and 24, respectively, against that of V351 Pup. The stretching factors are also obtained in each figure against V351 Pup. The apparent distance moduli of V1668 Cyg, PW Vul, V1974 Cyg, and QU Vul were calibrated as $(m-M)_{V,\mathrm{V1668\ Cyg}} = 14.6$ in Section 2, $(m-M)_{V,\mathrm{PW\ Vul}} = 13.0$ in Hachisu & Kato (2015), and $(m-M)_{V,\mathrm{V1974\ Cyg}} = 12.2$ in Section 7, and $(m-M)_{V,\mathrm{QU\ Vul}} = 13.6$ in Section 3. These are all consistent with each other.

Thus, we obtained $(m-M)_V = 15.1 \pm 0.2$ for V351 Pup.

For V382 Vel, we obtain

$$\begin{aligned}(m-M)_{V,\mathrm{V1500\ Cyg}} &= 12.3 \\ &= (m-M)_{V,\mathrm{V382\ Vel}} + \Delta V - 2.5\log 0.89 \\ &\approx 11.5+0.7+0.13 = 12.33 \\ &= (m-M)_{V,\mathrm{GK\ Per}} + \Delta V - 2.5\log 0.63 \\ &\approx 9.3+2.5+0.50 = 12.30 \\ &= (m-M)_{V,\mathrm{V1974\ Cyg}} + \Delta V - 2.5\log 0.47 \\ &\approx 12.2-0.7+0.82 = 12.32 \\ &= (m-M)_{V,\mathrm{QU\ Vul}} + \Delta V - 2.5\log 0.166 \\ &\approx 13.6-3.0+1.7 = 12.3, \end{aligned} \quad \text{(A4)}$$

from Figure 1. Here, ΔV is the difference of brightness obtained in Figure 1 against that of V1500 Cyg. In Figure 1, the V data for V1500 Cyg are taken from Lockwood & Millis (1976) and Tempesti (1979) and the UBV data are from Pfau (1976), Arkhipova & Zaitseva (1976), Duerbeck & Wolf (1977), and Contadakis (1980). The optical V data for GK Per are the same as those in Figure 2 of Hachisu & Kato (2007). The stretching factors are also obtained against V1500 Cyg. The apparent distance moduli of V1500 Cyg, GK Per, V1974 Cyg, and QU Vul were calibrated as $(m-M)_{V,\mathrm{V1500\ Cyg}} = 12.3$ in Hachisu & Kato (2014), $(m-M)_{V,\mathrm{GK\ Per}} = 9.3$ in Harrison et al. (2013) from *HST* annual parallaxes, $(m-M)_{V,\mathrm{V1974\ Cyg}} = 12.2$ in Section 7, and $(m-M)_{V,\mathrm{QU\ Vul}} = 13.6$ in Section 3. These are all consistent with each other. Thus, we obtained $(m-M)_V = 11.5 \pm 0.2$ for V382 Vel.

For V693 CrA, we obtain

$$\begin{aligned}(m-M)_{V,\mathrm{V693\ CrA}} &= 14.4 \\ &= (m-M)_{V,\mathrm{V351\ Pup}} + \Delta V - 2.5\log 0.40 \\ &\approx 15.1-1.6+1.0 = 14.5 \\ &= (m-M)_{V,\mathrm{V1668\ Cyg}} + \Delta V - 2.5\log 0.37 \\ &\approx 14.6-1.2+1.07 = 14.47 \\ &= (m-M)_{V,\mathrm{V1500\ Cyg}} + \Delta V - 2.5\log 0.79 \\ &\approx 12.3+1.8+0.25 = 14.35 \\ &= (m-M)_{V,\mathrm{QU\ Vul}} + \Delta V - 2.5\log 0.25 \\ &\approx 13.6-0.7+1.5 = 14.4, \end{aligned} \quad \text{(A5)}$$

where ΔV is the difference of brightness obtained in Figures 33, 34, 35, and 36 against that of V693 CrA. The timescales are squeezed in these figures as $f_s = 0.40$ for V351 Pup (Figure 33), $f_s = 0.37$ for V1668 Cyg (Figure 34), $f_s = 0.79$ for V1500 Cyg (Figure 35), and $f_s = 0.25$ for QU Vul (Figure 36) against V693 CrA. The apparent distance moduli of V351 Pup, V1668 Cyg, V1500 Cyg, and QU Vul were calibrated as $(m-M)_{V,\mathrm{V351\ Pup}} = 15.1$ in Section 4, $(m-M)_{V,\mathrm{V1668\ Cyg}} = 14.6$ in Section 2, $(m-M)_{V,\mathrm{V1500\ Cyg}} = 12.3$ in Hachisu & Kato (2010, 2014), and $(m-M)_{V,\mathrm{QU\ Vul}} = 13.6$ in Section 3. These three are all consistent with each other. Thus, we obtained $(m-M)_V = 14.4 \pm 0.2$ for V693 CrA.

B. TIME-NORMALIZED LIGHT CURVES OF FREE-FREE EMISSION

B.1. *Free-free emission model light curves*

Hachisu & Kato (2006) made theoretical light curves of free-free emission from optically thin ejecta outside the photosphere on the basis of the optically thick wind theory (Kato & Hachisu 1994). They showed that these light curves reproduced the optical light curves of novae reasonably well.

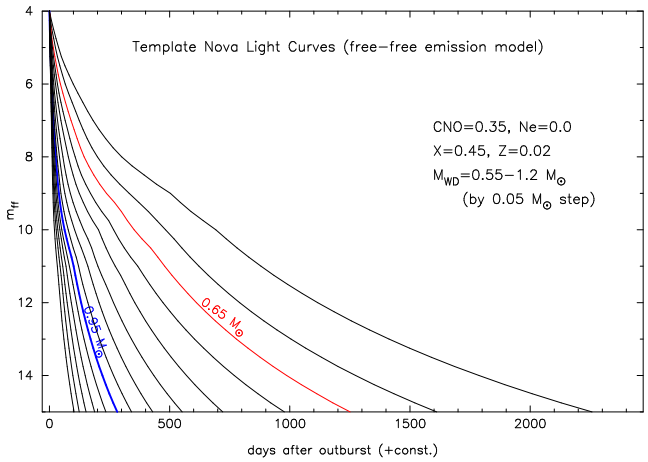

Figure 50. Magnitudes of our free-free emission model light curves for CO nova 3 and WD masses of $0.55-1.2\ M_\odot$ in $0.05\ M_\odot$ steps, numerical data of which are tabulated in Table 3. Two light curves are specified by the red thick solid line ($0.65\ M_\odot$) and blue thick solid line ($0.95\ M_\odot$).

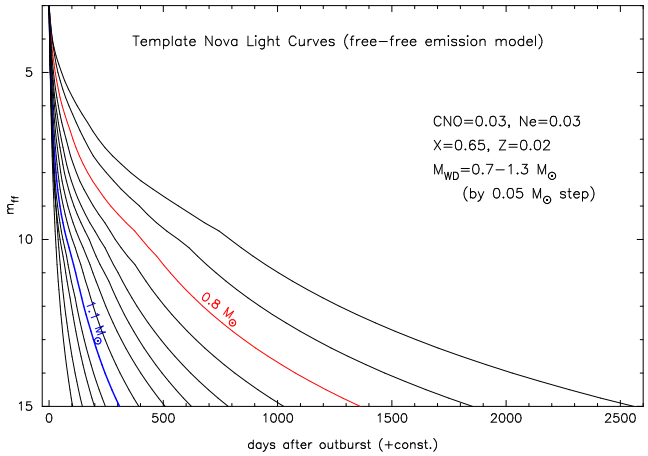

Figure 51. Same as Figure 50, but for Ne nova 3 and WD masses of $0.7-1.3\ M_\odot$. The numerical data are tabulated in Table 4. Two light curves are specified by the red thick solid line ($0.8\ M_\odot$) and blue thick solid line ($1.1\ M_\odot$).

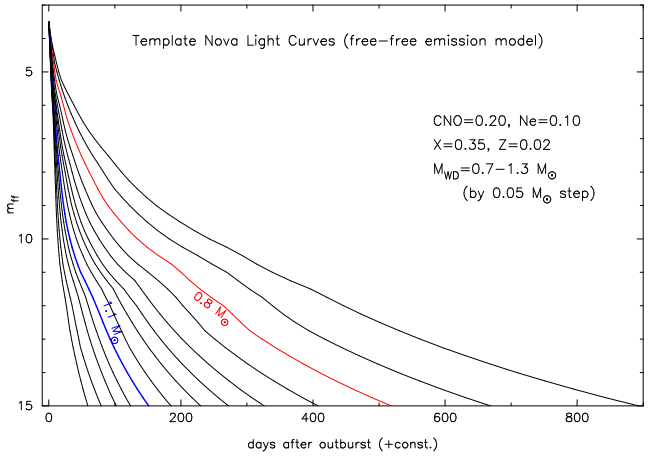

Figure 52. Same as Figure 50, but for Ne nova 1 and WD masses of $0.7-1.3\ M_\odot$. The numerical data are tabulated in Table 5.

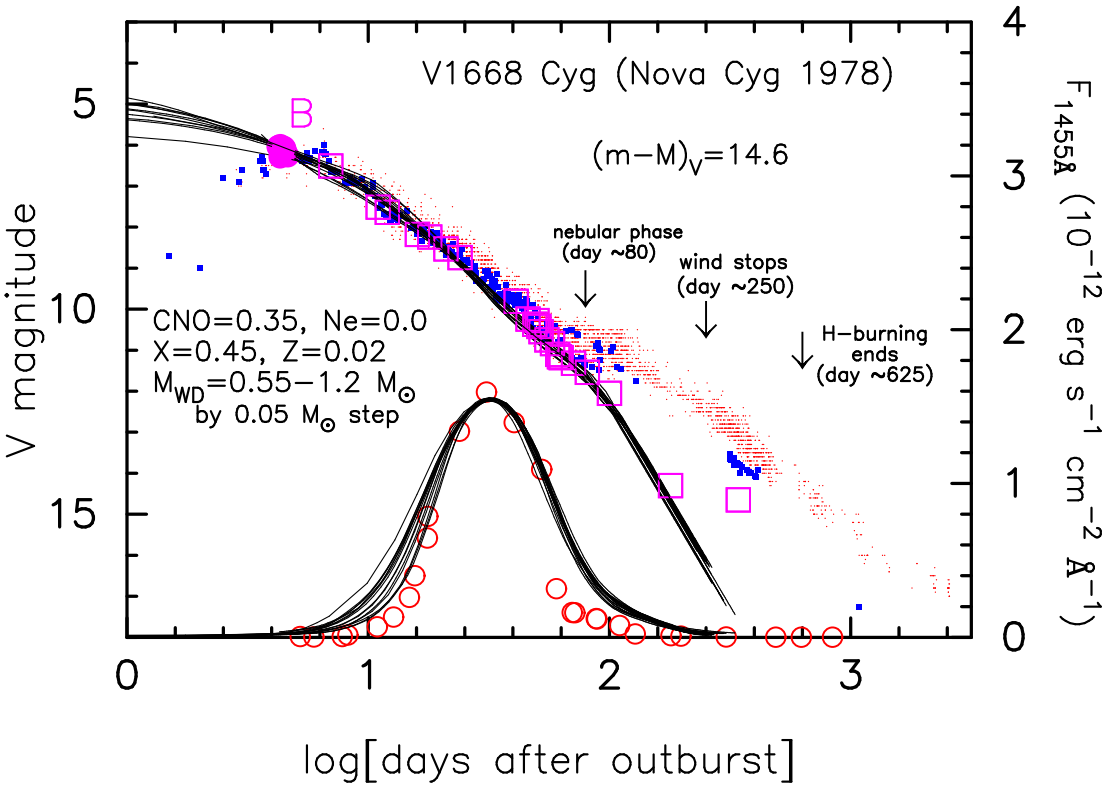

Figure 53. Same as the free-free emission model light curves in Figure 50 (CO nova 3), but all the light curves of free-free emission and UV 1455 Å blackbody emission are rescaled to overlap on the UV 1455 Å observation (red open circles) of V1668 Cyg. Each timescaling factor, f_s, is tabulated in Table 3. The right edge of each free-free emission model light curve corresponds to the epoch when the optically thick winds stop, i.e., ~ 250 days after the outburst for the 0.98 $M_\odot$ WD (denoted by an arrow). Point B (magenta filled circle) corresponds to the peak of the V magnitude of V1668 Cyg.

The flux of optically thin free-free emission is given by

$$j_\nu d\Omega dV dt d\nu = \frac{16}{3}\left(\frac{\pi}{6}\right)^{1/2}\frac{e^6 Z^2}{c^3 m_e^2}\left(\frac{m_e}{kT_e}\right)^{1/2} \times g\,\exp\left(-\frac{h\nu}{kT_e}\right) N_e N_i d\Omega dV dt d\nu, \quad \text{(B1)}$$

where j_ν is the emissivity at the frequency ν, Ω the solid angle, V the volume, t the time, e the electron charge, Z the ion charge in units of e, c the speed of light, m_e the electron mass, k the Boltzmann constant, T_e the electron temperature, g the Gaunt factor, h the Planck constant, and N_e and N_i are the number densities of electrons and ions (Allen 1973, p.103).

Electron temperatures of nova ejecta were suggested to be around $T_e \sim 10^4$ K, almost constant in time, during the nova outbursts (see, e.g., Ennis et al. 1977, for V1500 Cyg). If we further assume that the ionization degree of ejecta is constant during the outburst, we have the total flux of free-free emission, i.e.,

$$F_\nu \propto \int N_e N_i dV \propto \int_{R_{ph}}^{\infty} \frac{\dot{M}_{wind}^2}{v_{wind}^2 r^4} r^2 dr \propto \frac{\dot{M}_{wind}^2}{v_{ph}^2 R_{ph}} \quad \text{(B2)}$$

for optically thin ejecta, where F_ν is the flux at the frequency ν. For Kato & Hachisu's (1994) optically thick nova wind models, we have $N_e \propto \rho_{wind}$ and $N_i \propto \rho_{wind}$, where ρ_{wind} is the density of winds, $\dot{M}_{wind}$ is the wind mass-loss rate, v_{ph} and R_{ph} are the velocity and radius at the pseudophotosphere. Here, we integrate Equation (B2) outside the photosphere assuming that the wind velocity is $v_{wind} = v_{ph}$ (=constant in space) outside the photosphere and using the relation of continuity, $\rho_{wind} = \dot{M}_{wind}/4\pi r^2 v_{wind}$.

After the wind stops, the free-free emission light curve changes its decline shape as

$$F_\nu \propto \int N_e N_i dV \propto \frac{M_{ej}^2}{V^2} V \propto R^{-3} \propto t^{-3}, \quad \text{(B3)}$$

where the ejected mass of M_{ej} is constant in time and we assume that the ejecta volume, $V = 4\pi R^3/3$, expands as $R \propto t$.

Thus, Hachisu & Kato (2006) calculated free-free emission model light curves of novae for various chemical compositions, as tabulated in Table 2, based on the optically thick wind model of Kato & Hachisu (1994). Then, the free-free flux is given by

$$F_\nu^{\{M_{WD}\}}(t) = C\left[\frac{\dot{M}_{wind}^2}{v_{ph}^2 R_{ph}}\right]_{(t)}^{\{M_{WD}\}}, \quad \text{(B4)}$$

where C is the proportionality constant in Equation (B2). This equation is essentially the same as Equation (9) of Hachisu & Kato (2006). Note that the flux F_ν is independent of the frequency ν in the case of optically thin free-free emission. The details of calculations are presented in Hachisu & Kato (2006, 2010). The magnitudes of the model light curves are tabulated in Tables 3, 4, and 5 in a format of

$$m_{ff} = -2.5\,\log\left[\frac{\dot{M}_{wind}^2}{v_{ph}^2 R_{ph}}\right]_{(t)}^{\{M_{WD}\}} + G^{\{M_{WD}\}}, \quad \text{(B5)}$$

and are plotted in Figure 50 for 0.55 – 1.2 $M_\odot$ WDs in 0.05 $M_\odot$ steps (CO nova 3), in Figure 51 for 0.7 – 1.3 $M_\odot$

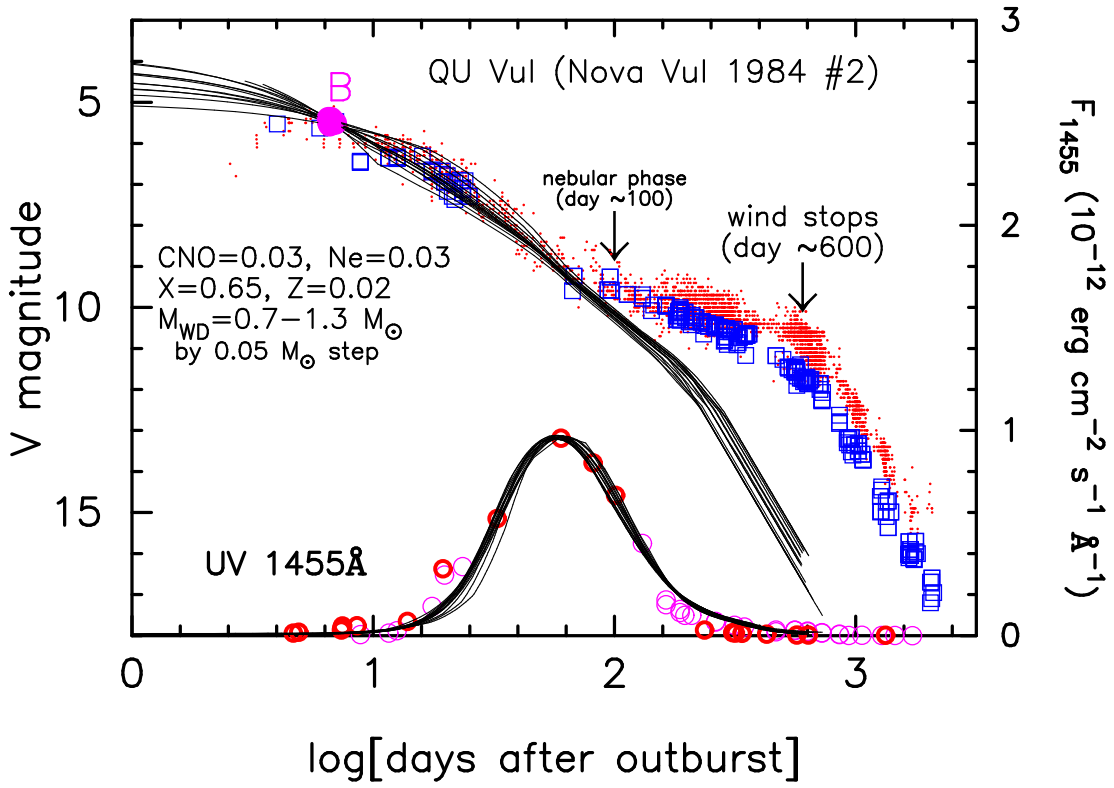

Figure 54. Same model light curves of free-free emission as those in Figure 51 (Ne nova 3), but all the light curves of free-free emission and UV 1455 Å blackbody emission are rescaled to overlap on the UV 1455 Å observation of QU Vul (magenta open circles) and PW Vul (red open circles). Each timescaling factor, f_s, is tabulated in Table 4. The right edge of each free-free emission model light curve corresponds to the epoch when the optically thick winds stop, i.e., $\sim$ 600 days after the outburst for the 0.96 $M_\odot$ WD model (denoted by an arrow). Point B (magenta filled circle) corresponds to the peak of the V magnitude.

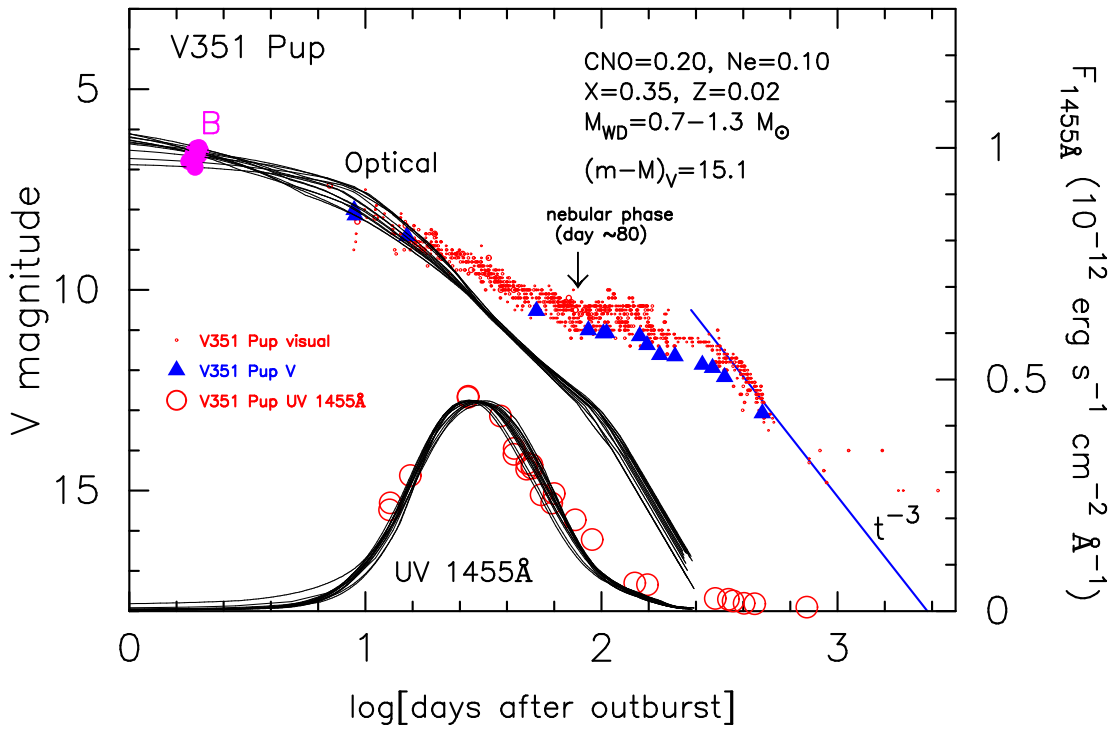

Figure 55. Same free-free emission model light curves as those in Figure 52 (Ne nova 1), but all the light curves of free-free emission and UV 1455 Å blackbody are rescaled to overlap on the UV 1455 Å observation (large red open circles) of V351 Pup. Each timescaling factor, f_s, is tabulated in Table 5. Points B (magenta filled circles) correspond to the peak of the V magnitude.

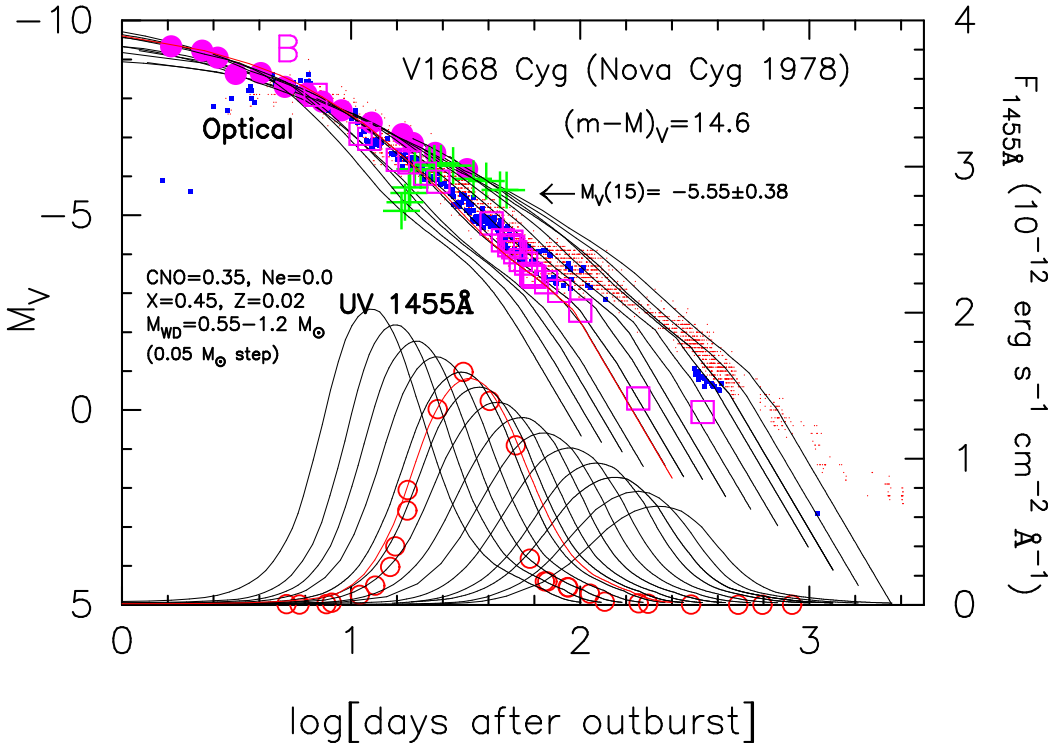

Figure 56. Same models as Figure 53 (CO nova 3), but for the absolute magnitudes and real timescales. We calibrated the free-free model light curves by the distance modulus of $(m-M)_V$ = 14.6 and calculated the absolute magnitude of each free-free emission light curve (labeled "Optical") from Equation (B11). The position at point B in Figure 53 is indicated by a magenta filled circle for each light curve. We also show the magnitude, $M_V(15)$, 15 days after the optical maximum, by green crosses. Their average value of $M_V(15) = -5.55 \pm 0.38$ is obtained for 0.55–1.2 $M_\odot$ WDs. The UV 1455 Å model light curves are also rescaled to recover the real timescale and flux. The red solid lines denote those for the 0.98 $M_\odot$ WD model.

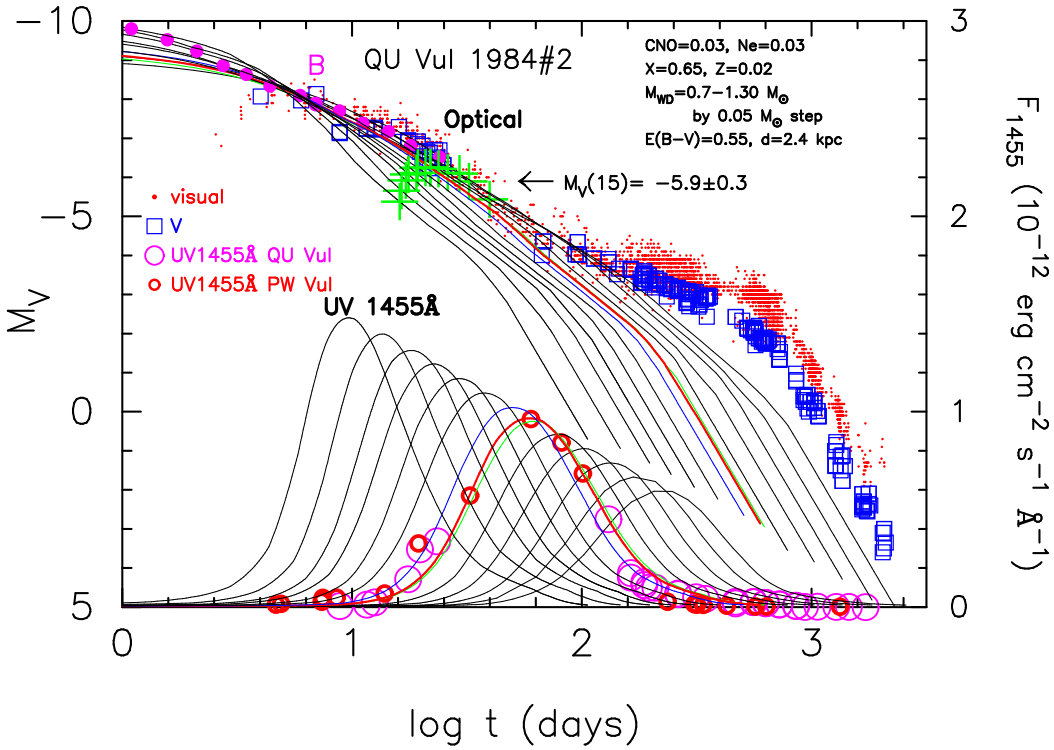

Figure 57. Same models as Figure 54 (Ne nova 3), but for the absolute magnitudes and real timescales. We calibrated the free-free model light curves with the distance modulus of $(m-M)_V$ = 13.6 in Figure 17(b) and calculated the absolute magnitude of each free-free emission light curve (labeled "Optical") from Equation (B11). The position at point B in Figure 54 is indicated by a magenta filled circle for each light curve. We also show the magnitude, $M_V(15)$, 15 days after the optical maximum, by green crosses. Their average value of $M_V(15) = -5.9 \pm 0.3$ is obtained for 0.7–1.3 $M_\odot$ WDs. Our UV 1455 Å model light curves are also rescaled to recover the real timescales and fluxes. The red thick, green thin, and blue thin solid lines denote those for the 0.96 $M_\odot$, 0.95 $M_\odot$, and 1.0 $M_\odot$ WDs, respectively.

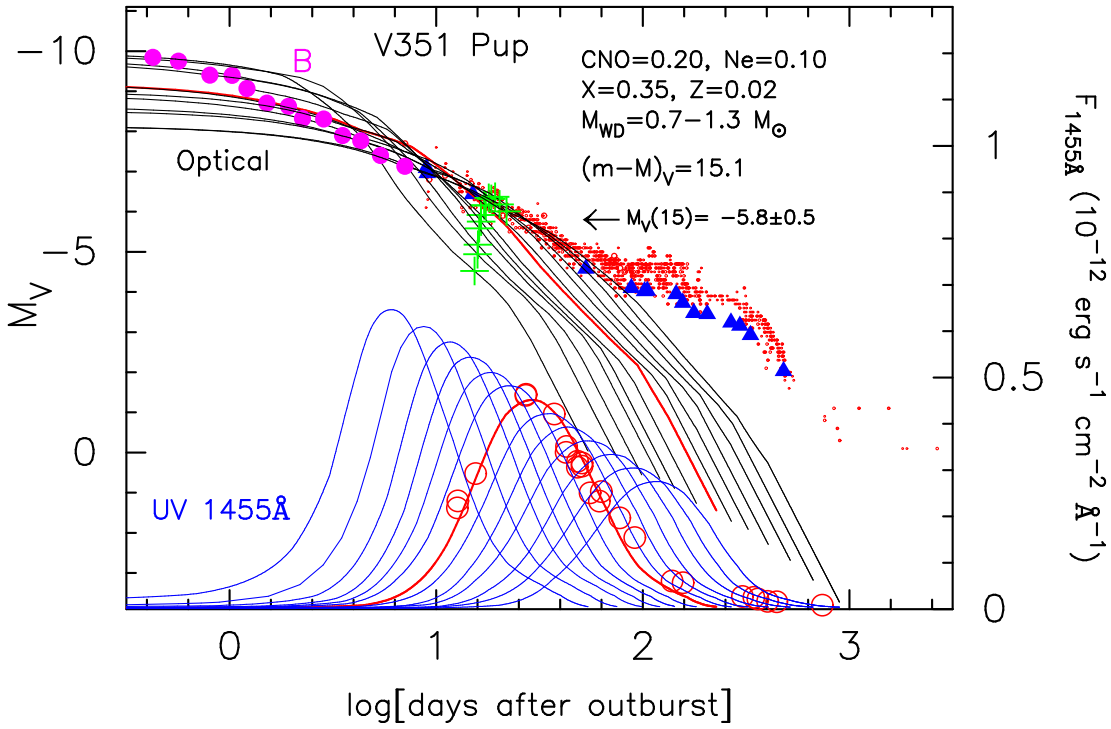

Figure 58. Same models as Figure 55 (Ne nova 1), but for the absolute magnitudes and real timescales. We calibrated the free-free model light curves using the distance modulus of $(m-M)_V$ = 15.1 and restored the absolute magnitude of each free-free emission model light curve (labeled "Optical") from Equation (B11). Each position at point B in Figure 55 is indicated by a magenta filled circle for each light curve. We also show the magnitude, $M_V(15)$, 15 days after the optical maximum, by green crosses. Their average value of $M_V(15) = -5.8 \pm 0.5$ is obtained for 0.7–1.3 $M_\odot$ WDs. The UV 1455 Å model light curves are also rescaled to recover the real timescales and fluxes. The red thick solid lines denote those for the 1.0 $M_\odot$ WD model.

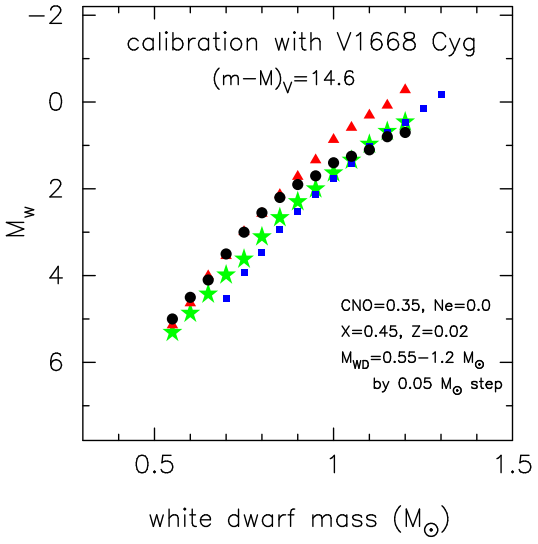

Figure 59. The absolute magnitudes at the end of the wind phase, M_w, against the WD mass for CO nova 3 (black filled circles) in the present work as well as CO nova 2 (red filled triangles) and Ne nova 2 (blue filled squares), the both of which are taken from Hachisu & Kato (2010), and CO nova 4 (green filled star-marks), taken from Hachisu & Kato (2015).

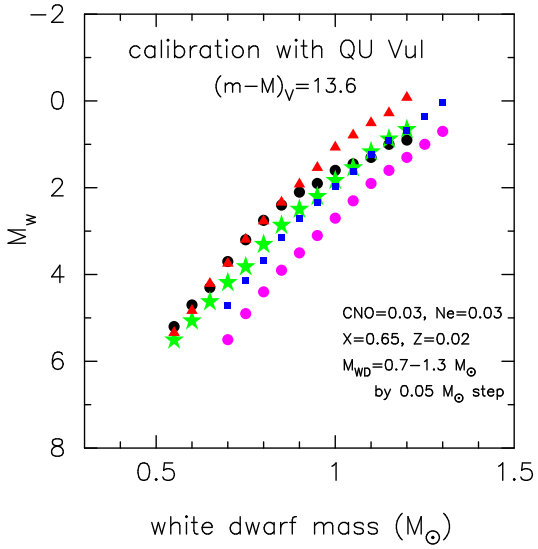

Figure 60. Same as Figure 59, but we added the end points of the wind phase for Ne nova 3 (magenta filled circles).

WDs in 0.05 $M_\odot$ steps (Ne nova 3), in Figure 52 for 0.7 – 1.3 $M_\odot$ WDs in 0.05 $M_\odot$ steps (Ne nova 1). The subscript (t) represents the dependence on time while the superscript $\{M_{\rm WD}\}$ corresponds to a model parameter. The last row (15th mag) of each column in Tables 3, 4, and 5 represents the magnitude at the end of the wind phase. Here, we define the constant $G^{\{M_{\rm WD}\}}$ in Equation (B5) such that the last (lowest) point of each light curve is 15th mag. This format helps to pack the light curve data into a short table.

B.2. *Absolute magnitudes of free-free model light curves*

The free-free emission model light curves in Figure 50 (also in Figures 51 and 52) have strong similarity in their shapes. For the chemical compositions of CO nova 2, CO nova 4, and Ne nova 2, Hachisu & Kato (2006, 2010, 2015) showed that the model light curves are homologous among various WD masses and almost overlap each other if they are properly squeezed/stretched along time. Here, we show the same

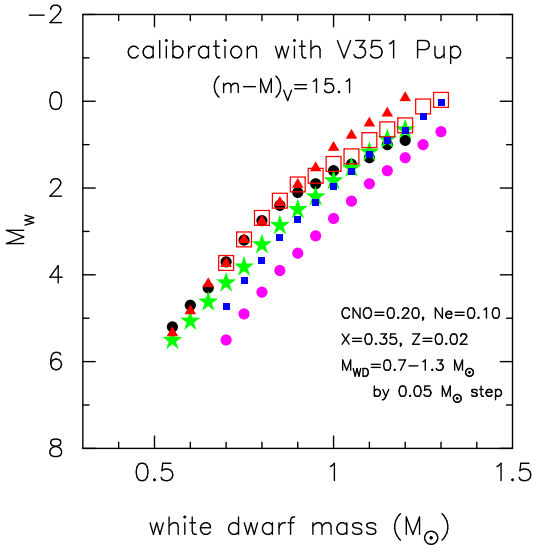

Figure 61. Same as Figure 60, but we added the end points of the wind phase for Ne nova 1 (red open squares).

properties of light curves for other chemical compositions of CO nova 3, Ne nova 3, and Ne nova 1. Figures 53, 54, and 55 clearly show that free-free emission model light curves overlap each other after they are properly squeezed/stretched along time. We determine the stretching factor, f_s, of each UV 1455 Å model light curve by increasing or decreasing f_s until the model light curve shape matches the observational data. For example, we see that the evolution of the 0.95 $M_\odot$ WD model light curve is 1.05 times slower than the QU Vul observation ($f_s \approx 1.05$) and the 1.0 $M_\odot$ WD model light curve evolves 1.15 times faster ($f_s \approx 0.87$). In Figure 54, in this way, all the UV 1455 Å model light curves overlap each other, if we squeeze/stretch the time as $t' = t/f_s$ and normalize the peak flux of UV 1455 Å. The values of $\log f_s$ are tabulated in Tables 3, 4, and 5. Using this time-stretching factor f_s, we can rewrite these timescaled light curves of free-free emission as

$$m'^{\{M_{\rm WD}\}}_V(t') = -2.5\ \log \left[\frac{\dot{M}^2_{\rm wind}}{v^2_{\rm ph}R_{\rm ph}}\right]^{\{M_{\rm WD}\}}_{(t'\,f_s)} + K_V, \qquad \text{(B6)}$$

where K_V is a constant common for all the WD masses. Because they all overlap each other (i.e., the universal decline law), it indicates that

$$\left[\frac{\dot{M}^2_{\rm wind}}{v^2_{\rm ph}R_{\rm ph}}\right]^{\{M_{\rm WD}\}}_{(t'\,f_s)} = \left[\frac{\dot{M}^2_{\rm wind}}{v^2_{\rm ph}R_{\rm ph}}\right]^{\{0.98\ M_\odot\}}_{(t')}, \qquad \text{(B7)}$$

for all $M_{\rm WD}$ of CO nova 3. Note that $f_s = 1$ for the 0.98 $M_\odot$ WD of CO nova 3 ($f_s = 1$ for the 0.96 $M_\odot$ WD of Ne nova 3, and $f_s = 1$ for the 1.0 $M_\odot$ WD of Ne nova 1). If we squeeze the timescale of a physical phenomenon by a factor of f_s (i.e., $t' = t/f_s$), we covert the frequency to $\nu' = f_s\nu$ and the flux of free-free emission to $F'_{\nu'} = f_s F_\nu$ because

$$\frac{d}{dt'} = f_s \frac{d}{dt}. \qquad \text{(B8)}$$

Substituting $F'_{\nu'} = F'_\nu$ (independent of the frequency in optically-thin free-free emission) into $F'_{\nu'} = f_s F_\nu$ and integrating $F'_\nu = f_s F_\nu$ with the V-filter response function, we have the following relation, i.e.,

$$m'_V(t/f_s) = m_V(t) - 2.5\log f_s. \qquad \text{(B9)}$$

Substituting Equation (B7) into (B6), and then Equation (B6) into (B9), we obtain the apparent V magnitudes of

$$m_V^{\{M_{\rm WD}\}}(t) = 2.5\log f_s - 2.5\ \log \left[\frac{\dot{M}^2_{\rm wind}}{v^2_{\rm ph}R_{\rm ph}}\right]^{\{0.98\ M_\odot\}}_{(t/f_s)} + K_V, \qquad \text{(B10)}$$

where note that f_s is the time-scaling factor for the WD with mass of $M_{\rm WD}$, generally not for the 0.98 $M_\odot$ WD (CO nova 3).

The corresponding absolute magnitudes of the light curves can be readily obtained from Equation (B10) and from the distance modulus of V1668 Cyg, i.e.,

$$\begin{aligned} M_V^{\{M_{\rm WD}\}}(t) &= m_V^{\{M_{\rm WD}\}}(t) - (m-M)_{V,\rm V1668\ Cyg} \\ &= 2.5\log f_s - 2.5\ \log \left[\frac{\dot{M}^2_{\rm wind}}{v^2_{\rm ph}R_{\rm ph}}\right]^{\{0.98\ M_\odot\}}_{(t/f_s)} \\ &\quad + K_V - (m-M)_{V,\rm V1668\ Cyg} \\ &= m'^{\{M_{\rm WD}\}}_V(t/f_s) + 2.5\log f_s - (m-M)_{V,\rm V1668\ Cyg}, \end{aligned} \qquad \text{(B11)}$$

where $(m-M)_{V,\rm V1668\ Cyg} = 14.6$ is the distance modulus of V1668 Cyg harboring a 0.98 $M_\odot$ WD (CO nova 3), and we use Equation (B7) in a different form of

$$\left[\frac{\dot{M}^2_{\rm wind}}{v^2_{\rm ph}R_{\rm ph}}\right]^{\{M_{\rm WD}\}}_{(t)} = \left[\frac{\dot{M}^2_{\rm wind}}{v^2_{\rm ph}R_{\rm ph}}\right]^{\{0.98\ M_\odot\}}_{(t/f_s)}, \qquad \text{(B12)}$$

and Equation (B6) also in a different form of

$$m'^{\{M_{\rm WD}\}}_V(t/f_s) = -2.5\ \log \left[\frac{\dot{M}^2_{\rm wind}}{v^2_{\rm ph}R_{\rm ph}}\right]^{\{M_{\rm WD}\}}_{(t)} + K_V, \qquad \text{(B13)}$$

to derive the last line of Equation (B11). The last line in Equation (B11) simply means that the model light curve $m'^{\{M_{\rm WD}\}}_V(t')$ in Figure 53 is shifted horizontally by $\log f_s$ and vertically by $2.5\log f_s - (m-M)_{V,\rm V1668\ Cyg}$ to retrieve the absolute magnitude and real timescale.

These retrieved absolute magnitudes and real timescales are plotted in Figure 56 for CO nova 3, in Figure 57 for Ne nova 3, in Figure 58 for Ne nova 1. We also tabulate the absolute magnitude, $M_{\rm w}$, at the end point of winds in Tables 3, 4, and 5 and plot them in Figures 59, 60, and 61, for CO nova 3, Ne nova 3, and Ne nova 1, respectively. The values of Ne nova 3 are slightly lower than those for the other chemical compositions (Figure 60). Then, we retrieve the absolute magnitudes of all model light curves in Tables 3, 4, and 5, as

$$M_V = m_{\rm ff} - (m_{\rm w} - M_{\rm w}) = m_{\rm ff} - (15.0 - M_{\rm w}). \qquad \text{(B14)}$$

Note that K_V is a constant for all WD masses. For Ne nova 3, K_V is related to $G^{\{0.98\ M_\odot\}}$ of V1668 Cyg as $K_V = G^{\{0.98\ M_\odot\}} + 1.3$ because $m_{\rm ff} - m'_V = m_{\rm ff} - m'_{\rm w} = G^{\{0.98\ M_\odot\}} - K_V = 15.0 - 16.3 = -1.3$ at the bottom of the light curve (at the end of winds). Here we use $m'_{\rm w} = m_{\rm w}$ because $f_s = 1$ for the 0.98 $M_\odot$ WD for V1668 Cyg and we directly read $m'_{\rm w} = m_{\rm w} = 16.3$ from the 0.98 $M_\odot$ WD model in Figure 17(b).

Then, we obtain $M_{\rm w}$ = 1.7 for the 0.98 $M_\odot$ WD model because $M_{\rm w} = m_{\rm w} - (m-M)_V$ = 16.3 − 14.6 = 1.7.

In the same way, we have $K_V = G^{\{0.96\ M_\odot\}} + 1.6$ for QU Vul of Ne nova 3 because $G^{\{0.96\ M_\odot\}} - K_V = m_{\rm ff} - m'_{\rm w}$ = 15.0 − 16.6 = −1.6, and $K_V = G^{\{1.0\ M_\odot\}} + 1.5$ for V351 Pup of Ne nova 1 because $G^{\{1.0\ M_\odot\}} - K_V = m_{\rm ff} - m'_{\rm w}$ = 15.0 − 16.5 = −1.5.

B.3. *MMRD relation*

B.3.1. *CO Nova 3 based on V1668 Cyg*

We calculated free-free model light curves of various WD masses for the chemical composition of CO nova 3. We plot them in Figure 50 and tabulate them in Table 3. These curves almost overlap each other if they are properly stretched/squeezed along time, as shown in Figure 53. Using Equation (B11), we obtain the absolute magnitude of each model light curve, as shown in Figure 56. (Note that the ordinates of the figure is the absolute magnitude of each light curve.) The absolute magnitude at the end point of the wind phase, $M_{\rm w}$, is also plotted in Figure 59 (and also listed in Table 3).

Figure 56 clearly shows that a more massive WD tends to have a brighter maximum magnitude (smaller $M_{V,\rm max}$, denoted by a magenta filled circle) and a faster decline rate (smaller t_2 or t_3 time). The apparent maximum brightness $m_{V,\rm max}$ of each light curve with a different WD mass is expressed as $m_{V,\rm max} = m'_{V,\rm max} + 2.5\log f_{\rm s}$ from Equation (B9). The t_3 time of each model light curve with a different WD mass is squeezed to be $t_3 = f_{\rm s} t'_3$. Eliminating $f_{\rm s}$ from these two relations, we have $m_{V,\rm max} = 2.5\log t_3 + m'_{V,\rm max} - 2.5\log t'_3$. If we adopt the free-free model light curves, point B (magenta filled circle) corresponds to the V maximum of V1668 Cyg, as shown in Figure 53. Then, we read t'_3 = 26 days and $m'_{V,\rm max}$ = 6.2 along our free-free model light curves in Figures 53 and 56. We obtained our MMRD relation as

$$\begin{aligned} M_{V,\rm max} &= m_{V,\rm max} - (m-M)_V \\ &= 2.5\log t_3 + m'_{V,\rm max} - 2.5\log t'_3 - (m-M)_V \\ &= 2.5\log t_3 - 11.94. \end{aligned} \quad \text{(B15)}$$

We plot this MMRD relation in Figure 47 together with the MMRD point of V1668 Cyg (based on our model light curve, green filled square). Note that we updated the distance modulus to $(m-M)_V$ = 14.6 for V1668 Cyg from its previous value of $(m-M)_V$ = 14.25 in Hachisu & Kato (2010).

B.3.2. *Ne Nova 3 based on QU Vul*

We obtained the theoretical MMRD relation for Ne nova 3 based on QU Vul. We calculated free-free model light curves of various WD masses for the chemical composition of Ne nova 3 (Figure 51 and Table 4). These curves almost overlap each other if they are properly stretched/squeezed along time (Figure 54). Using Equation (B11) for QU Vul, we obtain the absolute magnitude of each model light curve (Figure 57).

In the same way as for V1668 Cyg, we obtain our MMRD relation as

$$\begin{aligned} M_{V,\rm max} &= m_{V,\rm max} - (m-M)_V \\ &= 2.5\log t_3 + m'_{V,\rm max} - 2.5\log t'_3 - (m-M)_V \\ &= 2.5\log t_3 - 11.88, \end{aligned} \quad \text{(B16)}$$

where we adopt t'_3 = 32.7 days, $m'_{V,\rm max}$ = 5.5, and $(m-M)_V$ = 13.6 for QU Vul. Note that we read t'_3 = 32.7 days and $m'_{V,\rm max}$ = 5.5 along our free-free model light curves in Figures 54 and 57. We plot this MMRD relation in Figure 47 together with the MMRD point of QU Vul. A large black open circle corresponds to the MMRD point based on our model light curve while a large red filled circle represents the MMRD point obtained by Downes & Duerbeck (2000).

B.3.3. *Ne Nova 1 based on V351 Pup*

We calculated free-free model light curves of various WD masses for the chemical composition of Ne nova 1 (Figure 52 and Table 5). These curves almost overlap each other if they are properly stretched/squeezed along time (Figure 55). Using Equation (B11) for V351 Pup, we obtain the absolute magnitude of each model light curve (Figure 58).

In the same way as for V1668 Cyg, we obtained our MMRD relation as

$$\begin{aligned} M_{V,\rm max} &= m_{V,\rm max} - (m-M)_V \\ &= 2.5\log t_3 + m'_{V,\rm max} - 2.5\log t'_3 - (m-M)_V \\ &= 2.5\log t_3 - 11.98, \end{aligned} \quad \text{(B17)}$$

where we adopt t'_3 = 20.4 days, $m'_{V,\rm max}$ = 6.4, and $(m-M)_V$ = 15.1 for V351 Pup. Note that we read t'_3 = 20.4 days and $m'_{V,\rm max}$ = 6.4 along our free-free model light curves in Figures 55 and 58. We plot this MMRD relation in Figure 48 together with the MMRD point of QU Vul. A large black open circle corresponds to the MMRD point based on our model light curve while a large red filled circle represents the MMRD point obtained by Downes & Duerbeck (2000).

B.4. *Other empirical relations*

It is interesting to examine various empirical relations of classical novae on the basis of our free-free model light curves. Here we check the empirical formula that the absolute magnitude 15 days after optical maximum, $M_V(15)$, is almost common among various novae. This relation was proposed by Buscombe & de Vaucouleurs (1955) with $M_V(15) = -5.2 \pm 0.1$. Subsequently, the value of $M_V(15) = -5.60 \pm 0.43$ was reported by Cohen (1985); $M_V(15) = -5.23 \pm 0.39$ by van den Bergh & Younger (1987); $M_V(15) = -5.69 \pm 0.42$ by Capaccioli et al. (1989); and $M_V(15) = -6.05 \pm 0.44$ by Downes & Duerbeck (2000). This relation was sometimes called the $t15$ relation (e.g., Darnley et al. 2006).

We already obtained $M_V(15) = -5.95 \pm 0.25$ for 0.55 – 1.2 $M_\odot$ WDs with the chemical composition of CO nova 2 (Hachisu & Kato 2010), $M_V(15) = -5.6 \pm 0.3$ for 0.7 – 1.3 $M_\odot$ WDs with Ne nova 2 (Hachisu & Kato 2010), and $M_V(15) = -5.4 \pm 0.4$ for 0.7 – 1.05 $M_\odot$ WDs with CO nova 4 (Hachisu & Kato 2015). These three relations calculated from the model light curves are consistent with the above empirical relations obtained from the observations.

Point B (magenta filled circle) in Figure 53 represents the peak of V magnitude of the V1668 Cyg outburst. In the real timescale and absolute magnitude, this peak is different for different WD masses as shown in Figure 56. The position of the absolute magnitude 15 days after the peak is shown by green crosses. The distribution of the green crosses is given by $M_V(15) = -5.55 \pm 0.38$ for 0.55–1.2 $M_\odot$ WDs with CO nova 3, as shown in Figure 56. Note that this relation is obtained for the chemical composition of CO nova 3. In the same way, we obtained $M_V(15) = -5.9 \pm 0.3$ for 0.7–1.3 $M_\odot$ WDs with Ne nova 3, as shown in Figure 57, $M_V(15) = -5.8 \pm 0.5$ for 0.7–1.3 $M_\odot$ WDs with Ne nova 1, as shown in Figure 58. These new three relations calculated from our model light curves

are all roughly consistent with the above empirical and model relations.

It should be noted that, however, recent extra-galactic nova surveys show no clear evidence of the so-called $t15$ relation (e.g., Ferrarese et al. 2003; Darnley et al. 2006). The $t15$ relation is a statistical relation like the MMRD relation. We suppose that the maximum magnitude of a nova depends not only on the WD mass but also on the initial hydrogen-rich envelope mass as explained in the MMRD relation. Therefore, the $M_V(15)$ is also affected by the initial envelope mass, even if the WD mass is the same. This could explain the large scatter of $M_V(15)$ distribution.

REFERENCES

Allen, C. W. 1973, Astrophysical Quantities (3rd ed.; London: Athlone)
Andreaë, J., Drechsel, H., Snijders, M. A. J., & Cassatella, A. 1991, A&A, 244, 111
Andreä, J., Drechsel, H., & Starrfield, S. 1994, A&A, 291, 869
Arkhipova, V. P., & Zaitseva, G. V. 1976, Astron. Lett., 2, 35
Arkhipova, V. P., Esipov, V. F., & Sokol, G. V. 1997, Astron. Lett., 23, 713
Augusto, A., & Diaz, M. P. 2003, AJ, 125, 3349
Austin, S. J., Wagner, R. M., Starrfield, S., et al. 1996, AJ, 111, 869
Bergner, Iu. K., Miroshnichenko, A. S., Iudin, R. V., Iutanov, N. Iu., & Dzakusheva, K. G. 1988, Ap&SS, 149, 63
Bohlin, R. C., Savage, B. D., & Drake, J. F. 1978, ApJ, 224, 132
Brosch, N. 1981, IAU Circ., 3601, 2
Brosch, N. 1982, A&A, 107, 300
Bruch, A. 1992, Inf. Bul. Var. Stars, 3745, 1.
Budding, E. 1983, IAU Circ., 3853, 2
Burwitz, V., Starrfield, S., Krautter, J., & Ness, J.-U. 2002, Classical Nova Explosions, eds. M. Hernanz & J. José (New York: AIP), 377
Buscombe, W., & de Vaucouleurs, G. 1955, The Observatory, 75, 170
Caldwell, J. A. R. 1981, Inf. Bull. Variable Stars, 1981, 1
Caldwell, J. A. R. 1982, Inf. Bull. Variable Stars, 2147, 1
Camilleri, P., McNaught, R. H., Gilmore, A. C., & Kilmartin, P. M. 1992, IAU Circ., 5422, 1
Capaccioli, M., della Valle, M., Rosino, L., D'Onofrio, M. 1989, AJ, 97, 1622
Cassatella, A., Altamore, A., & González-Riestra, R. 2002, A&A, 384, 1023
Chochol, D., Grygar, J., Pribulla, T., et al. 1997a, A&A, 318, 908
Chochol, D., Hric, L., Urban, Z., Komzik, R., Grygar, J., & Papousek, J. 1993, A&A, 277, 103
Cohen, J. G. 1985, ApJ, 292, 90
Collins, P., Hurst, G. M., Wils, P., et al. 1984, IAU Circ., 4023, 1
Contadakis, M. E. 1980, Inf. Bull. Variable Stars, 1818, 1
Darnley, M. J., Bode, M. F., Kerins, E., et al. 2006, MNRAS, 369, 257
Darnley, M. J., Henze, M., Steele, I. A., et al. 2015, A&A, 580, A45
della Valle, M., Gilmozzi, R., Bianchini, A., & Esenoglu, H. 1997, A&A, 325, 1151
della Valle, M., & Livio, M. 1995, ApJ, 452, 704
della Valle, M., Pasquini, L., Daou, D., & Williams, R. E. 2002, A&A, 390, 155
di Paolantonio, A., Patriarca, R., & Tempesti, P. 1981, Inf. Bull. Variable Stars, 1913
Downes, R. A., & Duerbeck, H. W. 2000, AJ, 120, 2007
Downen, L. N., Iliadis, C., José, J., Starrfield, S. 2013, ApJ, 762, 105
Duerbeck, H. W. 1981, PASP, 93, 165
Duerbeck, H. W., Rindermann, R., & Seitter, W. C. 1980, A&A, 81, 157
Duerbeck, H. W., & Wolf, B. 1977, A&AS, 29, 297
Ennis, D., Becklin, E. E., Beckwith, S., Elias, J., Gatley, I., Matthews, K., Neugebauer, G., & Willner, S. P. 1977, ApJ, 214, 478
Ferland, G. J., & Shields, G. A. 1978, ApJ, 226, 172
Ferrarese, L., Côté, P., & Jordán, A. 2003, ApJ, 599, 1302
Gallagher, J. S.; Holm, A. V. 1974, ApJ, 189, L123
Gallagher, J. S., Kaler, J. B., Olson, E. C., Hartkopf, W. I., & Hunter, D. A. 1980, PASP, 92, 46
Gallagher, J. S., & Ney, E. P. 1976, ApJ, 204, L35
Gehrz, R. D., Hackwell, J. A., Grasdalen, G. I. et al. 1980, ApJ, 239, 570
Gehrz, R. D., Grasdalen, G. I., & Hackwell, J. A. 1985, ApJL, 298, L47
Gehrz, R. D., Grasdalen, G. L., & Hackwell, J. A. 1986, ApJL, 298, L47 (erratum 306, L49)
Gehrz, R. D., Truran, J. W., Williams, R. E., & Starrfield, S. 1998, PASP, 110, 3
Gil-Pons, P., & García-Berro, E. 2001, A&A, 375, 87
Gil-Pons, P., García-Berro, E., José, J., Hernanz, M., & Truran, J. W. 2003, A&A, 407, 1021
Green, G. M., Schlafly, E. F., Finkbeiner, D. P., et al. 2015, ApJ, in press (arXiv:1507.01005))
Grevesse, N., & Anders, E. 1989, Cosmic Abundances of Matter, ed. C. J. Waddington (New York: AIP), 1
Güver, T., & Özel, F. 2009, MNRAS, 400, 2050
Hachisu, I., & Kato, M. 2001, ApJ, 558, 323
Hachisu, I., & Kato, M. 2006, ApJS, 167, 59
Hachisu, I., & Kato, M. 2007, ApJ, 662, 552
Hachisu, I., & Kato, M. 2010, ApJ, 709, 680
Hachisu, I., & Kato, M. 2014, ApJ, 785, 97
Hachisu, I., & Kato, M. 2015, ApJ, 798, 76
Hachisu, I., Kato, M., & Cassatella, A. 2008, ApJ, 687, 1236
Harman, D. J., & O'Brien, T. J. 2003, MNRAS, 344, 1219
Harrison, T. E., Bornak, J., McArthur, B. E., & Benedict, G. F. 2013, ApJ, 767, 7
Hayward, T. L., Saizar, P., Gehrz, R. D., et al. 1996, ApJ, 469, 854
Hopp, U. 1979, Inf. Bull. Variable Stars, 1633, 1
Iijima, T. 2006, A&A, 451, 563
Kato, M., & Hachisu, I., 1994, ApJ, 437, 802
Kato, M., & Hachisu, I., 2007, ApJ, 657, 1004
Kato, M., Hachisu, I., & Cassatella, A. 2009, ApJ, 704, 1676
Kato, M., Mikołajewska, J., & Hachisu, I. 2012, ApJ, 750, 5
Kato, M., Saio, H., Hachisu, I., & Nomoto, K. 2014, ApJ, 793, 136
Kato, M., Saio, H., & Hachisu, I. 2015, ApJ, 808, 52
Kiselev, N. N., & Narizhnaia, N. V. 1977, Soviet Astronomy, 21, 344
Klare, G., Wolf, B., & Krautter, J. 1980, A&A, 89, 282
Kolotilov, E. A. 1980, Soviet Astronomy Letters, 6, 268
Kolotilov, E. A., & Shenavrin, V. I. 1988, SvAL, 14, 29
Kozai, Y., Kosai, H., Honda, M., & Cragg, T. 1981, IAU Circ., 3590, 1
Krautter, J., Ögelman, H., Starrfield, S., Wichmann, R., & Pfeffermann, E. 1996, ApJ, .456, 788
Lance, C. M., McCall, M. L., & Uomoto, A. K. 1988, ApJS, 66, 151
Lindgren, H. 1979, Inf. Bull. Variable Stars, 1543, 1
Liszt, H. S. 2014, ApJ, 780, 10
Livio, M., & Truran, J. W. 1994, ApJ, 425, 797
Lockwood, G. W., & Millis, R. L. 1976, PASP, 88, 235
Lyke, J. E., & Campbell, R. D. 2009, AJ,
Lyke, J. E. et al. 2003, AJ, 126, 993
Mallama, A. D., & Skillman, D. R. 1979, PASP, 91, 99
Marshall, D. J., Robin, A. C., Reylé, C., Schultheis, M., & Picaud, S. 2006, A&A, 453, 635
Miroshnichenko, A. S. 1993, Perem. Zvezdy, 23, 175
Mukai, K., & Ishida, M. 2001, ApJ, 551, 1024
Ness, J.-U., Starrfield, S., Jordan, C., Krautter, J., & Schmitt, J. H. M. M. 2005, MNRAS, 364, 1015
Orio, M., Balman, S., della Valle, M., Gallagher, J., & Ögelman, H. 1996, ApJ, 466, 410
Orio, M., Parmar, A. N., Greiner, J., et al. 2002, MNRAS, 333, L11
Paresce, F., Livio, M., Hack, W., & Korista, K. 1995, A&A, 299, 823
Payne-Gaposchkin, C. 1957, The Galactic Novae (Amsterdam: North-Holland)
Pfau, W. 1976, Inf. Bul. Variable Stars, 1106
Piccioni, A., Guarnieri, A., Bartolini, C., & Giovannelli, F. 1984, Acta Astron., 34, 473
Retter, A., Leibowitz, E. M., & Ofek, E. O. 1997, MNRAS, 286, 745
Robb, R. M., & Scarfe, C. D. 1995, MNRAS, 273, 347
Rosino, L., & Iijima, T. 1987, Ap&SS, 130, 157
Rosino, L., Iijima, T., Benetti, S., et al. 1992, A&A, 257, 603
Saizar, P., Starrfield, S., Ferland, G. J., et al. 1992, ApJ, 398, 651
Saizar, P., Pachoulakis, I., Shore, S. N., et al. 1996, MNRAS, 279, 280
Sala, G., & Hernanz, M. 2005, A&A, 439, 1057
Schlafly, E. F., & Finkbeiner, D. P. 2011, ApJ, 737, 103
Schmidt, Th. 1957, Z. Astrophys., 41, 181
Schwarz, G. J. 2002, ApJ, 577, 940
Schwarz, G. J., Shore, S. N., Starrfield, S., & Vanlandingham, K. M. 2007, ApJ, 657, 453
Seaton, M. J. 1979, MNRAS, 187, 73
Shafter, A. W., Misselt, K. A., Szkody, P., & Politano, M. 1995, ApJ, 448, L33
Shore, S. N., Schwarz, G., Bond, H. E., et al. 2003, AJ, 125, 1507
Slovak, M. H. & Vogt, S. S. 1979, Nature, 277, 114
Snijders, M. A. J., Batt, T. J., Roche, P. F., et al. 1987, MNRAS, 228, 329
Sokoloski, J. L., Crotts, A. P. S., Lawrence, S., & Uthas, H. 2013, ApJ, 770, L33
Stickland, D. J., Penn, C. J., Seaton, M. J., Snijders, M. A. J., & Storey, P. J. 1981, MNRAS, 197, 107
Strope, R., Schaefer, B. E., & Henden, A. A. 2010, AJ, 140, 34
Taylor, A. R., Pottasch, S. R., Seaquist, E. R., & Hollis, J. M. 1987, A&A, 183, 38
Tempesti, P. 1979, Astronomische Nachrichten, 300, 51
Umeda, H., Nomoto, K., Yamaoka, H., & Wanajo, S. 1999, ApJ, 513, 861
van den Bergh, S., & Younger, P. F. 1987, A&AS, 70, 125
Vanlandingham, K. M., Starrfield, S., & Shore, S. N. 1997, MNRAS, 290, 87
Vanlandingham, K., Starrfield, S., Wagner, R. M., Shore, S. N., & Sonneborn, G. 1996, MNRAS, 282, 563
Vanlandingham, K. M., Schwarz, G.J., Shore, S.N., Starrfield, S., & Wagner, R.M. 2005, ApJ, 624, 914
Verbunt, F. 1987, A&AS, 71, 339
Walker, W. S. G., & Marino, B. F. 1982, Publ. Variable Star Sect., R. Astron. Soc. N.Z., 10, 48
Wanajo, S., Hashimoto, M., Nomoto, K. 1999, ApJ, 523, 409

Warner, B. 1995, Cataclysmic variable stars, (Cambridge: Cambridge Univ. Press)
Weidemann, V. 2000, A&A, 363, 647
Whitelock, P. A., Carter, B. S., Feast, M. W., Glass, I. S., Laney, D., et al. 1984, MNRAS, 211, 421
Williams, R. E., Phillips, M. M., & Hamuy, M. 1994, ApJS, 90, 297
Williams, R. E., Ney, E. P., Sparks, W. M., et al. 1985, MNRAS, 212, 753
Woodward, C. E., Wooden, D. H., Pina, R. K., & Fisher, R. S. 1999, IAU Circ., 7220, 3
Woudt, P. A., Warner, B. 2001, MNRAS, 328, 159
Woudt, P. A., Warner, B., & Spark, M. 2005, MNRAS, 364, 107
Wu, C.-C., Holm, A. V., Panek, R. J., et al. 1989, ApJ, 339, 443